博　士　論　文

Effects of environmental factors on the mechanical properties of carbon fiber paper reinforced polyamide 6

(炭素繊維ペーパー強化ポリアミド6の力学特性に対する環境要因の影響に関する研究)

何　向東

Abstract

Carbon fiber reinforced plastics (CFRP) have a wide range of applications in the fields of aerospace, transportation, sports, automobiles, etc. Compared to ceramic and metal materials, CFRP have lower weight at the same level of mechanical performance because of the excellent properties of carbon fibers (CF). Recently, carbon fiber reinforced thermoplastics (CFRTP) have been used extensively in order to reduce costs and improve productivity. For matrix used in CFRTP, polyamide 6 (PA6) is highly expected due to its excellent mechanical properties, low cost and great cohesiveness with carbon fibers. However, environmental factors such as moisture, sea water, temperature, thermo- oxidation, etc. may result in negative effect on CFRTP material. So, in this research, with the aim of confirming the mechanical performance of CFRTP in various environments, the effects of different environmental factors were investigated experimentally and analytically.

Chapter 1 presented the current state and pressing issues of recycling CFRP and recycled carbon fibers (rCF). The importance of studying short carbon fibers and carbon fiber mat reinforced thermoplastics were discussed. The reason for choosing carbon fiber paper reinforced thermoplastics (CPT) with the matrix of polyamide 6 (PA6) as the research objective was described. Different environmental factors, such as moisture, sea water, cyclic absorption-desorption, and thermo-oxidation and their effects were shown respectively.

Chapter 2 introduced the water absorption behavior of CPT material in fresh and sea water. Water absorption ratio and diffusion coefficient were calculated by Fick's diffusion law to evaluate the water diffusion behavior in CPT. The flexural properties of CPT with different water contents and under different temperatures were studied by three-point bending test. The fracture surface after the flexural test was observed by scanning electron microscope (SEM). Droplet test was conducted to clarify the change of interfacial shear strength (IFSS) before

and after water absorption. Cyclic water absorption-desorption test was conducted to analyze the role of water molecules in water-absorbed CPT materials. The role of water molecules as plasticizers was identified and a relatively stable mechanical properties of CPT after several cycles of absorption-desorption was found.

Chapter 3 introduced the performance of CPT material after long-term aging in fresh water and sea water environment. Surface morphology of these specimens was observed by microscope, indicating more serious effects of fresh water than that of sea water. Thermodynamic properties were studied by differential scanning calorimetry (DSC) to analyze the aging effect from the perspective of resin crystallization. The analysis of the chemical structure of matrix by Fourier-transform infrared (FTIR) proved that polymer chain scission and degradation happened during aging test. Discussion on critical length of fibers and factor *C* confirmed that the degradation of resin has a great influence on the decline of mechanical properties of CPT.

Chapter 4 studied the thermo-oxidative effects on CPT material in order to evaluate the high temperature tolerance. The highest use temperature of CPT materials was determined by thermo-oxidative aging test. Micromorphology of specimens after aging test was observed. Thermo-oxidative resistance of CPT material was found, and the result provided a guidance for the application of CPT materials in fire rescue equipment.

Chapter 5 made a summary of this dissertation. The prospect of the application of short carbon fiber reinforced plastics and the outlook for future tasks were discussed.

Contents

List of Figures

List of Tables

List of Equations

List of Abbreviations

Abbreviation	Definition
C	
CF	Carbon fiber
CFRP	Carbon fiber reinforced plastics
CFRTP	Carbon fiber reinforced thermoplastics
CFRTS	Carbon fiber reinforced thermosetting plastics
CPT	Carbon fiber paper reinforced thermoplastics
D	
DSC	Differential scanning calorimetry
F	
FLD	Fiber length distribution
FOD	Fiber orientation distribution
FTIR	Fourier-transform infrared spectrum
I	
IFSS	Interfacial shear strength
M	
MRoM	Modified rule of mixture
P	
PA6	Polyamide 6
PAN	Polyacrylonitrile
R	
rCF	Recycled carbon fiber
RoM	Rule of mixture

Chapter 1. Introduction

1.1 Carbon fiber

Carbon fiber (CF) is a potential material usually used as reinforcement, which is widely developed in recent years. Carbon fibers were first made by Edison in 1879 by carbonizing cotton fibers, which was used to make filament of light bulb. In the 1950s, with the development of aerospace and technology, materials with excellent properties were widely in demand [1]. Many industrialized countries began to pay attention to the research and production development of carbon fibers. So far, the research and development technology of light and high strength carbon fibers has been mature, and carbon fibers have gradually entered people's daily life from the aerospace and other high-end fields. At the same time, the research and development work of carbon fibers with higher performance and high strength has never stopped. The application of new high-strength carbon fiber has brought great influence on and change human's technology and science. Because of their excellent

properties, carbon fibers are indispensable engineering material for aerospace, national defense and military industry, and also widely used in sports goods, transportation, medical equipment, civil construction and other fields [2-4].

Carbon fibers, which are used as reinforced material, are generally divided into two series: PAN based carbon fibers and pitch-based carbon fibers. PAN based carbon fibers are made from polyacrylonitrile (PAN), which was first recognized as a suitable precursor of carbon fiber in 1961. It is now the most important starting material for carbon fibers. PAN based carbon fibers are compatible with relatively high strength and elastic modulus. Besides, they also show low density, high temperature resistance, friction resistance, corrosion resistance, good thermal conductivity, low coefficient of thermal expansion, and other excellent properties. So, PAN based carbon fibers have been developed rapidly [5-7]. Pitch-based carbon fibers are made from coal pitch, petroleum and other materials rich in polycyclic aromatic hydrocarbons by polymerization, spinning, non-melting and carbonization [8]. In accordance with the different performance, pitch-based carbon fibers are usually divided into general-purpose pitch carbon fiber and high-performance pitch carbon fiber. The former is made from isotropic pitch, which is also known as isotropic pitch carbon fiber, and the latter is made from mesophase pitch, so it is also called mesophase pitch carbon fiber. The strength and modulus of general-purpose pitch carbon fibers are worse than PAN based carbon fiber, so it cannot be used as reinforcement materials for aerospace, sports and entertainment products. However, high performance pitch carbon fibers have high mechanical properties, good heat transfer performance, good conductivity and low coefficient of thermal expansion [7-10]. It can be compounded with resin and metal to make high performance composite materials. Currently, PAN based carbon fibers are widely used, which account for about 90% of total carbon fiber production over the world.

1.2 Recycling of carbon fibers

1.2.1 CFRP and CFRP waste

Carbon fiber reinforced plastics, which is called CFRP, is one of the important uses of carbon fiber materials. Carbon fibers are used as reinforcement in plastics, making composites obtain better processability, lower cost and lighter weight, which are the advantages of plastics. On the other hand, the addition of carbon fibers can help composites obtain high mechanical properties, high thermal conductivity and other excellent properties of carbon fibers. So, CFRP material has excellent mechanical properties and relatively low weight comparing to metal and ceramic materials, leading to a wide application in many fields [11-16].

Because of the excellent properties, the demand for carbon fibers and CFRP has increased year by year. According to some research, the global carbon fiber and carbon fiber reinforced plastics markets are expected to reach US $37.23 billion, growing at a compound annual growth rate of more than 10%. In addition, the growing demand for automotive fuel efficiency, coupled with the growing focus on renewable energy, will drive market growth over the forecast period. Based on this application, it is expected that by 2023, due to the growing demand for lightweight, safe and cost-effective vehicles, the automotive segment is expected to lead the market. Global CF and CFRP market size are shown in Figure 1-1 [17]. It can be found that the demand over the world is showing obvious growth.

However, as Figure 1-2 [18] shows, carbon fibers have relatively high production cost, compared to metallic materials, such as steel, aluminum, and alloy. Therefore, it is difficult to apply CFRP to commercial mass-production such as vehicles, sports productions, unmanned machinery etc., which limits their further development.

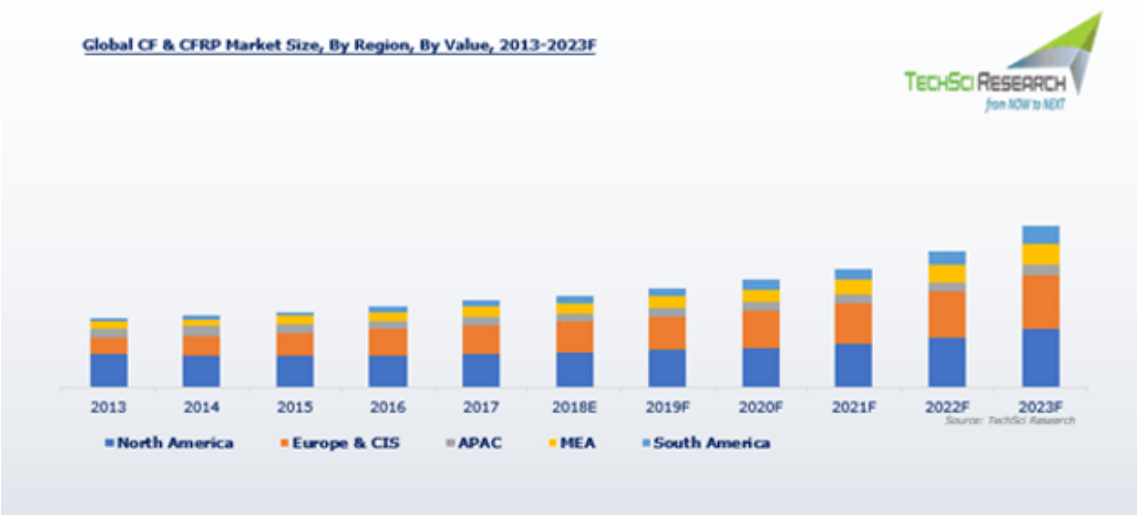

Figure 1-1 Global CF and CFRP market size [17]

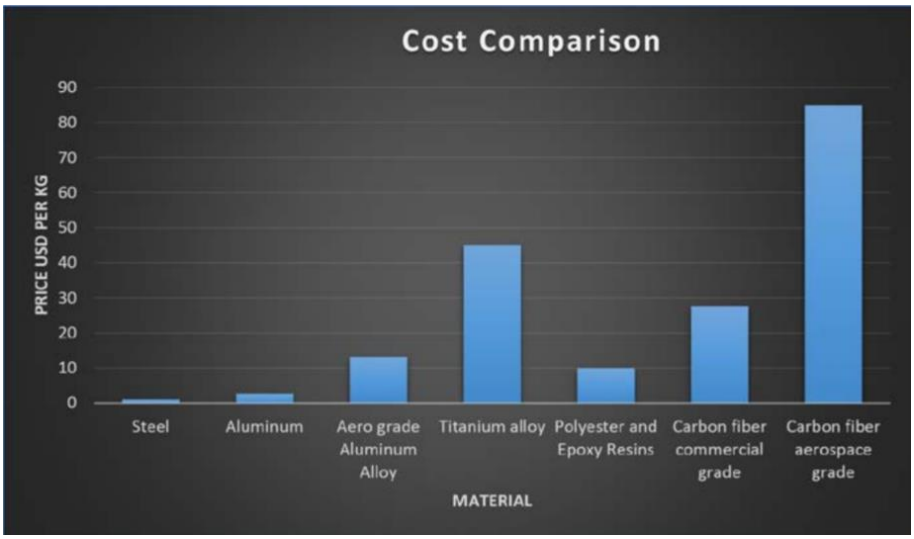

Figure 1-2 Cost comparison of materials [18]

Synchronizing with the increasing demand of CF and CFRP, CFRP wastes is also increasing with the continuous expansion of the utilization every year. Among the CFRP wastes, unused prepreg CFRP and retired CFRP products take a large part. Most of them are just shape damaged, but the internal carbon fibers still retain their original performance, owning to their stability and corrosion resistance [19-22]. Therefore, if there are some effective methods to

recycle and reuse carbon fibers with good performance from these CFRP waste, it can effectively alleviate the current contradiction between the insufficient capacity and the huge demand of carbon fibers.

Nowadays, most of CFRP waste are used as landfill and incinerated as energy provider, which is a huge waste for carbon fibers [23]. Considering the stable state of carbon fibers in these products, if they can be recycled and reused, the tension of carbon fibers demand can be relieved to some extent. The problem is whether the recycled carbon fibers (rCF) can meet the requirements of product quality. So, new and effective methods of recycling of carbon fibers need to be developed.

1.2.2 Recycling techniques

At present, several methods are normally applied for carbon fiber recycling as shown in Figure 1-3. Mechanical recycling includes shredding, crushing, grinding, etc. CFRP wastes are treated to fine particles or powder [24-26]. These particles or powder will be used in cement, paving material, blast furnace material, i.e. landfill and incineration as mentioned above, or used as fillers to reinforce composites. After mechanical recycling, carbon fibers and resin cannot be separated from each other, so, the use of recycled products will be limited.

Carbon fibers recycled by mechanical recycling can hardly keep their original shapes, so rCF are difficult to continue to be applied in the same fields. Thus, novel recycling methods have been proposed and studied in recent decades, including pyrolysis recycling, fluidized bed recycling, and chemical recycling [27-32]. CFRP can be separated as rCF and byproducts. Different from mechanical recycling, carbon fibers can almost keep their shapes and properties after these new methods. So, the reuse of rCF to their original fields becomes possible.

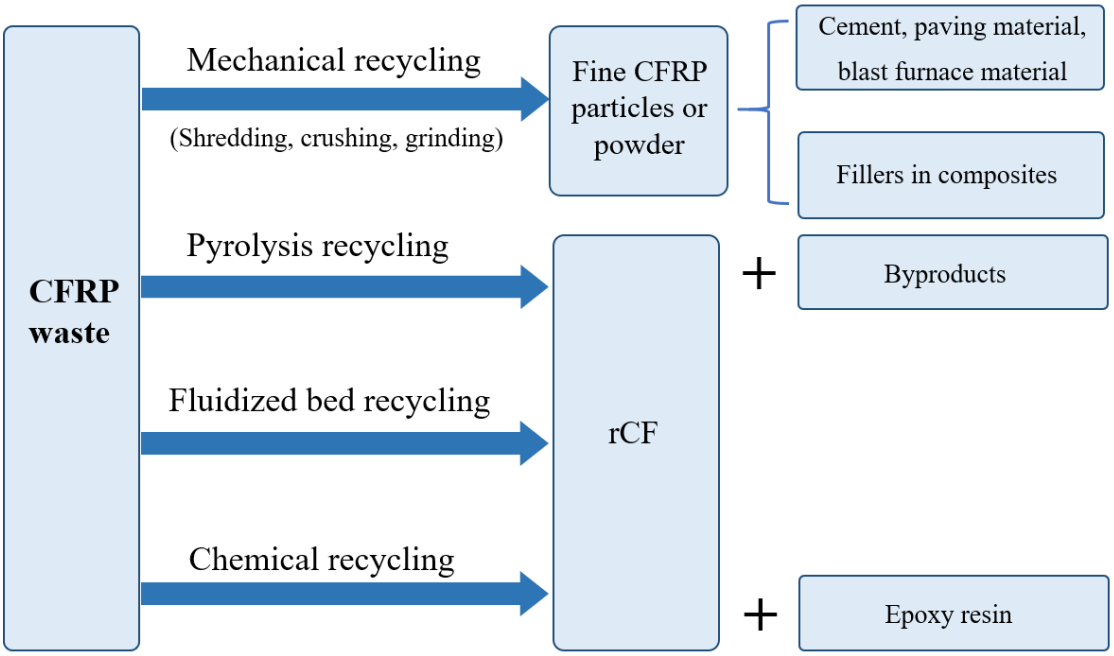

Figure 1-3 Main technologies to recycle CF in CFRP waste

1.3 Re-manufacturing of CFRP by recycled carbon fibers

1.3.1 Recycled carbon fibers

The purpose of CFRP recycling is not only to recycle carbon fibers, but the reuse of rCF should be considered as the ultimate target. Figure 1-4 [33] shows the expected life-cycle for CFRP materials. At this stage, after recycling carbon fibers from CFRP wastes, the re-manufacturing of rCF and whether the rCF can meet the use requirements needs to be investigated emphatically.

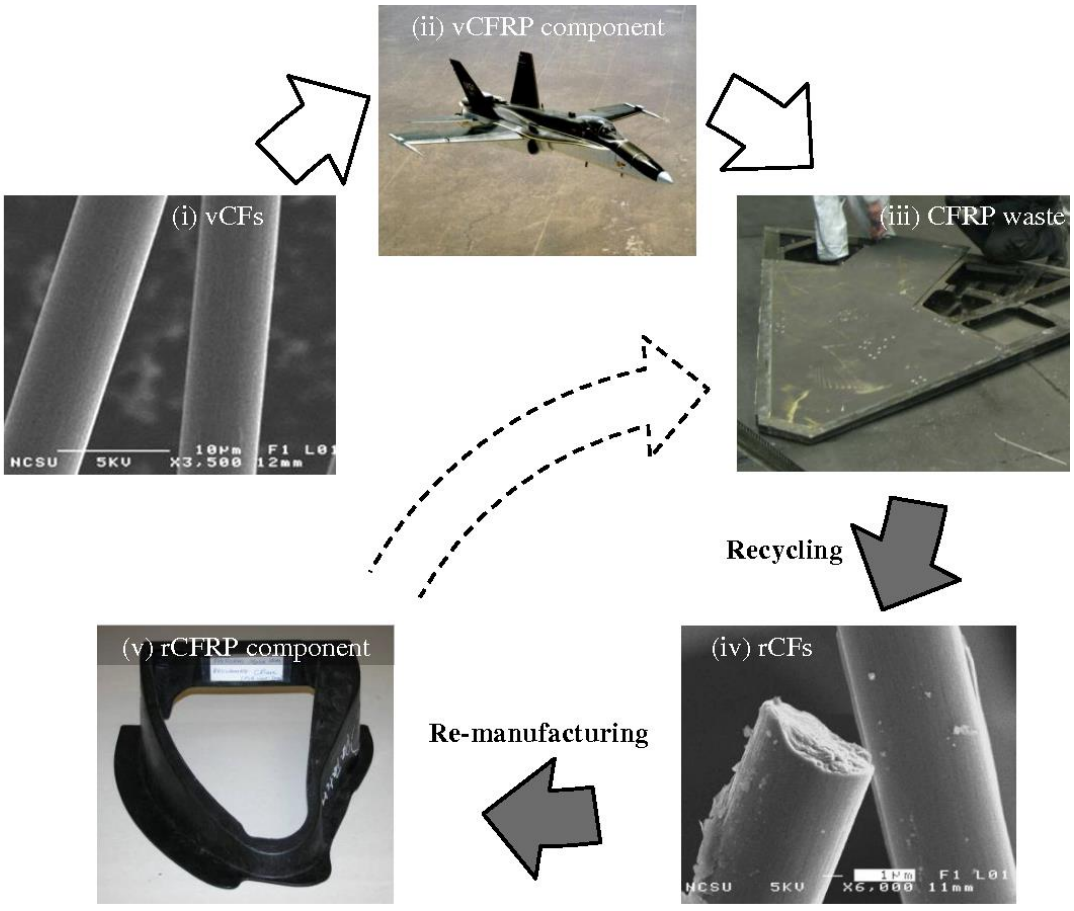

Figure 1-4 Close life-cycle for CFRP [33]

However, when the new developed methods described in 1.2.2 are adopted in industry for recycling carbon fibers, limited by the factors such as equipment sizes, production cost, etc., CFRP wastes are usually cut and crushed into smaller pieces. So, the continuous carbon fibers in the parts that needed to be recycled are likely to be cut off into discontinuous carbon fibers during the recycling process. Figure 1-5 [34] shows the length distribution of rCF after fluidized bed recycling. After recycling, continuous carbon fibers cannot maintain their original length and become discontinuous and short carbon fibers, which forces researchers to reconsider and plan the re-manufacturing methods for rCF.

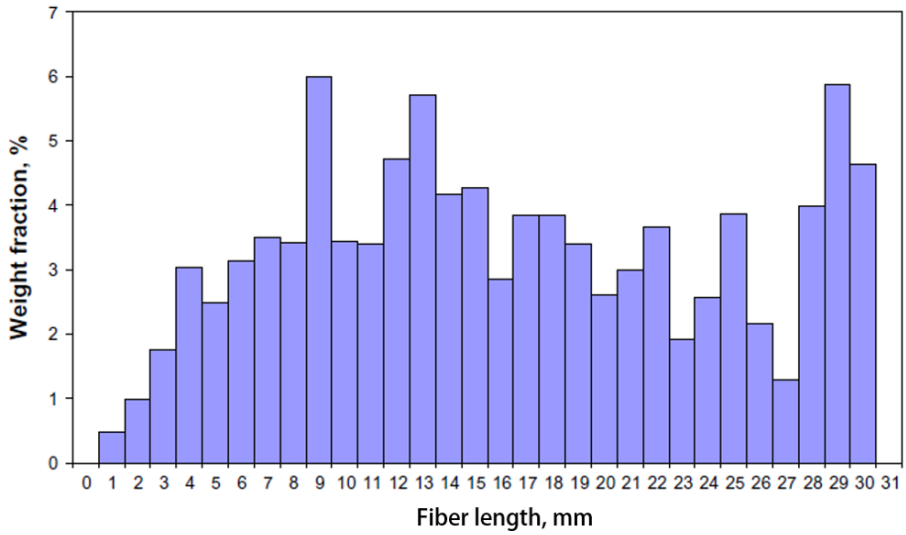

Figure 1-5 Weight average length distribution of rCF [34]

Figure 1-6 [35] shows the re-manufacturing process of rCF after pyrolysis recycling, fluidized bed recycling, and chemical recycling process shown in Figure 1-3. Reclaimed fibers are usually in “fluffy” form. Depending on the length of rCF, different manufacture approaches are employed. Short fibers are evenly mixed with chosen resin and the final products are isotropic in plane. Fibers with medium length are usually preformed and then impregnated in resin to make prepreg materials. Long fibers are firstly aligned, in order to restore their original state in CFRP waste as much as possible, and then impregnated in chosen resin.

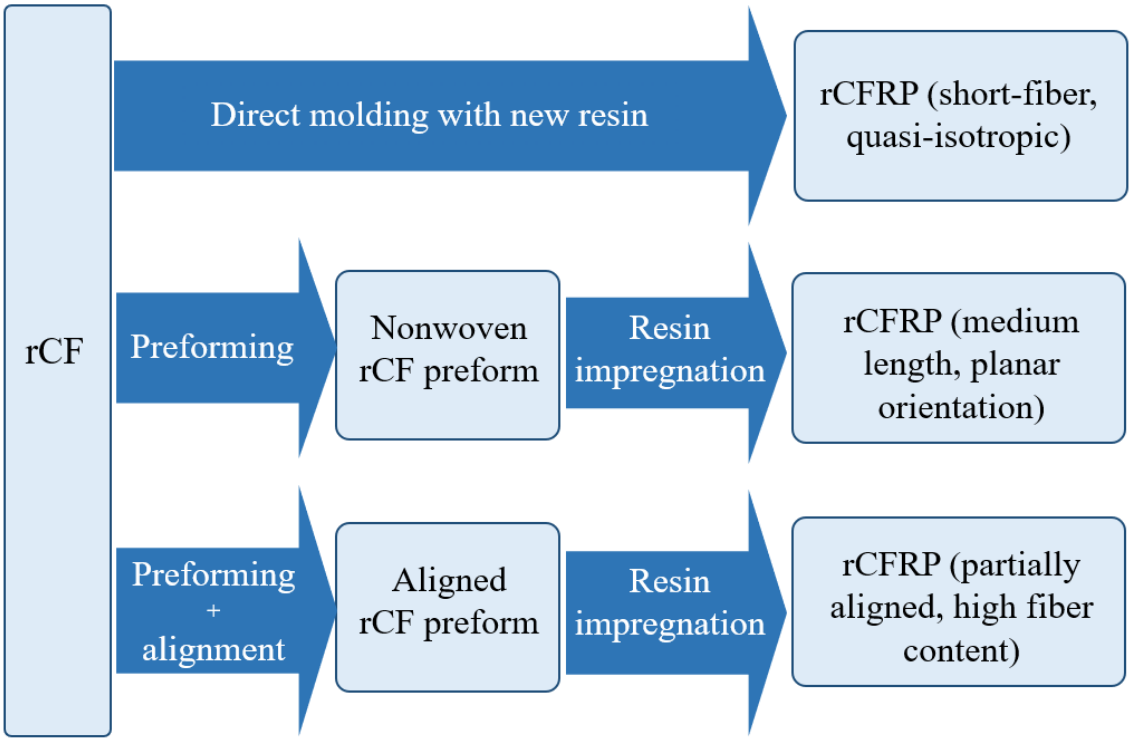

Figure 1-6 Re-manufacturing process of CFRP by rCF after new recycling methods [35]

1.3.2 Matrix choosing

As Figure 1-6 shows, rCF should be well-mixed with new resin to produce new CFRP raw material. Depending on the nature of resin, it can be divided into two types: thermosetting resin and thermoplastics resin. The features of the two types are described below.

Thermosetting resin refers to a kind of resin that has chemical changes after heating, gradually hardens, and does not soften or dissolve when heated again. The most common resins used as the matrix material of CFRP are epoxy resin, phenolic resin, unsaturated polyester resin, and so on. Due to the low viscosity and good liquidity of some thermosetting resins, they are widely used for the impregnation of rCF. Therefore, carbon fiber reinforced thermosettings (CFRTS) are commonly applied in various fields [36].

Thermoplastic resins usually melt after heating and solidify after cooling. This property can be maintained no matter how many times heating and cooling are repeated. Therefore, different from CFRTS, carbon fiber reinforced thermoplastics (CFRTP) can be processed several times by heating. Furthermore, the molecular structures of thermoplastic resins are linear, and no chemical reactions happen during heating and cooling process. So, thermoplastics have faster molding speed than thermosetting resins because they do not need curing time for chemical reactions. Besides, universal thermoplastic resins are cheaper than thermosetting resins [37]. Commonly used thermoplastic resins are polyamide 6 (PA6), polypropylene, polycarbonate, polyamide 66, phenylene sulfide, etc.

Among the general thermoplastic resins, PA6 is a promising resin because it is relatively inexpensive as a kind of engineering plastic. It has a low melting point and a wide range of process temperature. Its impact and solubility resistance are better than polyamide 66, but its moisture absorption is also stronger. The effect of moisture absorption is the subject of this research, and detailed information will be discussed in chapter 2 and 3. Because of the great mechanical performance of PA6 itself among thermoplastic resins, relatively low cost and good adhesion with carbon fibers, PA6 resin is often used as the matrix material of CFRTP.

Therefore, when choosing suitable resin for the re-manufacturing of CFRP by rCF, considering the cost, resin properties, the combination of CF and resin, the difficulty of forming, the difficulty in recycling and other factors, PA6 is a promising choice. However, as mentioned above, environmental factors may have negative influence on the performance of PA6 composite, so it is necessary to comprehensively consider and evaluate the impact of these environmental factors.

1.4 Environmental factors

When considering the application of CFRTP to mass-production, the evaluation of the change of mechanical properties and stability due to diverse environment is critical. Various environmental factors lead to the deterioration of plastics, such as moisture, temperature, sea water, heat, oxygen, etc. So, it is necessary to study the influence of environment before the mass-production and application to market. In this research, moisture, hydrothermal environment, sea water, thermo-oxidation are taken as the objective environmental factors.

1.4.1 Moisture

Owning to the existing of hydrophilic groups in some polymer chains, such as amide bond, carbonyl, hydroxyl, amino group, etc. and various possible additives that may be added to improve the processing properties of materials, composites show certain water absorption characteristics [38]. Generally, two steps happen during the water absorption process. First, water molecules are absorbed by dry polymer. The absorbed water builds hydrogen bonds with hydrophilic groups on polymer chains and breaks secondary bonds between nearby polymer chains. When all the hydrophilic groups on polymer chains are all occupied by water molecules, water continues to penetrate into the inner part of composite, forming clusters between polymer chains [39].

Different polymer-based composites may exhibit different water absorption behavior and characteristics due to different resins and additives. Figure 1-7 [39] gives a typical result concerning water diffusion parameters identification on the chosen pure PA6 specimens. The great agreement between the experimental data and the Fick's model shows that the studied material absorbed moisture according to a Fickian diffusion law.

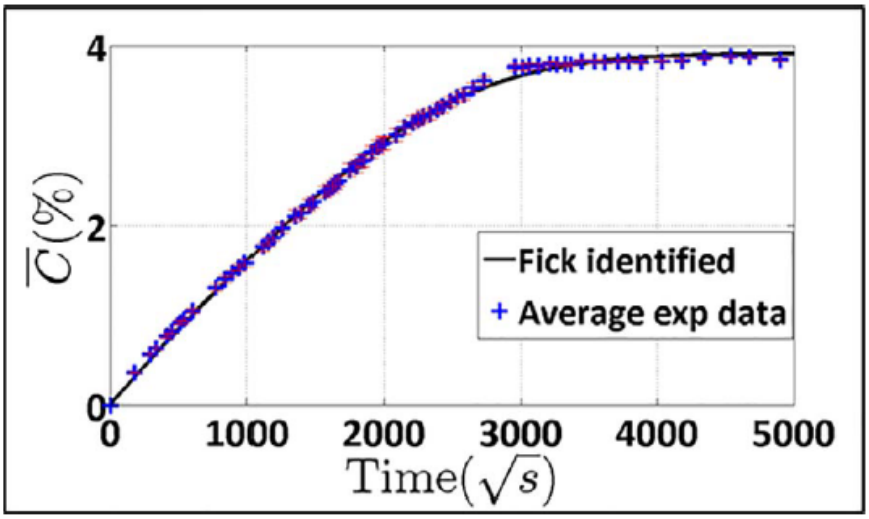

Figure 1-7. Average experimental and identified data with Fick solution for one specimen of neat resin [39]

E. Picard et al. [40] investigated the additive state on the water transport properties of polyamide 6 based nanocomposites. The amount of absorbed water increased with the increase in water activity, which ranged from 0 to 0.9. And when the additives increased, the absorbed water contents at a given activity decreased and the saturated state of water absorption reached more slowly. Furthermore, the water absorption behavior of studied specimens all followed Fickian diffusion law, indicating a possible law of water absorption of PA6 resin-based composite. Relative results are shown in Figure 1-8. However, results from Y. Lei et al. [41] of PA6 based carbon fiber composites show different water absorption behavior, which is shown in Figure 1-9. Fickian diffusion law can only be used to describe the initial stage of water absorption process and its value is lower than experimental data. Langmuir diffusion model can describe the experimental data better than Fickian diffusion law in the second stage of water absorption. Besides, pure polymer absorbs more water and show higher water-uptake than PA6/CF composite at the same temperature because carbon fibers exhibit barrier effect to water absorption behavior. Similar results of water absorption were also reported in different polymer-based composites [42-45].

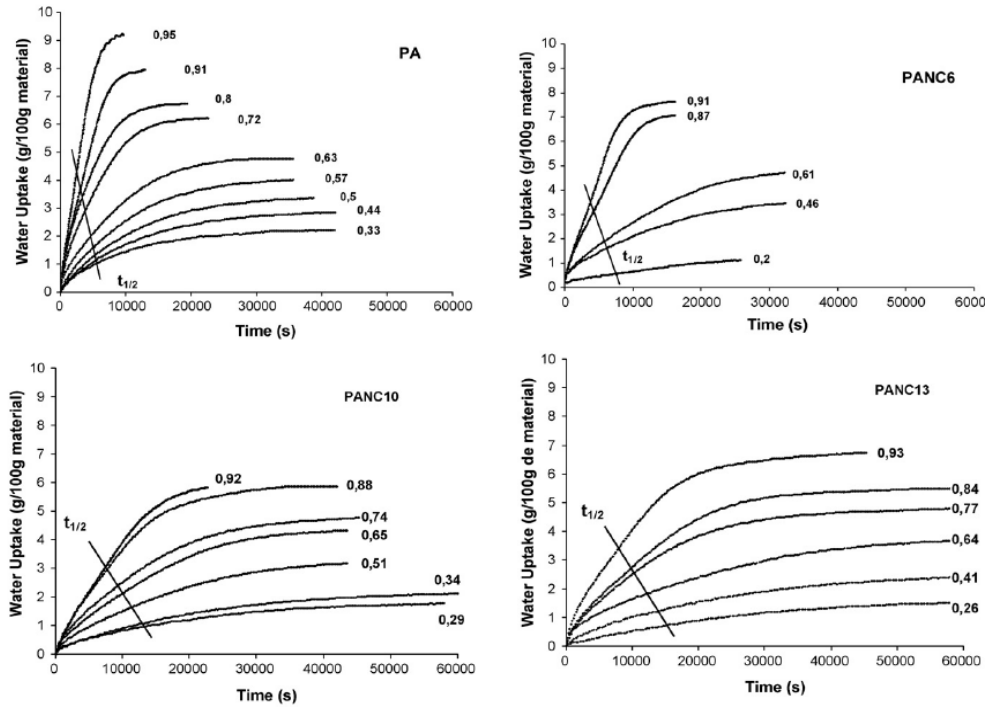

Figure 1-8. Water vapor uptake in the PA6 and nanocomposites films as a function of the activity [40]

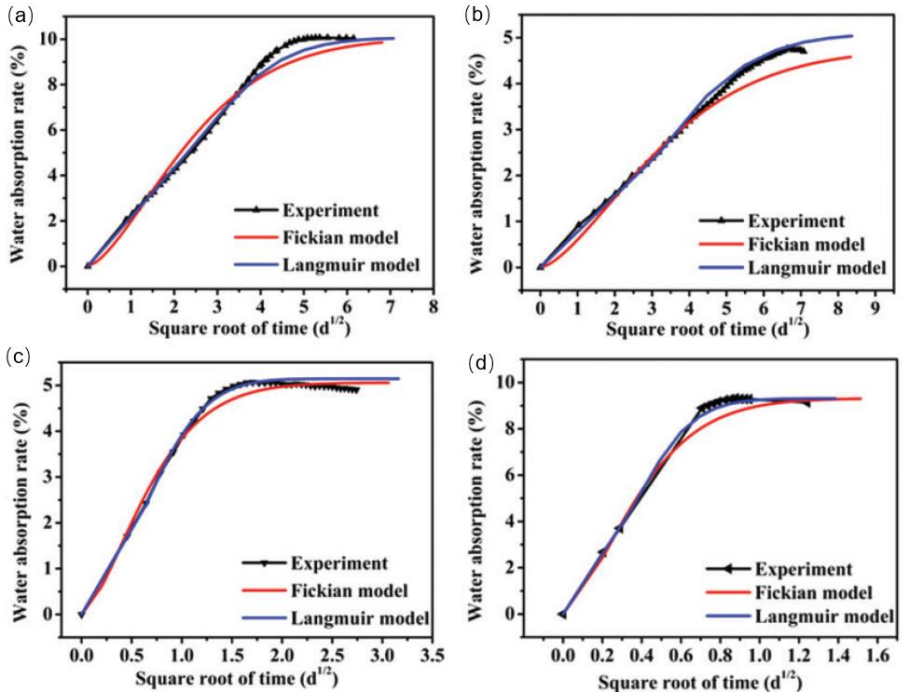

Figure 1-9. Experimental and analytical curves at two water temperature; (a) 25 ℃ of PA6; (b) 70 ℃ of PA6; (c) 25 ℃ of CF/PA6; (d) 70 ℃ of CF/PA6 [41]

Therefore, when the water absorption time is short, Fickian diffusion law is suitable to describe the water absorption behavior of PA6 material. In short carbon fiber reinforced material, the dynamics of water absorption needs to be studied in order to clarify the water absorption characteristics of this material in water rich environment and build solid foundation for further research.

1.4.2 Hydrothermal environment

As mentioned above, two steps usually exist in the water absorption process. The first step of water absorption induces a decrease in the modulus of matrix, while the second step does not result in significant drop of the stiffness of specimens anymore because forming water clusters do not cause further physico-chemical alteration of polymer chains. H. Obeid et al. [39] investigated the relation between moisture contents and mechanical properties in PA6 resin, and the results proved the two-step absorption behavior and their effects on the mechanical properties of PA6, as Figure 1-10 shows. Kusmono et al. [46] pointed out that after water absorption, both the tensile strength and modulus of PA6-based composite decreased but the elongation increased at break. C. Huang et al. [47] studied the tensile properties of water absorbed PA6 material, and they identified that after water absorption, the mechanical strength and modulus of PA6 material were reduced by 20% and 50% respectively, while the elongation at break were increased by around 900%. This result is attributed to the plasticization of the resin after water absorption. Similar results were also reported by V. Do et al. [48] No matter whether the matrix is pure resin or composite resin obtained by mixing two resins, as long as one of the resins contains hydrophilic group, the composite material absorbs moisture, and the mechanical properties decrease with the increase of the percentage of hydrophilic resin, as Figure 1-11 shows.

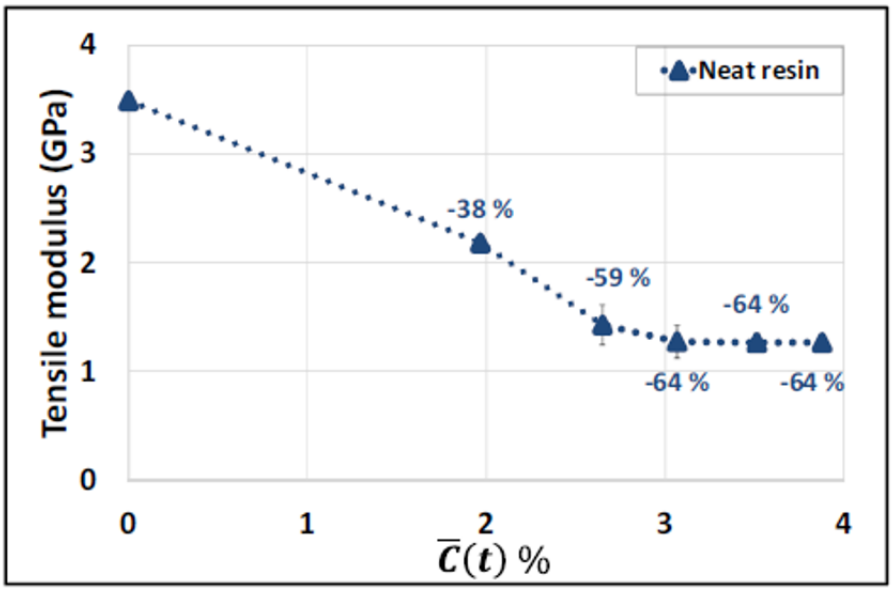

(a)

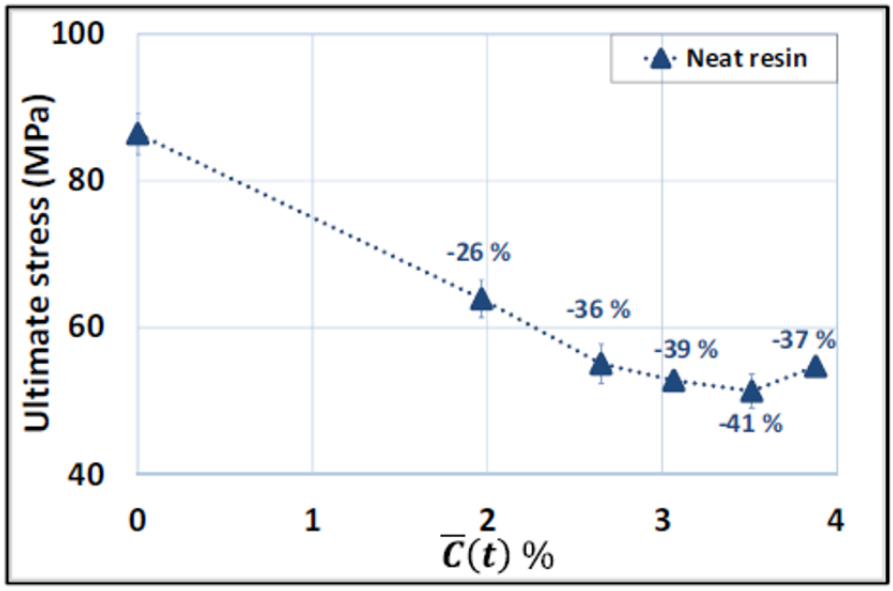

(b)

Figure 1-10 Evolution of (a) the average tensile modulus as a function of global water content; (b) the ultimate tensile stress as a function of global water content in PA6 resin [39]

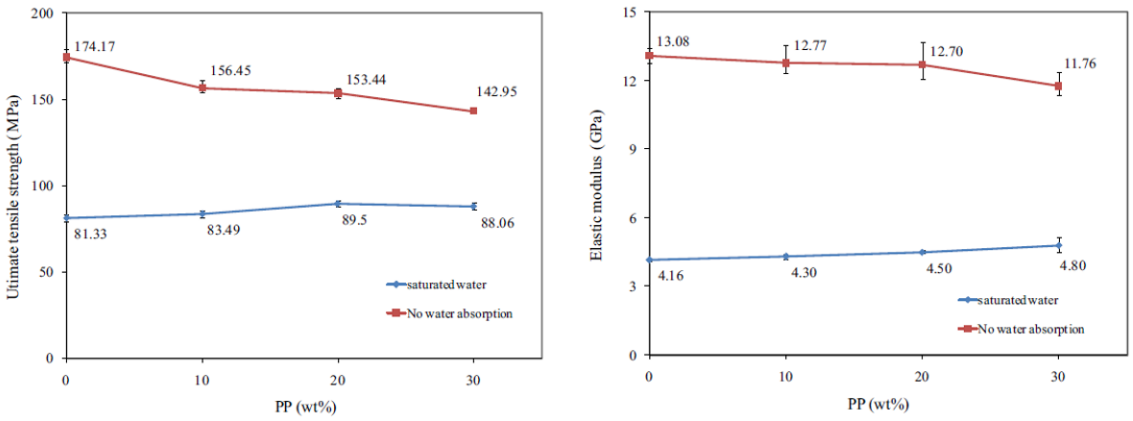

Figure 1-11. Ultimate tensile strength and elastic modulus according to wt% of polypropylene in the composites [48]

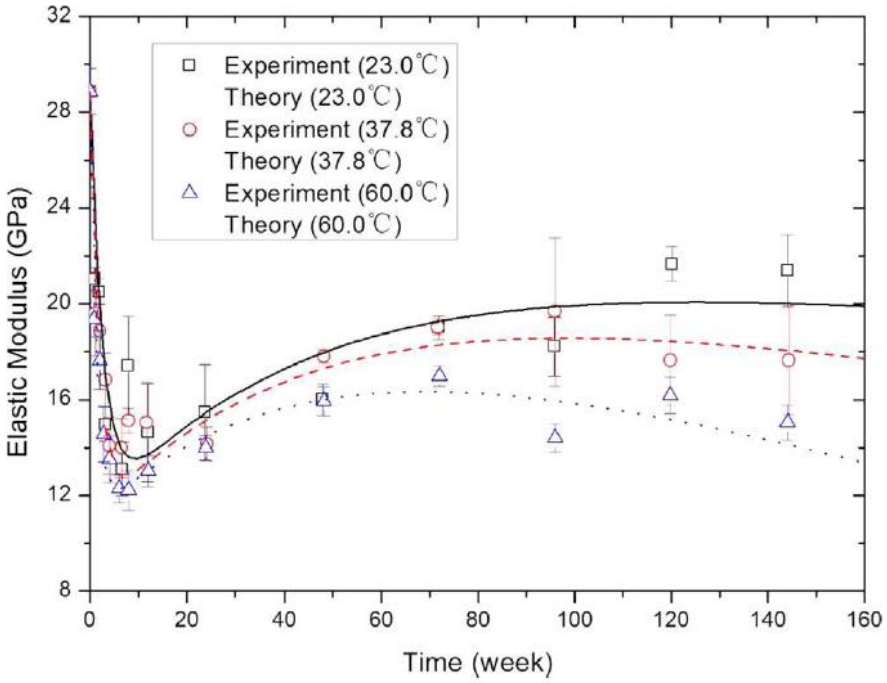

Figure 1-12 Elastic modulus of fiber reinforced composite at different temperature [49]

Polymers used as the matrix material in composites are usually sensitive to temperature changes. The crystallinity and amorphous structure of polymer change with the change of temperature, which affect sits mechanical properties, So, the performance of polymer based

composite materials will be detectably affected when the using temperature changes sharply. As the results reported by F. Tian et al [49], when the ambient temperature changed within the suitable application temperature of the chosen polymer-based composite, the higher the temperature is, the relatively lower the elastic properties are. The relative results are shown in Figure 1-12.

Meanwhile, because both moisture and temperature have negative effects on the properties of materials, and in practical use, these two environmental conditions often appear at the same time, the synergistic effects of moisture and temperature also reduce the performance of the composite, especially after long-term aging in the chosen environment. Therefore, it is critical to study the long-term performance of composite material exposed to the target environment before applied to practical use [50-57].

I. Ksouri et al. [58] reported the morphological, physicochemical and mechanical characterization of fibers reinforced PA6 material after long-term aging in fresh water at 90 °C for 80 days. Surface morphology showed in Figure 1-13 presented damages on the material surface after long-term aging, which was due to thermal effect and water absorption. The mechanical properties presented in Figure 1-14 showed that long-term aging led to the decrease, but the decline kept stable when the aging time was extended, suggesting that short-term aging had obvious effect on the performance of material.

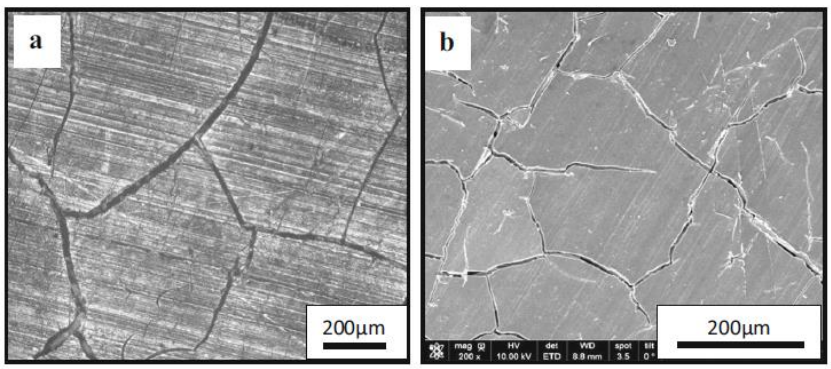

Figure 1-13 Surface damages of pure PA6 and studied fiber reinforced PA6 aged in fresh water at 90 °C for 80 days [58]

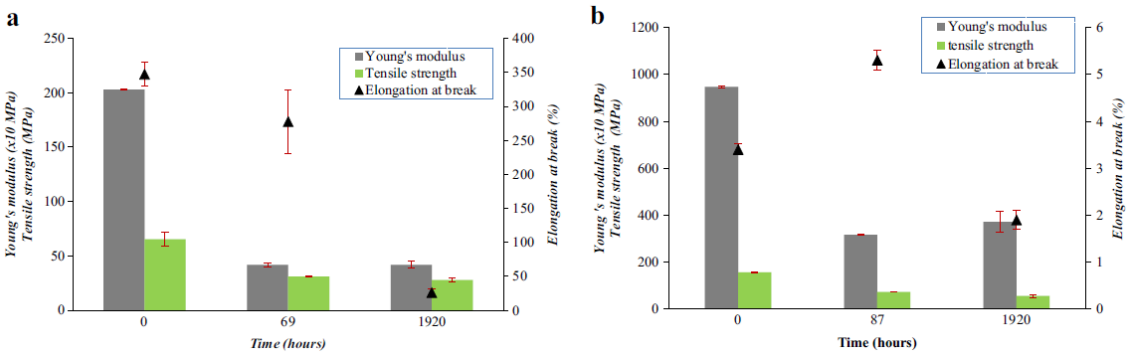

Figure 1-14 Mechanical properties of (a) PA6 and (b) reinforced PA6 after immersion in distilled water at 90 °C at different times [58]

Infrared spectra results explained the degradation mechanism of PA6 resin in detail, which is presented in Figure 1-15. After long-term aging, typical peaks in carbonyl area gave the evidence of polymer chain scission.

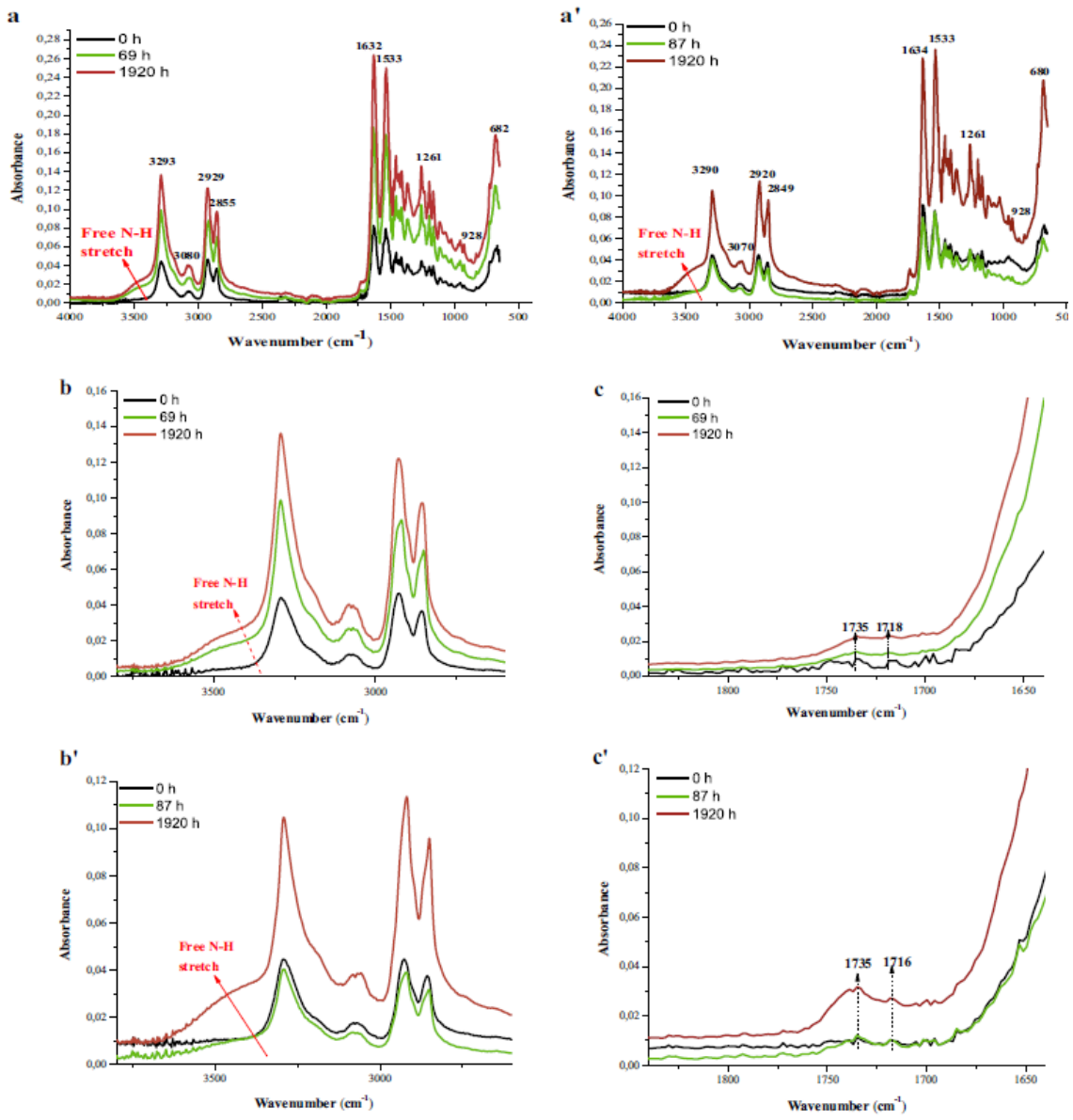

Figure 1-15 Infrared spectra submerged in fresh water for different aging time: (a) PA6; (a') PA6 composite, (b, b') from 2600 to 3800 cm^{-1} and (c, c') in the carbonyl area[58]

R. Li et al. [59] investigated the behavior of PA 6 composites after long-term hydrothermal aging. They pointed that the addition of reinforcement phase in PA6 resin would accelerate the degradation process of resin. Aged specimens indicated an obvious interfacial debonding phenomenon, which leed to the final failure of specimens and brought a serious deterioration on the mechanical properties. I. Ksouri et al.[60] also suggested a yellowing phenomenon of

color change and crazing formation after hydrothermal aging. The scission of the molecular chains was mainly responsible for the fall of tensile properties. And the fracture topography of specimens also changed with aging temperatures. B. Yang et al. [61] indicated that moisture had less effect on the mechanical property of poly cyclic butylene terephthalate (pCBT) composites at lower temperature but the influence at high temperature was obvious. Mechanical properties results shown in Figure 1-16 presented the synergistic effect of moisture and high temperature on the decline of mechanical properties of composite. Aged materials mainly showed a brittle failure while unaged materials had plastic yielding feature obviously, which also suggested the plasticization of water molecules.

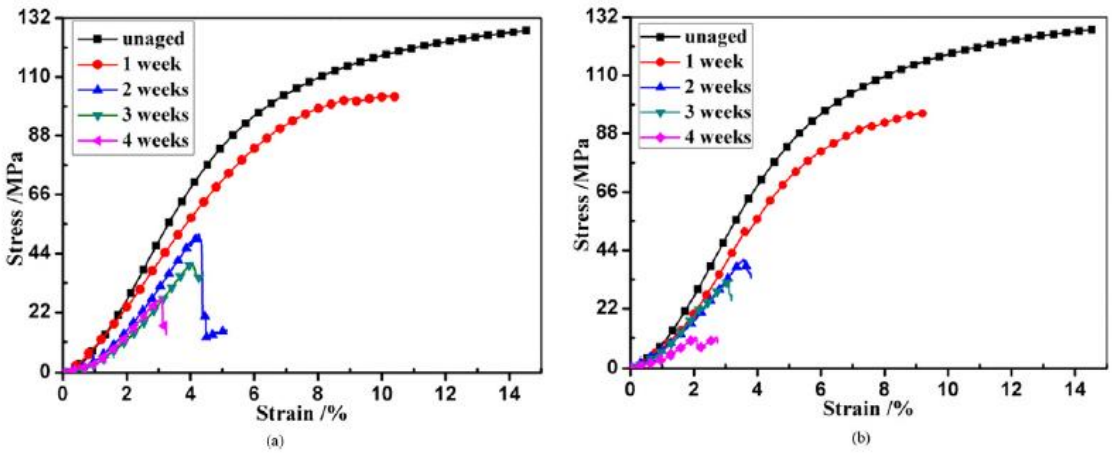

Figure 1-16 Stress-strain curves of pCBT composites after exposed in various conditions: (a) relative humidity 60%, 90 °C, and (b) relative humidity 90%, 90 °C [61]

1.4.3 Sea water

At present, with the pace of economic globalization, the marine industry is becoming a new economic growth point of coastal countries and regions. Products that can adapt to the marine environment are becoming a requirement. The influence of sea water certainly affects the comprehensive application performance and service life of products. M. Arhant et al. [62]

studied the effects of sea water on carbon-polyamide 6 laminates. The immersion of sea water definitely decreased the mechanical performance of studied material but the difference between sea water and humidity was not obvious. P. Davies et al. [63] suggested that the effects of sea water were small on the carbon fiber reinforced acrylic matrix composite, and the drop could be fully recoverable after drying, as Figure 1-17 shows.

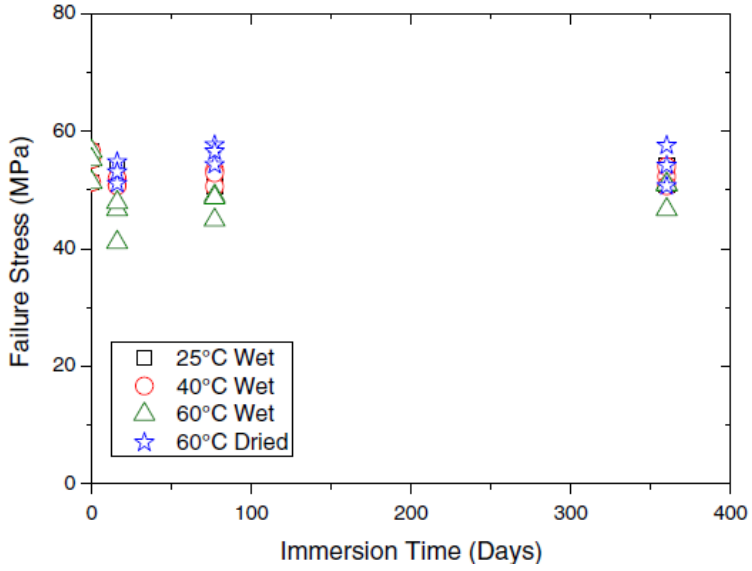

Figure 1-17 Tensile failure stress of carbon fiber reinforced acrylic matrix composite after aging in sea water to different times at 3 temperatures, all samples saturated with water from 77 days on [63]

The influence of different aquatic environments, including distilled water, river water and sea water, on the mechanical properties of polycaprolactone (PCL) was reported by B. Lu et al. [64] Relative results are shown in Figure 1-18. Mechanical properties of studied material underwent sharp decrease when the aquatic body was sterilized. The difference between fresh water and sea water with the same sterilized conditions were not detectable. They showed similar trend of changing with the extension of experiment time.

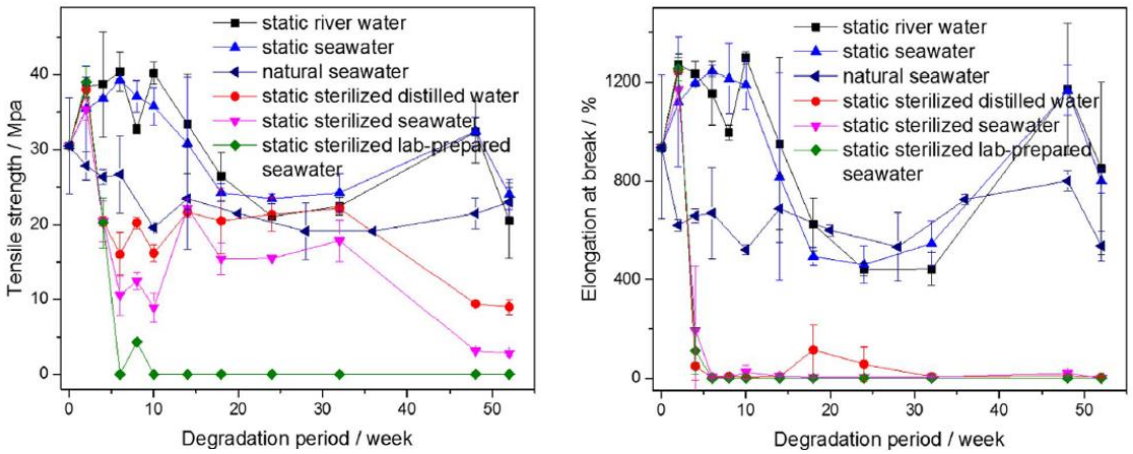

Figure 1-18. Changes in the tensile strength and ultimate elongation of PCL samples in different water bodies with degradation period [64]

P. Davies [65] also focused on the environmental degradation of composites for marine structures. As his results show, which is presented in Figure 1-19, tensile properties of acrylic matrix resin were sensitive to sea water contents. More water absorption leads to a detectable reduction in tensile modulus.

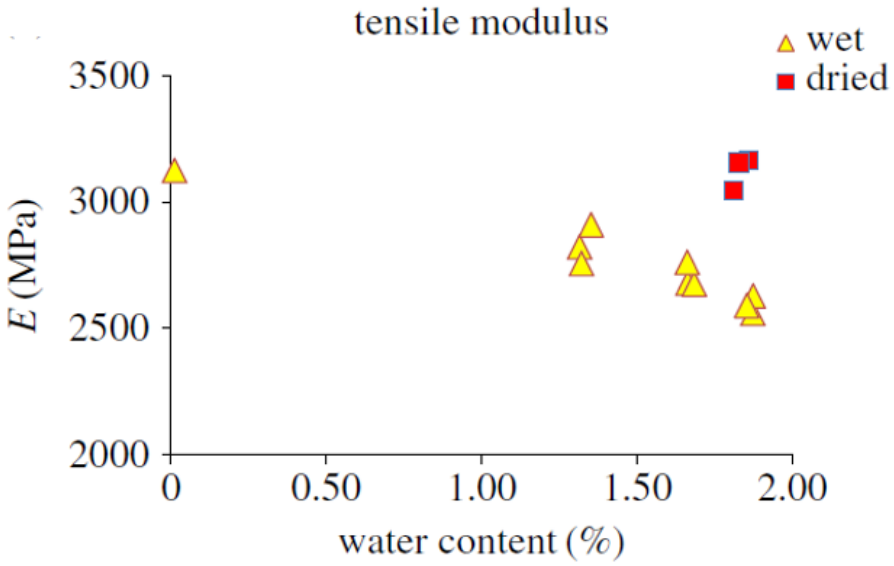

Figure 1-19 Tensile strength of aged acrylic matrix resin in the wet and dry state [65]

1.4.4 Thermo-oxidation

Thermo-oxidative aging, which is a synergistic effect of heat and oxygen, is one of main reason of degradation of composite materials. High temperature accelerates the process of polymer oxidation, and the oxygen leads to the main chain scission of polymer, which results in the severe decline of mechanical properties. As L. Sang et al.[66] reported, the average tensile strength of studied material increased at the initial stage and then decreased in the high temperature exposure process. Compared to a pure resin, the studied material showed higher retention ratio of tensile properties, which may indicate a weaker degradation of resin after thermo-oxidative aging, as Figure 1-20 shows. Surface morphology shown in Figure 1-21 exhibited better thermo-oxidative stability provided by carbon fibers during the ageing process because of the smaller cracks, and less carbon fibers exposed to the outside.

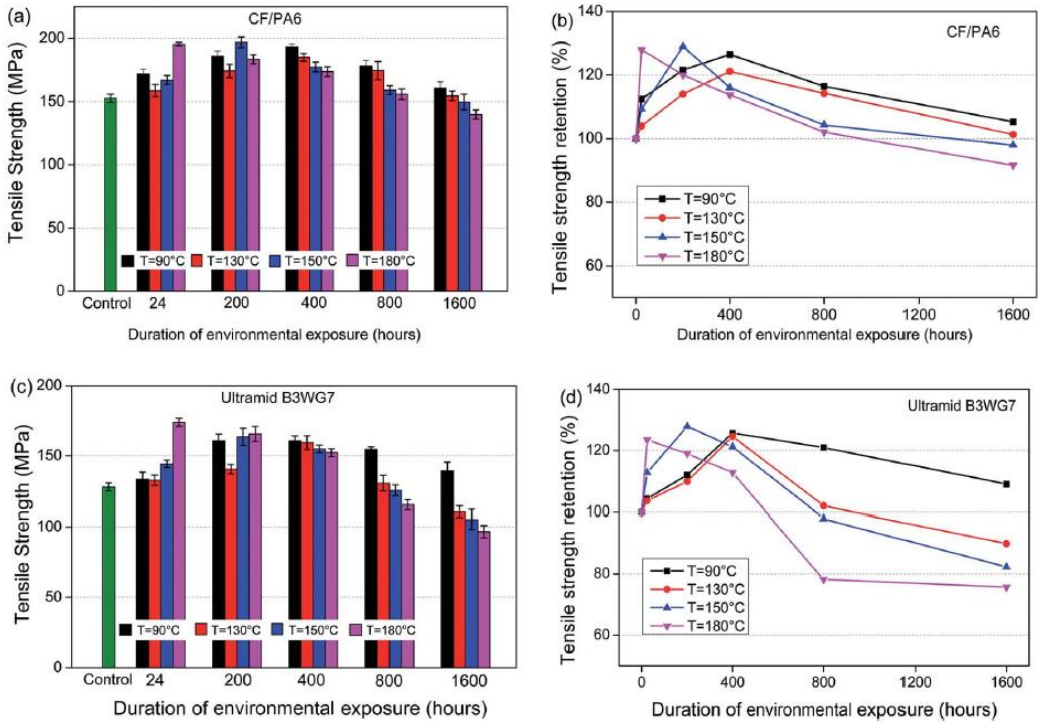

Figure 1-20 Effect of different ageing temperature on CF/PA specimen: (a) tensile strength, (b) tensile strength retention; Ultramid® B3WG7 (pure PA6) specimen: (c) tensile strength (d) tensile strength retention [66]

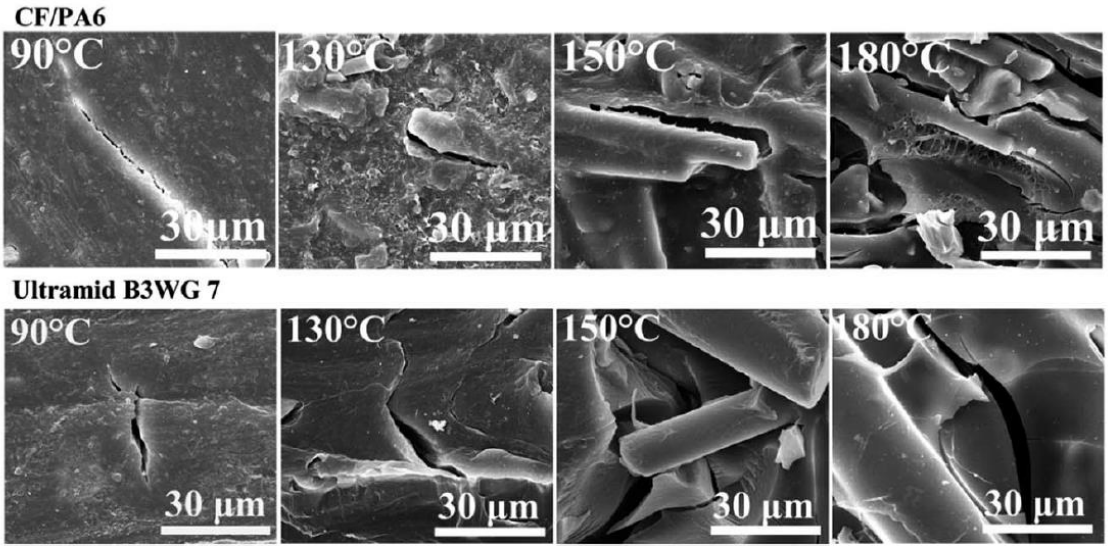

Figure 1-21 SEM micrographs of surface microstructure of CF/PA6 and Ultramid® B3WG7 specimen at varying ageing temperatures for 1600 hours [66]

Since the mechanical performance of composite materials is closely related to the properties of resin matrix, the stability of the resin under thermo-oxidative environment is also an important topic. W. Dong et al. [67] investigated the influence of temperature on the thermo-oxidative degradation of PA6 resin. As the results shown in Figure 1-22 and 1-23, the increase of carbonyl at high temperature proves the decomposition of PA6. Meanwhile, elongation at break in tensile test also proved the serious degradation of PA6 resin when the temperature was above 140 °C. Carbonyl index and oxygen uptake relies closely on the aging temperature, which provided a method to predict the performance of PA6-based composites under high temperature exposure.

Other researcher also reported the performance of PA6-based composite under the thermo-oxidative environment [68-75]. PA6 shows weak thermo-oxidative resistance to some extent. However, the addition of inorganic refractory can enhance the thermo-oxidative resistance of the material. Therefore, CFRTP material may also show thermo-oxidative resistance because

of the flame retardancy of carbon fibers.

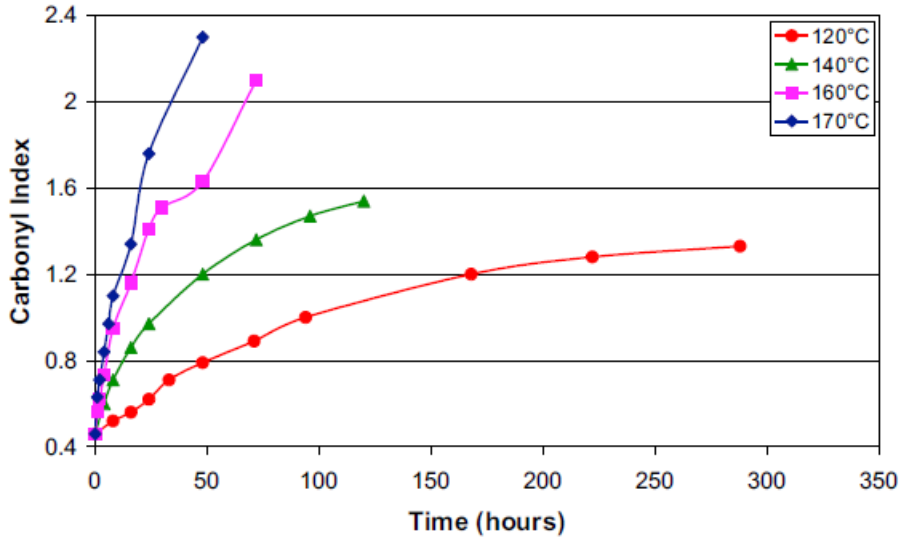

Figure 1-22 Carbonyl index as a function of time of PA6 degraded at 120, 140, 160 and 170 °C [67]

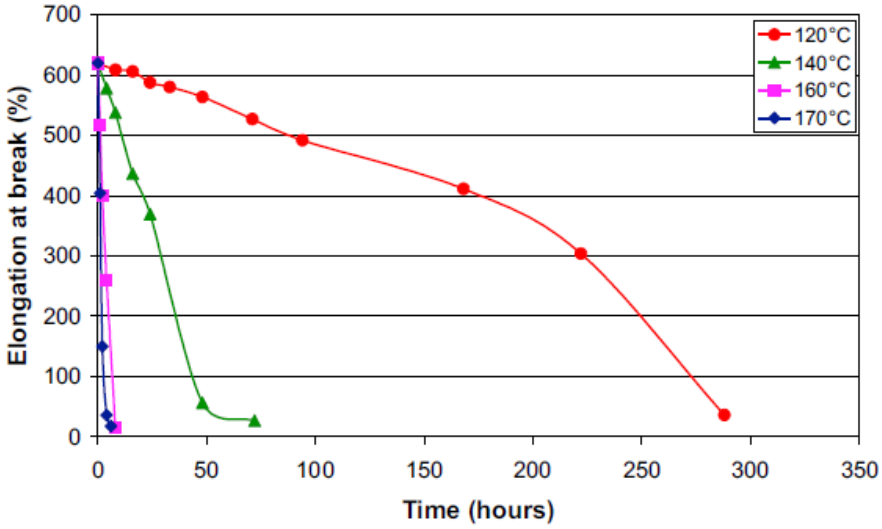

Figure 1-23 Elongation at break (%) as a function of time of PA6 degraded at 120, 140, 160 and 170 °C [67]

1.5 Objective and outline

As mentioned in section 1.4, environmental factors, like moisture, sea water, temperature, hydrothermal environment and thermo-oxidation are inevitable in the actual use of products. These factors may bring fatal effects on the performance of polymer or resin-based composites. Therefore, when evaluating the practicability and usability of rCF reinforced plastics composites, it is essential to clarify the influence of the environmental factors.

The material chosen in this study is carbon fiber paper reinforced thermoplastics (CPT). Because CPT is a kind of new material, researches on CPT are limited. The study on the effects of the environmental factors on CPT is of vital importance. The structure of this doctoral thesis is shown in Figure 1-24.

In chapter 1, the general introduction of carbon fiber and CFRP were given. Then, the existing problems on CFRP waste were described and recycling technologies of carbon fibers were introduced. Problems on reuse of rCF were also mentioned and the importance of studying short fibers reinforced plastics was also elucidated. Besides, influence of environment factors on composite materials were introduced by literature reviews. And finally, the outline of this thesis was given in this part.

In chapter 2, first, the water absorption behavior of carbon fiber paper reinforced thermoplastics (CPT) in fresh water and sea water was investigated. The flexural properties of these CPT specimens were studied by three-point bending test. The micromorphology of CPT after three-point bending test was observed by scanning electron microscope. Moreover, the interfacial shear strength between carbon fiber and resin before and after water absorption were tested by droplet test. In addition, the cyclic absorption-desorption behavior of CPT in fresh water and sea water was also studied. The effects of absorption-desorption on the performance of CPT were analyzed by three-point bending test.

In chapter 3, the performance of CPT after long-term aging in hydrothermal environment was studied. Long-term aging test in fresh and sea water at high temperature was conducted. Barcol hardness test, differential scanning calorimetry test, Fourier-transform infrared spectrum test were conducted to clarify the influence on the physical and chemical properties of CPT. The micromorphology of the aged CPT was observed by microscope and 3D laser scanning microscope. The mechanical properties of the aged CPT were investigated by three-point bending test. Then rules of mixture and factor C were employed to explain the hydrothermal effects.

In chapter 4, thermo-oxidative aging test was conducted on CPT in order to study the thermo-oxidative resistance of CPT. The weight loss on the unit area of the specimens was weighed, calculated and compared. The micromorphology of the aged CPT was observed by scanning electron microscope and 3D laser scanning microscope. Then, the mechanical properties of aged CPT were also investigated by three-point bending test. Finally, an explanation of the thermo-oxidative resistance of CPT was put forward.

Chapter 5 gives conclusions of this research and makes an outlook for future's work.

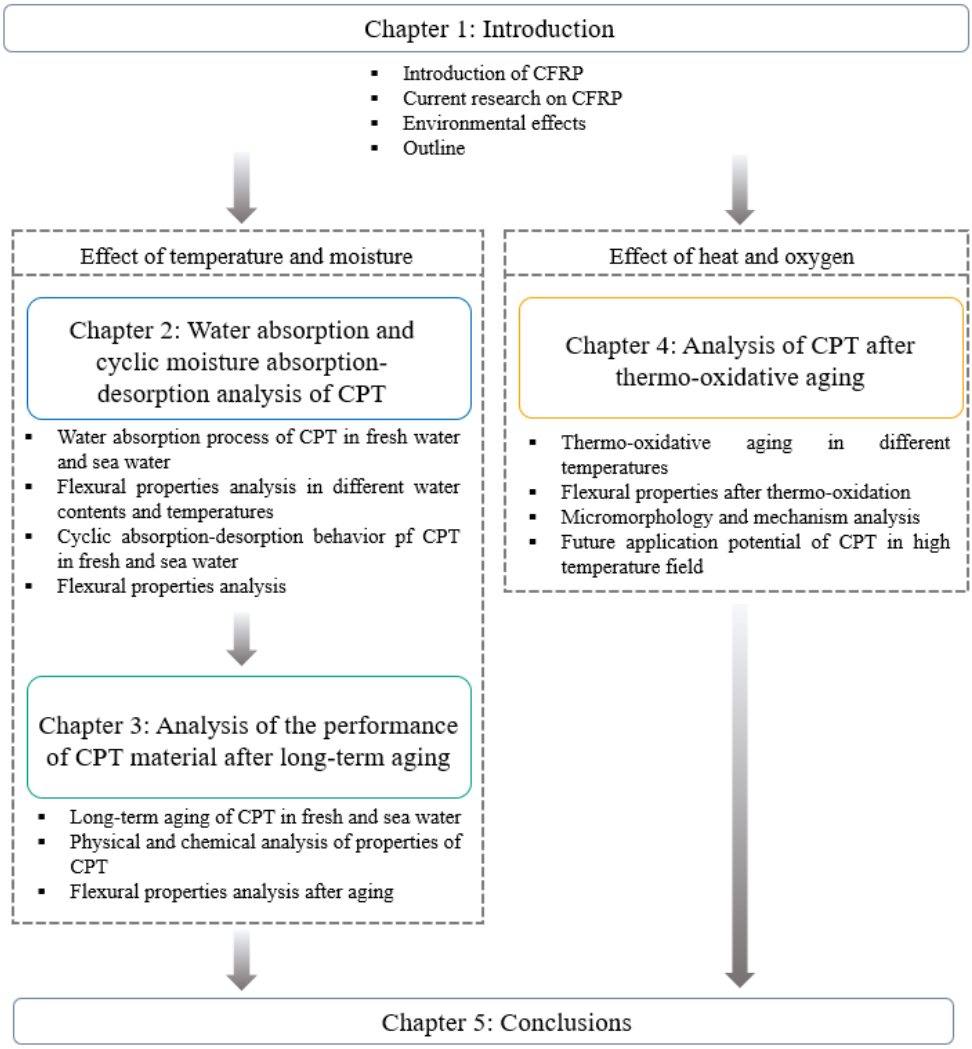

Figure 1-24 The structure of this doctoral thesis

1.6 Materials

1.6.1 Carbon fiber paper reinforced thermoplastics (CPT)

CPT refers to CFRTP which is produced by a new original paper making methods. In this research, CARMIX® (manufactured by Awa Paper Mfg. Co., Ltd) was used. As shown in Figure 1-25, monofilament carbon fibers and resin fibers cut into 6 mm were mixed simultaneously in water. After water was drained, fibers remaining on mesh were dried,

pressed and made into CPT sheet. The volume fraction (V_f) of carbon fiber was about 20%. Since CPT shows uniform dispersion of fibers, it has an in-plane isotropy, and its mechanical properties are stable.

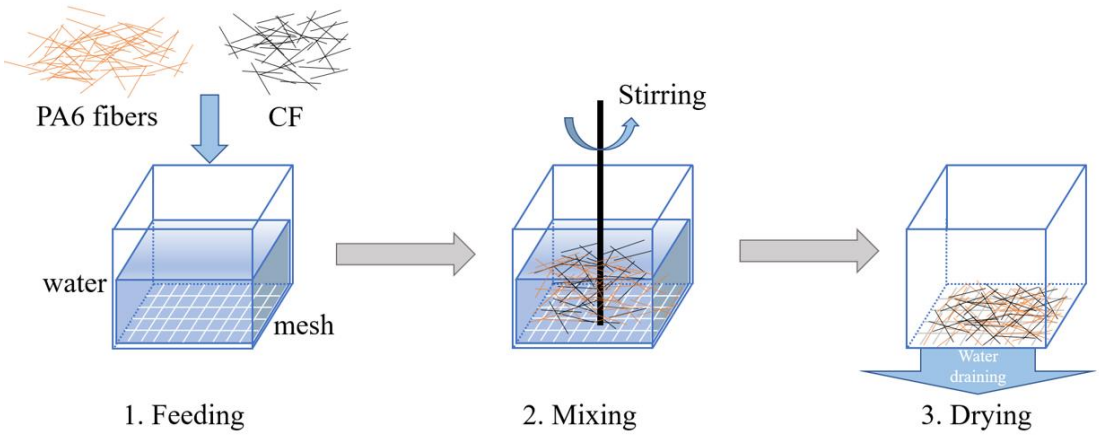

Figure 1-25 Molding process of CPT sheet

In this study, CPT sheets were cut into 250 mm × 120 mm and dried in vacuum oven at 90 ℃ for 24 hours. CPT specimens were made by compression molding. The molding program is shown in Figure 1-26, an automatic press machine (manufactured by Pinette Emidecau Industries, with a maximum output of 30 tons was employed. A two-step molding was used. In the preheating stage, the temperature was set at 260 ℃, and the molding time was 15 minutes. The pressure was kept as 1 MPa. Then, the pressure was removed for 3 seconds to avoid bubbles within the plate. After that, the pressure was added to 5 MPa and maintained until the end of molding process. After pressed for 10min at 5 MPa, the molded plate was cooled to 50 ℃ and taken out from the mold.

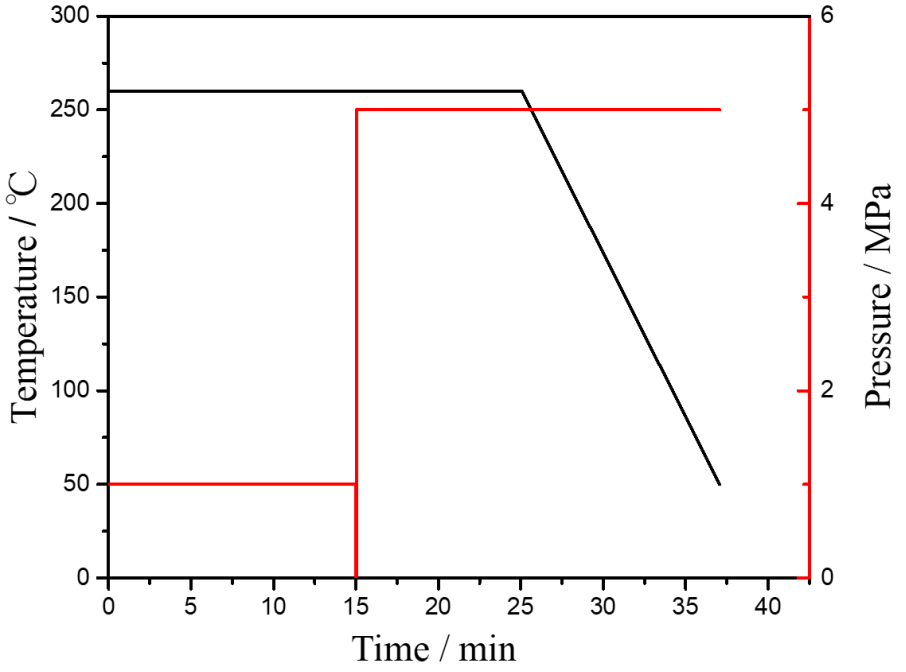

Figure 1-26 Molding program of CPT specimens

1.6.2 Polyamide 6 specimens

Polyamide 6 (PA6) specimens used in this study were manufactured by PA6 film (DIAMIRON®C, manufactured by Mitsubishi Chemical Co., Ltd) using a simple injection molding machine as shown in Figure 1-27. The PA6 film was cut into a size of about 3 mm × 3 mm so that it could be put into the cylinder of 1 cm diameter in the injection molding machine. PA6 film was dried for 72 hours in a vacuum dryer held at 90 ℃. The chamber temperature of the injection molding machine was set at 260 ℃. The melting time was 2 minutes and the mold temperature was set at 90 ℃. The specimen size was 135 mm × 15 mm × 3 mm.

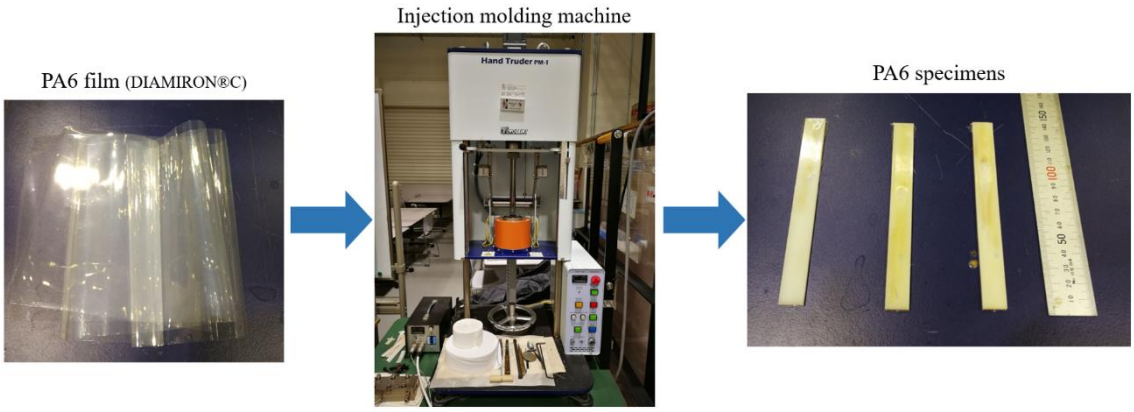

Figure 1-27 Molding process of PA6 specimens

Chapter 2. Water absorption and cyclic moisture absorption-desorption analysis of CPT

2.1 Introduction

Among these different environmental factors, moisture may cause degradation of the polymer matrix and weakens the mechanical properties of products during their service life [76]. Because carbon fibers absorb little or no water compared to PA6, the absorption is largely PA6 dominated [39, 77]. At present, with the pace of economic globalization, the marine industry is becoming a new economic growth point of coastal countries and regions. Products that can adapt to the marine environment are becoming a requirement. The marine environment certainly affects the comprehensive application performance and service life of products. Sea water is the predominant hazard, where not only the influence of water, but also the effects of inorganic salts should be considered [78]. So, if it is shown that the effect of salt water is small, it becomes bright information for the application of CFRTP such as amphibious vehicle, drone and water competition in the future.

2.2 Materials and experiments

2.2.1 Materials

CPT specimens used in this study were made by the molding methods mentioned in 1.6.1. The thickness of the molded plates was controlled in 3 mm. The molded plates were cut into specimens with dimensions of 120 mm×20 mm×3mm using a diamond disc cutter.

2.2.2 Experiments

2.2.2.1 Water absorption test

The water absorption test was conducted in sea water with 3.4% mass fraction of salt and in fresh water, to analyze the water absorption properties of CPT composite specimens. Before immersion in water, all specimens were dried in a vacuum oven at 90 ℃ until their mass changes were less than 0.01%. Then, these specimens were immersed in water at 70 ℃, which is above the glass transition temperature of PA6, in order to accelerate the water absorption process. Dry PA6 specimens were used as a control.

The weight of the specimen s during the water absorption process was monitored. The weight gain ratio at any time *t* W_t (%) was calculated by the following equation:

$$W_t = \frac{m_t - m_0}{m_0} \times 100\% \qquad \text{Equation 2-1}$$

where m_0 is the initial specimen mass (prior to immersion in sea water) and m_t is the mass at any time *t* during the water absorption process. When calculating the weight uptake in sea water, it was assumed the solution was a homogeneous mixture of dissociated water molecules and aqueous salt ions.

According to Fick's diffusion law, the moisture distribution is solved subject to the initial and boundary conditions shown as following:

$$W = W_0\,, 0 < z < h, t \leq 0 \qquad \text{Equation 2-2}$$

$$W = W_\infty\,, z = 0;\ z = h;\ \ t > 0 \qquad \text{Equation 2-3}$$

where W_0 is the initial moisture concentration, W_∞ is the maximum moisture concentration in a specimen, t is the immersion time and h is the thickness of the specimen.

The moisture concentration is solved subject to the following equation:

$$\frac{W_t - W_0}{W_\infty - W_0} = 1 - \frac{4}{\pi}\sum_{n=1}^{\infty}\left(\frac{1}{2n+1} sin\frac{(2n+1)\pi z}{h} \times exp\left[-\frac{(2n+1)^2\pi^2 Dt}{h^2}\right]\right) \qquad \text{Equation 2-4}$$

D is the diffusion coefficient of water in the specimen, which can be used to evaluate the diffusivity of water.

The diffusion coefficient D is a constant at the initial stage of water absorption. So, D can be calculated by using the results at time t_1 and t_2 as the following equation:

$$D = \frac{\pi}{16}\left(\frac{W_1 - W_2}{W_\infty}\right)^2\left(\frac{h}{\sqrt{t_1} - \sqrt{t_2}}\right)^2 \qquad \text{Equation 2-5}$$

This leads to

$$D = \frac{\pi h^2}{16}\left(\frac{k}{W_\infty}\right)^2 \qquad \text{Equation 2-6}$$

where k is the initial slope of the plot of weight gain versus square root of time. According to Fick's diffusion law, Equation 2-6 can be employed to calculate D until the water absorption is at least 60% of the maximum state [79-85].

2.2.2.2 Cyclic water absorption-desorption test

Since the environment is not changeless, moisture may change from humid to dry and temperature also varies with the weather or season. So, the properties of the material after the treatment of dry and wet changes should be considered [86]. The cyclic water absorption-desorption test was employed to study this effect on CPT material. The process is shown in Figure 2-1.

The whole process includes three cycles. Each gray box represents one cycle. In the 1st cycle, dry specimens were immersed in fresh and sea water in 70 ℃, respectively, until the saturated state. Then, some of the specimens were taken out and named F-1S and S-1S, which means “saturated once in fresh water” and “saturated once in sea water”, respectively. Then, the rest of the specimens were put into vacuum oven until the weight change was below 0.01%. Some of the re-dried specimens were taken out and named “F-1C” and “S-1C”, which means “completed one cycle in fresh water” and “finished one cycle in sea water”, respectively. Then, the rest of specimens were taken into the 2nd and 3rd cycle. Similarly, specimens named as F-2S, S-2S F-2C and S-2C, can be obtained in the 2nd cycle and specimens named as F-3S, S-3S, F-3C and S-3C can be obtained in the 3rd cycle.

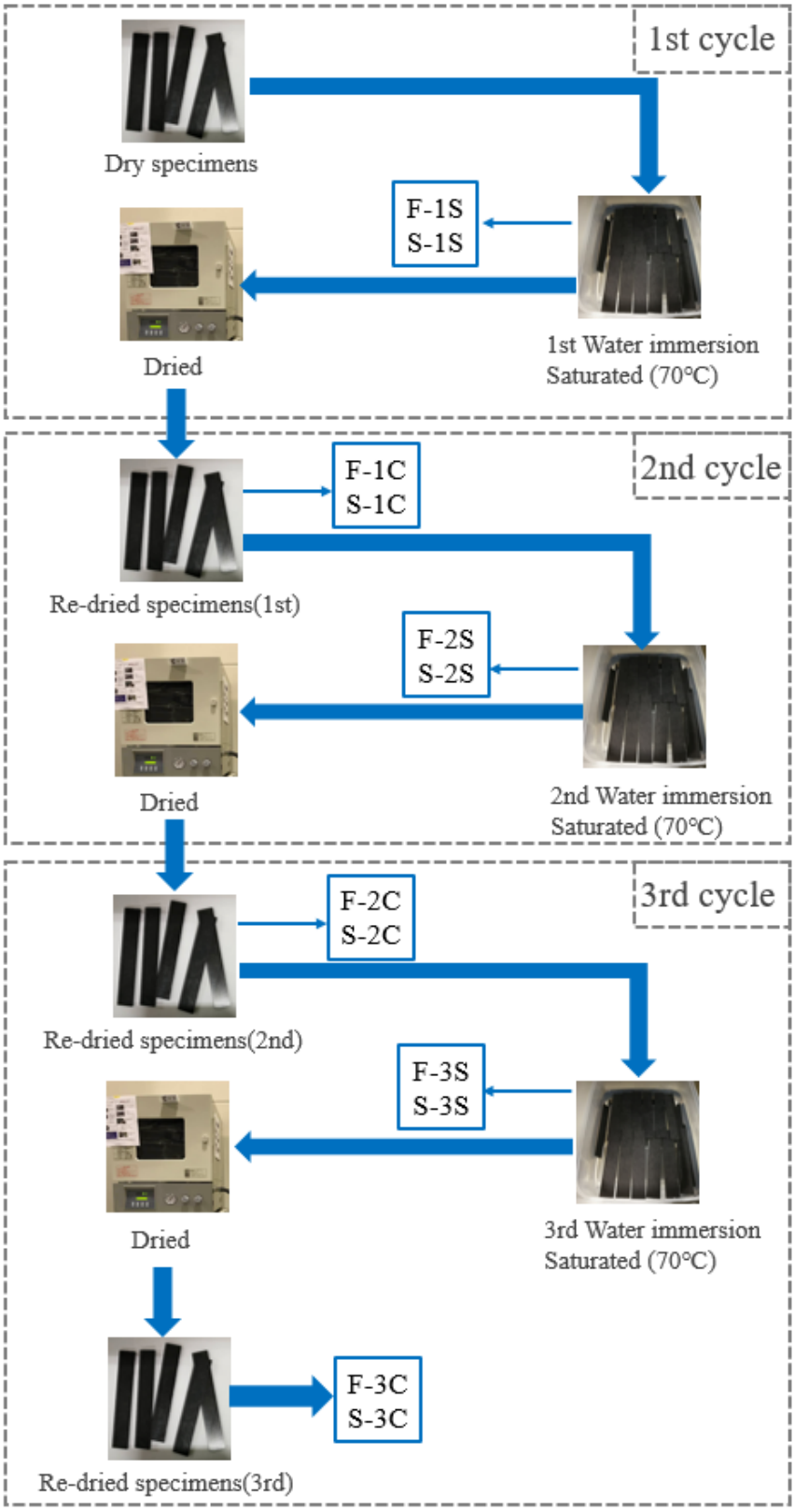

Figure 2-1 Process of cyclic water absorption-desorption test

2.2.2.3 Barcol hardness test

The Barcol hardness of the specimens was tested by Barcol hardness impressor (GYZJ934-I, Barber–Colman Co.) according to the standard JIS K 7051. Ten valid values were taken in each group. In practical use, “HBI-A” should be added before the measured hardness value.

2.2.2.4 Three-point bending test

The three-point bending test was conducted to determine the flexural properties of the CPT composite under different temperatures and moisture conditions. A universal testing machine (AUTOGRAPH AGXplus, Shimadzu Co.) was used. The span of the supporters (L) was determined by the thickness of specimens. The ratio of the span to the thickness was 16:1, as shown in Figure 2-2. The bending load point radius was 5mm. A thermostatic chamber was used to control the ambient temperature for the duration of the test and a thermometer was used to monitor the real-time temperature of specimens. The test was conducted at -25 ℃, 0 ℃, 25 ℃, 50 ℃, 75 ℃, and 100 ℃. Five specimens were tested under each condition. The load speed was 1 mm·min^{-1}.

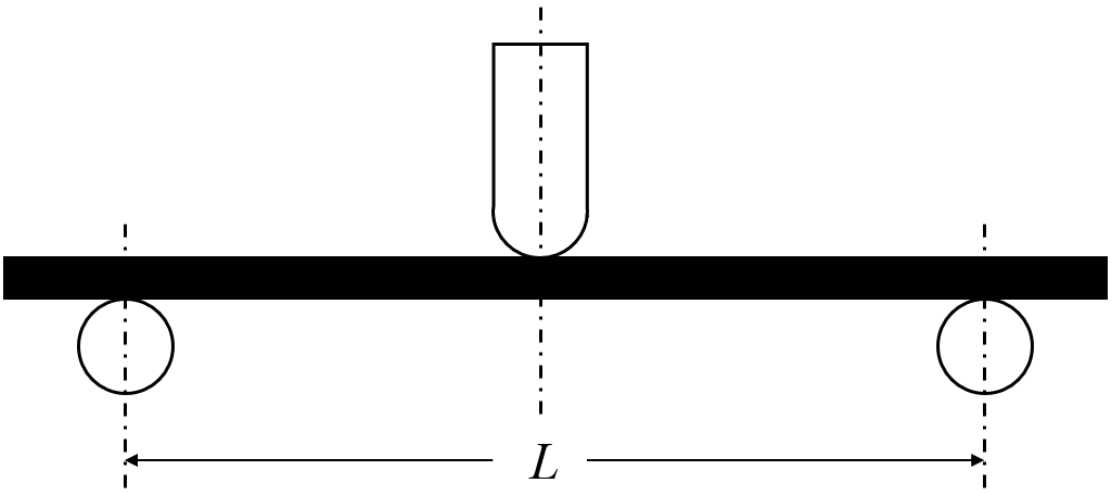

Figure 2-2 Setting of three-point bending test

The flexural stress was calculated by

$$\sigma_f = \frac{3FL}{2bh^2} \qquad \text{Equation 2-7}$$

where σ_f is the stress, F is the load, L is the span of the supporters, b is the specimen width and h is the specimen thickness.

The strain at the middle of the bottom specimen surface can be calculated by the following equation:

$$\varepsilon = \frac{600Sh}{L^2}\% \qquad \text{Equation 2-8}$$

where ε is the strain, and S is the displacement of the middle point of specimens.

2.2.2.4 Micromorphological analysis

The fracture surface of the specimens after the three-point bending test was observed by a scanning electron microscope (VE-8800, KEYENCE Co.).

2.2.2.5 Droplet test

The droplet test was conducted by an assessment device for interface properties of composite materials (HM 410, TOHEI SANGYO CO. LTD) to detect the interfacial shear strength (IFSS) between the carbon fiber and resin. Carbon fibers were purchased from Toho Tenax Co. Ltd (HTC 110, diameter d=6.9 μm), and PA6 resin was provided by Toray Industry, Inc. (strength σ_m = 85 MPa at room temperature). Carbon fibers and PA6 are the same types as these in CPT. The droplets of PA6 were immersed in fresh and sea water before the test for 24 hours, in order to simulate the state of the saturated CPT specimens. Dry PA6 was also studied as a control. Figure 2-3 shows the experimental arrangement of droplet test. Carbon fibers

encapsulated by PA6 droplets were prepared. The micro vise jaws were fixed. Carbon fiber was set on a load cell and pulled with a rate of 0.12 mm·min^{-1}. The center of the carbon fiber was positioned at the center of the gap between the micro vise jaws. We tried several embedded lengths, controlled between 50 and 80 μm so that the amount of resin is enough for droplets to form a sphere; while medium sized droplets can also guarantee that fibers do not break during the experiment. The droplet specimens were prepared at 210 ℃. First, the specimens were cooled to 180 ℃, then the cooling rate was controlled as 10 ℃ min^{-1} until 60 ℃, then the specimens were air-quenched to 25 ℃.

Figure 2-4 shows the cooling curve of CPT in differential scanning calorimetry (DSC) test, the sharp peak around 190 ℃ is the thermal crystallization peak of PA6 in CPT and 180 ℃ is the end crystallization temperature of PA6 in CPT. Therefore, this temperature was taken as the dividing point in preparing droplet specimens as mentioned above.

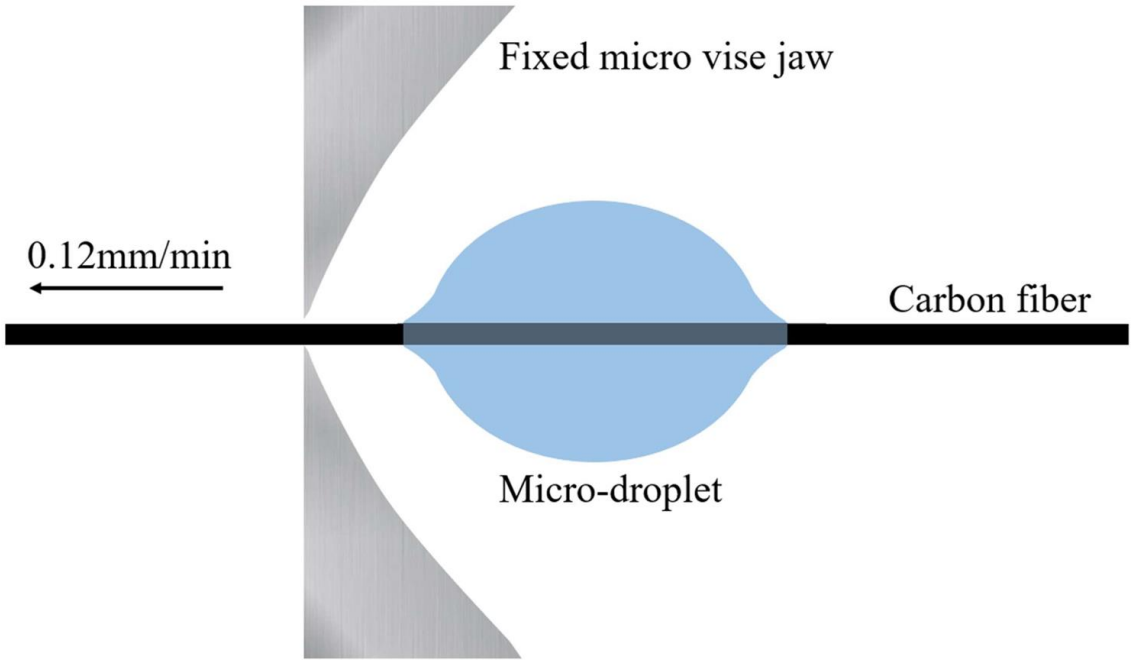

Figure 2-3 Experimental arrangement of the droplet test.

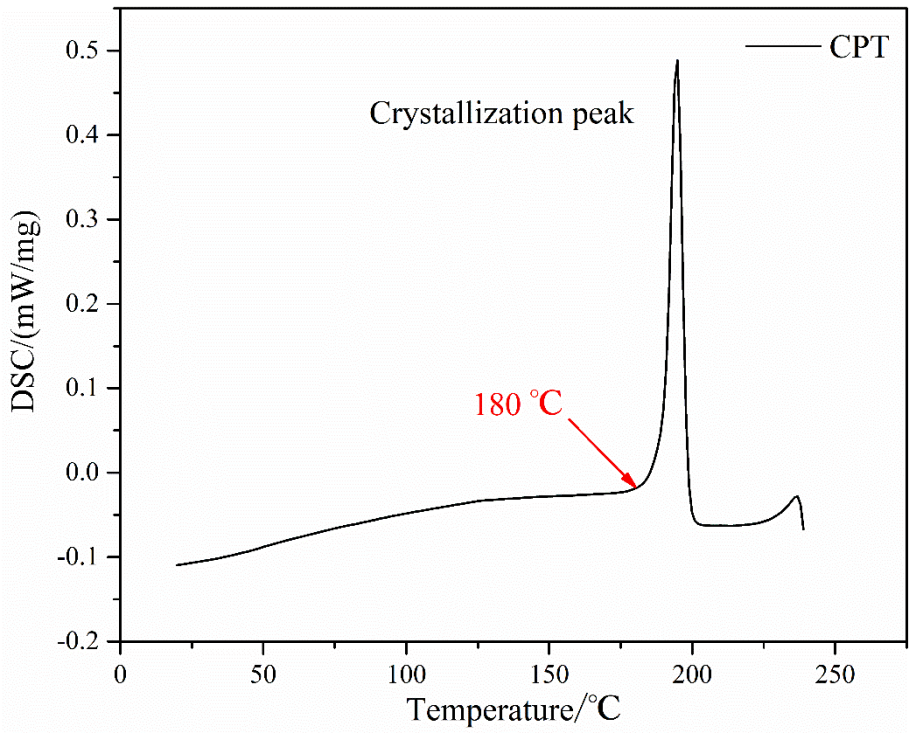

Figure 2-4 The cooling curve of CPT in differential scanning calorimetry test

The IFSS is calculated by the following equation:

$$\tau = \frac{F}{\pi d L_e} \qquad \text{Equation 2-9}$$

where τ is the IFSS, d is the diameter of the fiber, F is the maximum load and L_e is the embedded length. F and L_e can be obtained from the device [87-90]. So, the maximum load is proportional to the embedded length, and the IFSS can be calculated by the slope. In this study, 40 valid points were used for further analysis. Besides, two other methods can also be employed to the calculate the IFSS. First is the arithmetic mean of the IFSS of the 40 valid points obtained. Second one is shown in Equation 2-10, which is an empirical method. σ_m is the strength of resin.

$$\tau = \frac{\sigma_m}{\sqrt{3}} \qquad \text{Equation 2-10}$$

2.3 Results and discussions

2.3.1 Short-term water absorption

2.3.1.1 Water absorption test

The results of water absorption of the CPT material are shown in Figure 2-5, and the results calculated by using Fick's diffusion model are shown in Figure 2-6. The water absorption properties are shown in Table 2-1. Carbon fibers are considered non-absorbent, so any water absorption of the CPT material comes from PA6 [19]. As we can see, the diffusion behavior of pure PA6 and CPT is consistent with Fick's diffusion model. Whether the water environment is fresh or sea water, the diffusion coefficient D of CPT is lower than that of pure PA6 because of the lower resin content. The incorporation of carbon fiber increases the path length of the water molecules that have permeated into the composites, which slows down the water penetration process. The calculated weight gain of CPT (W_c) was calculated by the maximum weight gain of pure PA6 times the volume fraction of PA6 resin in CPT. The calculated weight gain in fresh water is 6.48%, which is larger than the experimental value (5.96%). Because more hydrogen bonds were formed between the amide group in polymer chains and water molecules, the formation of a hydrogen bond microstructure framework inhibits further water absorption by the matrix. Similar results can also be found in sea water, the calculated weight gain is 6.28%, which is larger than the experimental value (5.70%). Furthermore, it can be seen that the CPT material absorbed more fresh water than sea water. This may be caused by the dissociation of the amide bond in polymers. The attraction between the polymer chain with terminal ions and the inorganic salt ions in the sea water may hinder further infiltration of water molecules.

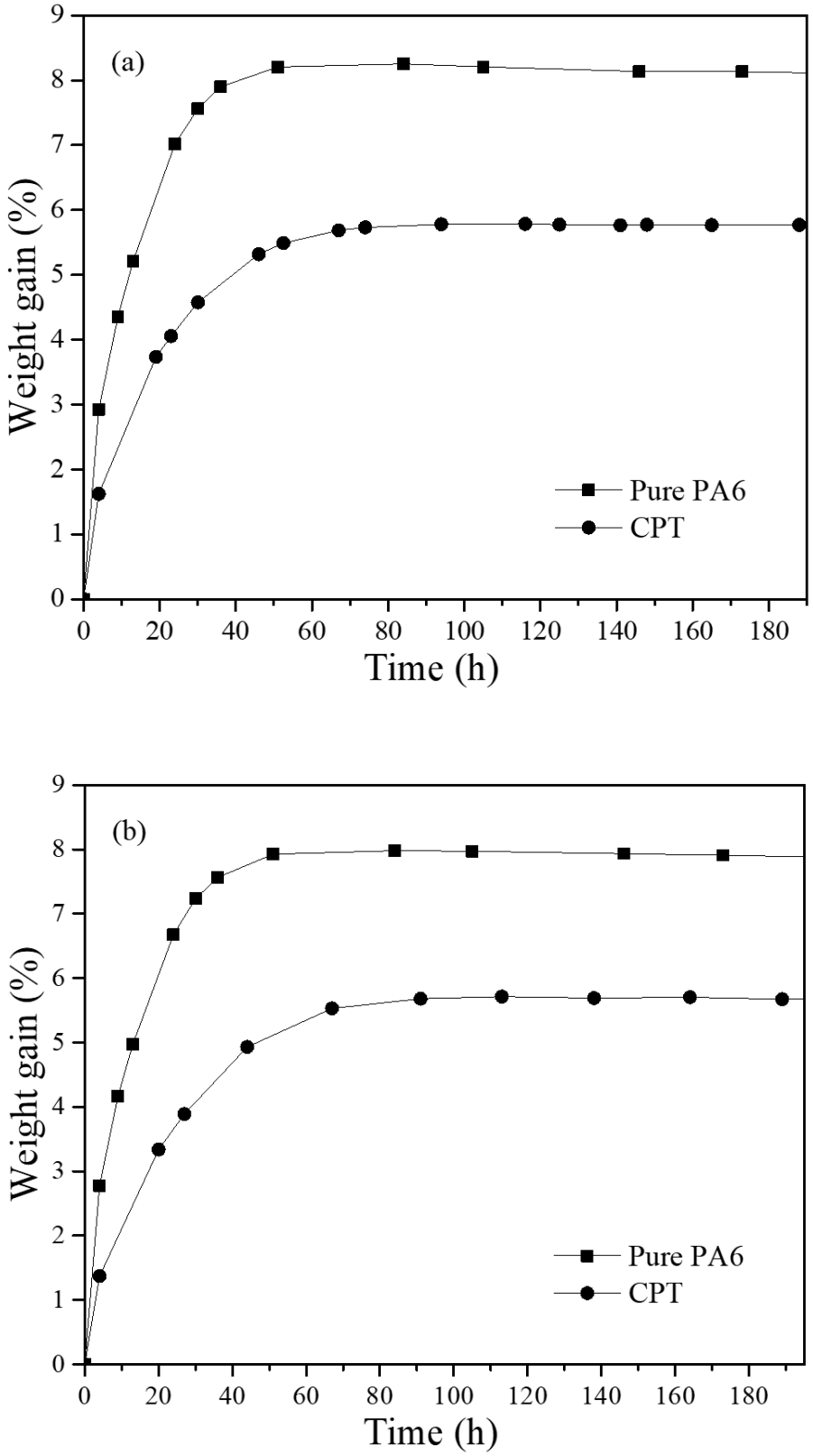

Figure 2-5 Weight gain of CPT material (a) in fresh water; (b) in sea water

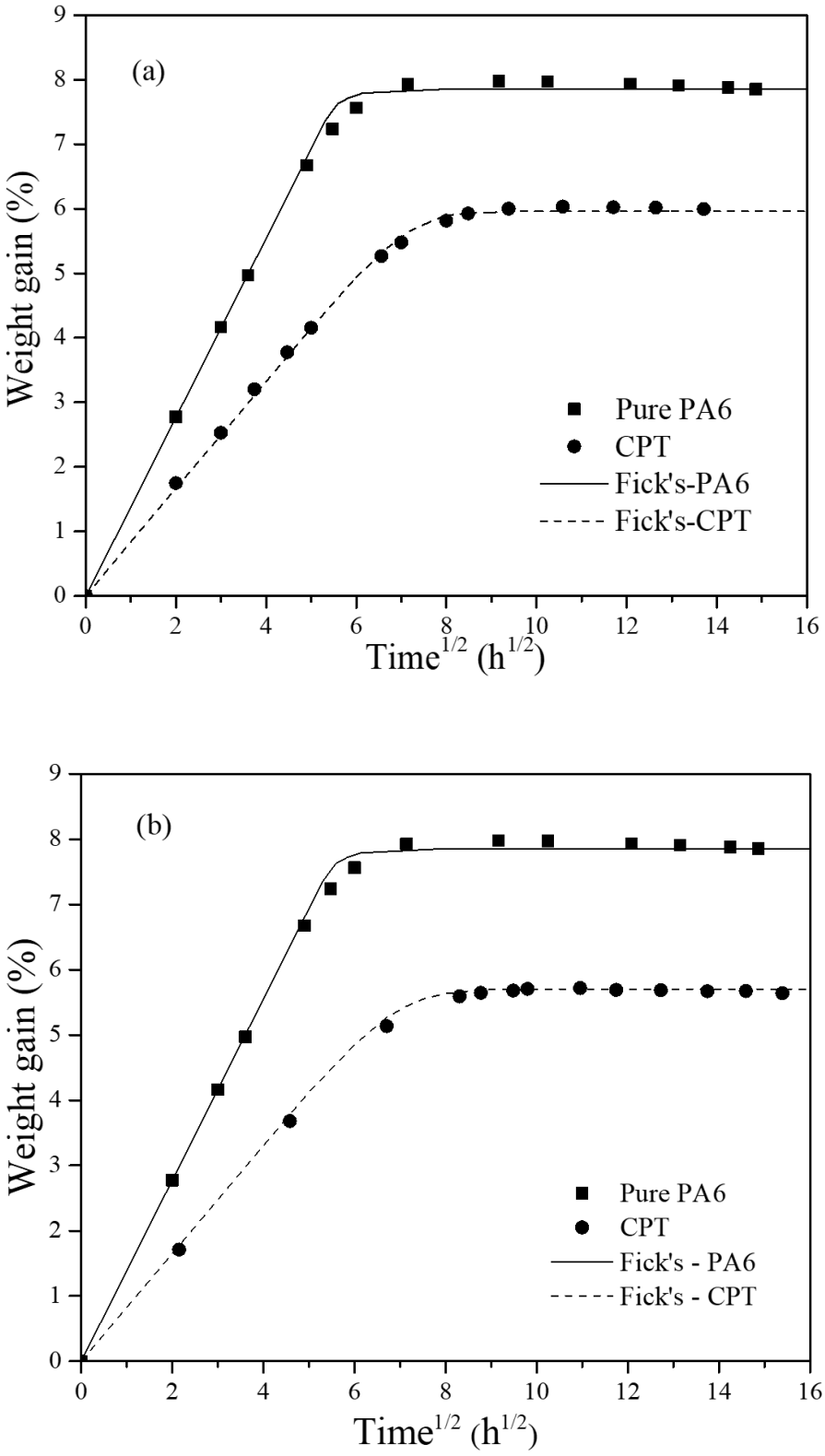

Figure 2-6 Weight gain of CPT material with Fick's diffusion law (a) in fresh water; (b) in sea water

Table 2-1. Water absorption properties of CPT and pure PA6 in fresh and sea water

		W (%)	W_c (%)	k	D ($\times 10^{-8}$ m^2 h^{-1})
Fresh water	Pure PA6	8.10	/	1.44681	5.64
	CPT	5.96	6.48	0.85111	3.59
Sea water	Pure PA6	7.85	/	1.38118	5.47
	CPT	5.70	6.28	0.75567	3.10

The diffusion coefficient in fresh and sea water also indicate the different water absorption dynamics. The diffusion coefficient of pure PA6 in fresh and sea water are 5.64×10^{-8} m^2 h^{-1} and 5.47×10^{-8} m^2 h^{-1}, respectively. Similarly, the diffusion coefficient of CPT in sea water also shows a smaller value, which is 3.10×10^{-8} m^2 h^{-1}, than that in fresh water, owning a D value of 3.59×10^{-8} m^2 h^{-1}. As mentioned above, the inorganic salt ions in the sea water and the polymer chain with terminal ions are probable to attract each other, so the absorption of CPT in sea water is impeded, resulting in a lower diffusion coefficient.

2.3.1.2 Barcol hardness test

The results of the Barcol hardness of specimens are shown in Figure 2-7. The hardness of dry specimens is HBI-A 55, and that of saturated specimens in fresh and sea water are HBI-A 36 and HBI-A 37, which is 65% and 67% of dry specimens, respectively. Although there is little difference between fresh water and sea water, at each moisture content, the hardness of the CPT in sea water is slightly larger than that in fresh water. Because the CPT specimens absorb less sea water than fresh water, the hardness of the specimens absorbing sea water is less affected by water molecules. When the water content is 1%, the hardness decreases by about 15% and kept a 10% decrease until the water content reached 3%. After 3% water content, the decrease in the hardness slows down, with a 1% decrease for every 1% increase of water content until the saturated state. This is caused by water concentration on the surface of specimens. At the initial stage, the resin near the specimen surface absorbs plenty of water

quickly due to the difference in water concentration between the exterior and interior of the specimen. Water molecules that act as plasticizer can reduce the hardness of the resin. At the same time, water infiltrating into the interface between the fiber and resin plays the role of lubricant, making the interface easy to slide. The resin close to the surface absorbs more moisture, so it leads to the rapid reduction of Barcol hardness at the initial stage. With the process of water absorption, the inner part of the specimen also reaches the saturated state. Therefore, compared with the initial stage, the plasticizing effect of water is weakened, leading to the slower hardness changes.

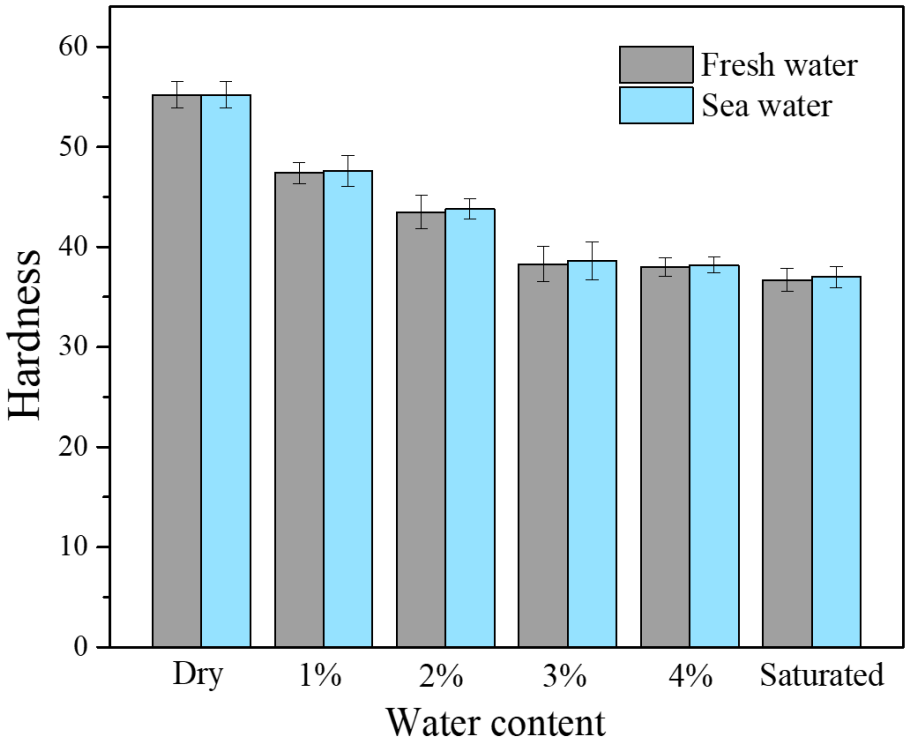

Figure 2-7 Barcol hardness of CPT material with different fresh and sea water contents

2.3.1.3 Three-point bending test

2.3.1.3.1 Effects of the temperature of water absorption

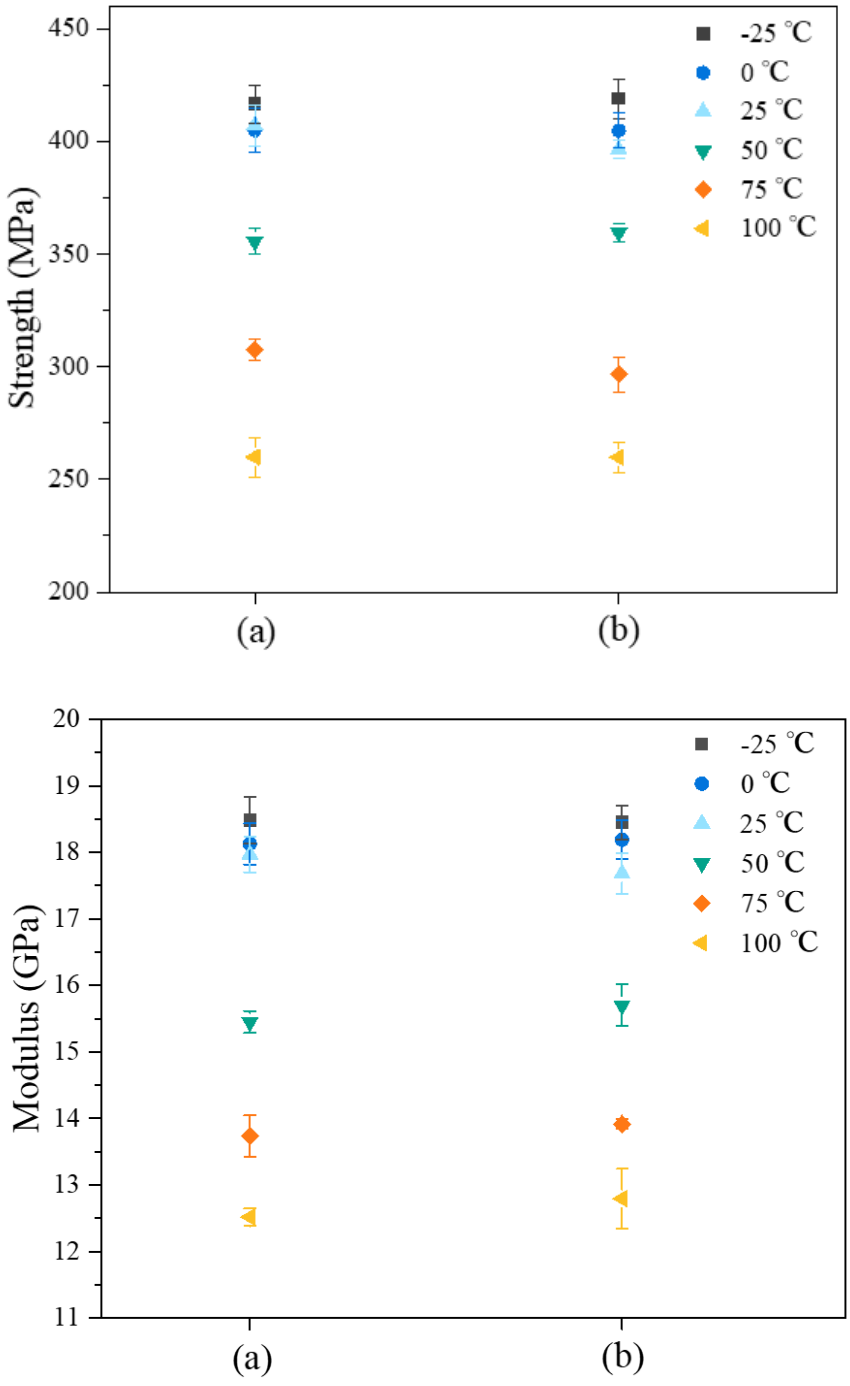

Figure 2-8 Flexural strength and modulus of (a) dry specimens; (b) dry specimens kept in a vacuum oven

The change in the mechanical properties by water absorption were studied by three-point bending test. The effects of water contents in specimens and test temperatures were researched, respectively. Before that, because the water absorption test was conducted at 70 ℃ for a period of time, the influence of temperature should be clarified. So, a group of dry CPT specimens were kept in a vacuum oven at 70 ℃ for the same time as the water absorption test. Then, the three-point bending test of these specimens was conducted. The results of flexural strength and modulus of these specimens are shown in Figure 2-8, and dry specimens are taken as a control.

As Figure 2-8 shows, even the CPT material is kept at 70 ℃ for a period of time, the flexural properties almost have no change at all the chosen temperatures. Therefore, the change in the flexural properties of water absorbed CPT specimens can be attributed to water absorption.

2.3.1.3.2 Effects of water contents in specimens

The flexural properties of CPT specimens with different water contents are shown in Figure 2-9. The test temperature was controlled at 25 ℃.

When the CPT specimens are immersed in fresh water, the strength decreases fast when the water absorption was 1%. At the initial stage, absorbed water only concentrates in the surface area of the specimens. Because composites are sensitive to surface properties, the flexural strength decreases fast when the surface layer absorbed water, even if the whole water absorption is only 1%. In the latter half part of water absorption, flexural strength almost keeps stable. As mentioned in chapter 1, two steps exist in the water absorption process. When the water content is below 2%, the absorbed water molecules builds hydrogen bonds with hydrophilic groups on PA6 chains. When the water content is above 3%, all the hydrophilic groups on PA6 chains are all occupied by water molecules, but water continues to penetrate into the inner part of composite, forming clusters between polymer chains. So, the critical

water content should between 2% and 3%.

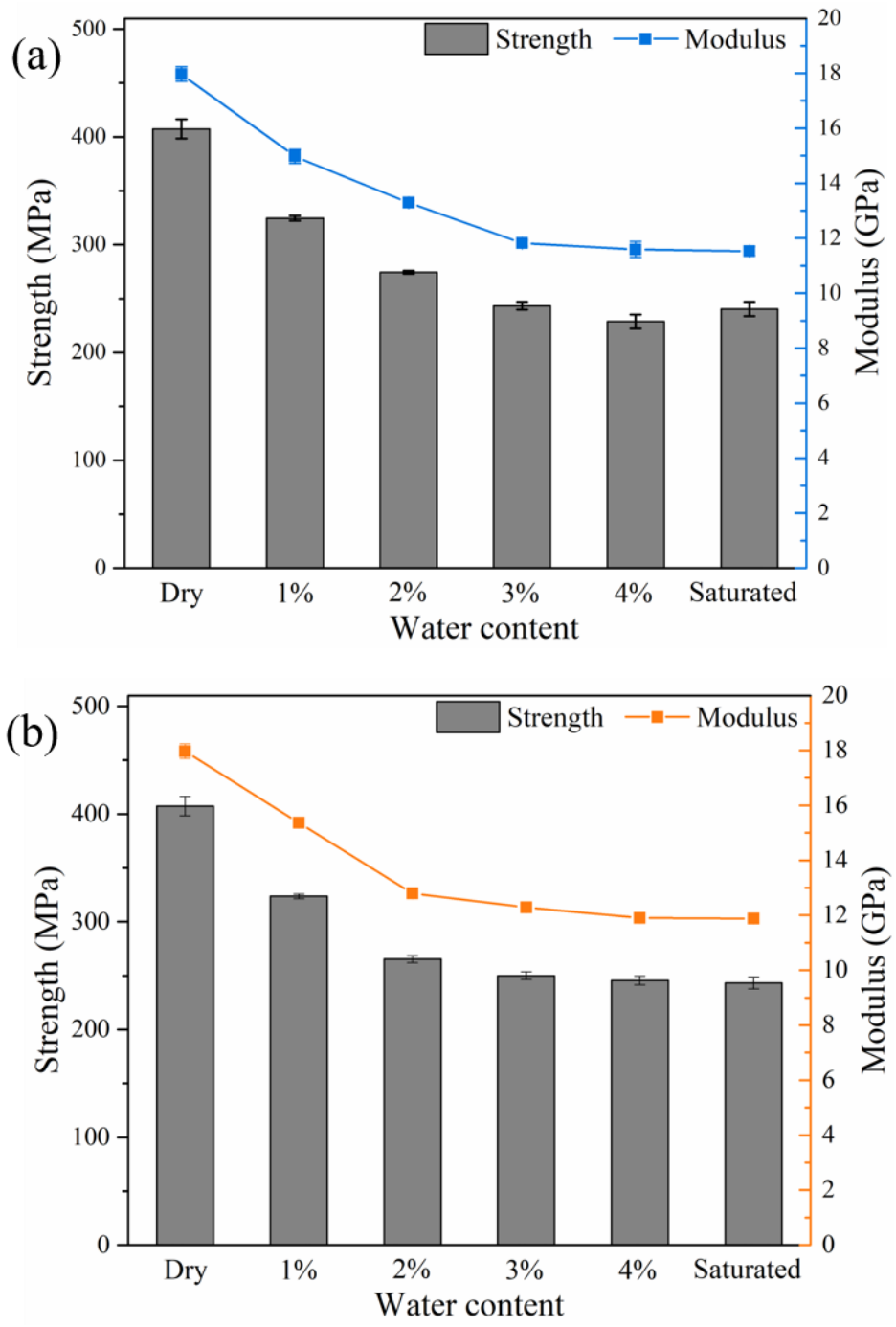

Figure 2-9 Flexural properties of CPT material with different water contents: (a) CPT immersed in fresh water; (b) CPT immersed in sea water.

Compared to dry state, the strength of the saturated specimens decreases by 41% . The similar trend is also found at the change in the modulus, which has a decrease by 33.9%. When the CPT specimens are immersed in sea water, the results are similar to that in fresh water. The flexural strength decreases by 40.2%, and modulus decreases by 35.9%.

Comparing the results of two different water media, it is found that the results are not significantly different with various water media. Besides, the effects of water absorption on the degradation of flexural properties are similar in the strength compared with the modulus. The reason is the decrease in the resin matrix strength, which weakens the combination between fibers and matrix, makes specimens more susceptible to damage, thus the strength of the specimens decrease more significantly; while the contribution of the resin matrix to the overall modulus of the specimen can be neglected. So the decrease in the interfacial force between fibers and matrix should be the main factor leading to the modulus decrease.

2.3.1.3.3 Effects of test temperature

The flexural properties of the CPT material absorbed different water under different temperatures are shown in Figure 2-10. Results of dry specimens are taken as a control. For dry specimens, the flexural strength has a little decrease when the temperature is below 50 ℃, which is lower than the glass transition temperature of PA6, which is 60 ℃. When the temperature increases from -25 ℃ to 100 ℃, the flexural strength has a decrease by 35%, and the flexural modulus decreases by about 32%. The results indicate that the mechanical properties of the CPT materials decrease obviously at higher temperature.

When the CPT specimens are saturated by fresh water, because of water absorption, mechanical properties are widely affected. Flexural strength and modulus show detectable decline in the whole range of temperature. Decrease in the modulus is milder than decrease in the strength. The strength decreases by almost 50% when the temperature increased from

-25 ℃ to 100 ℃, but the modulus decreases by 31% after the heating process. This may be due to the change in the thermodynamic properties of the resin after heating, resulting in the decrease in the flexural strength. However, due to the existence of carbon fibers, which are stable to the temperature range in this test, the modulus of the CPT decreases less.

Similar trend also appears in sea water saturated CPT as Figure 2-10 (c) shows. The strength decreases by 42% but the modulus decreases by 31% after heating process. At same test temperature, the flexural properties of CPT in fresh water and sea water show little difference. This result indicates that different water media have little effects on the macroscopic mechanical properties of CPT specimens.

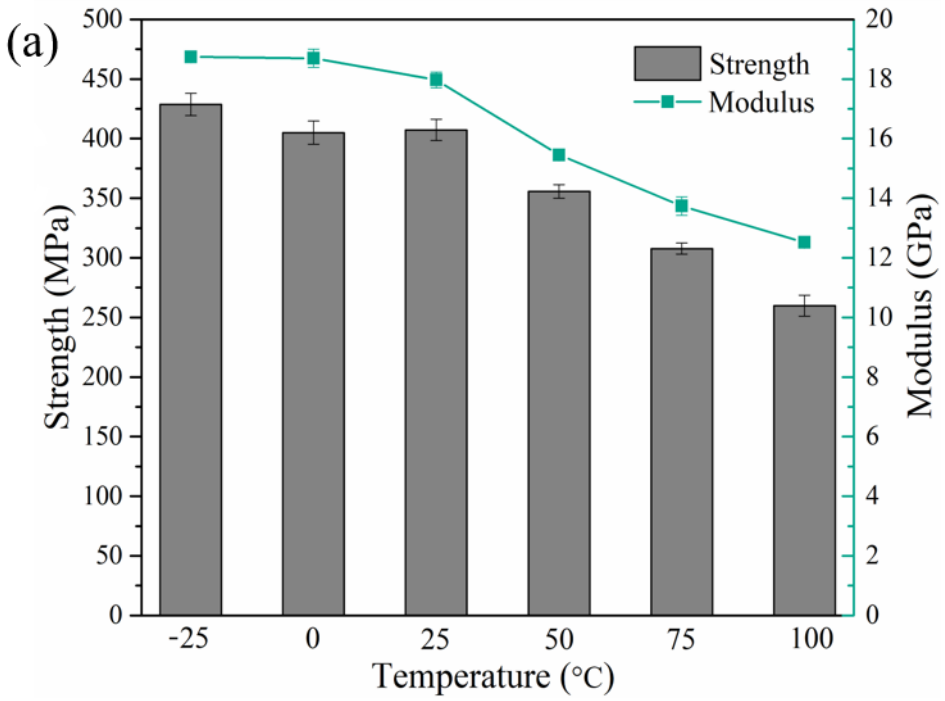

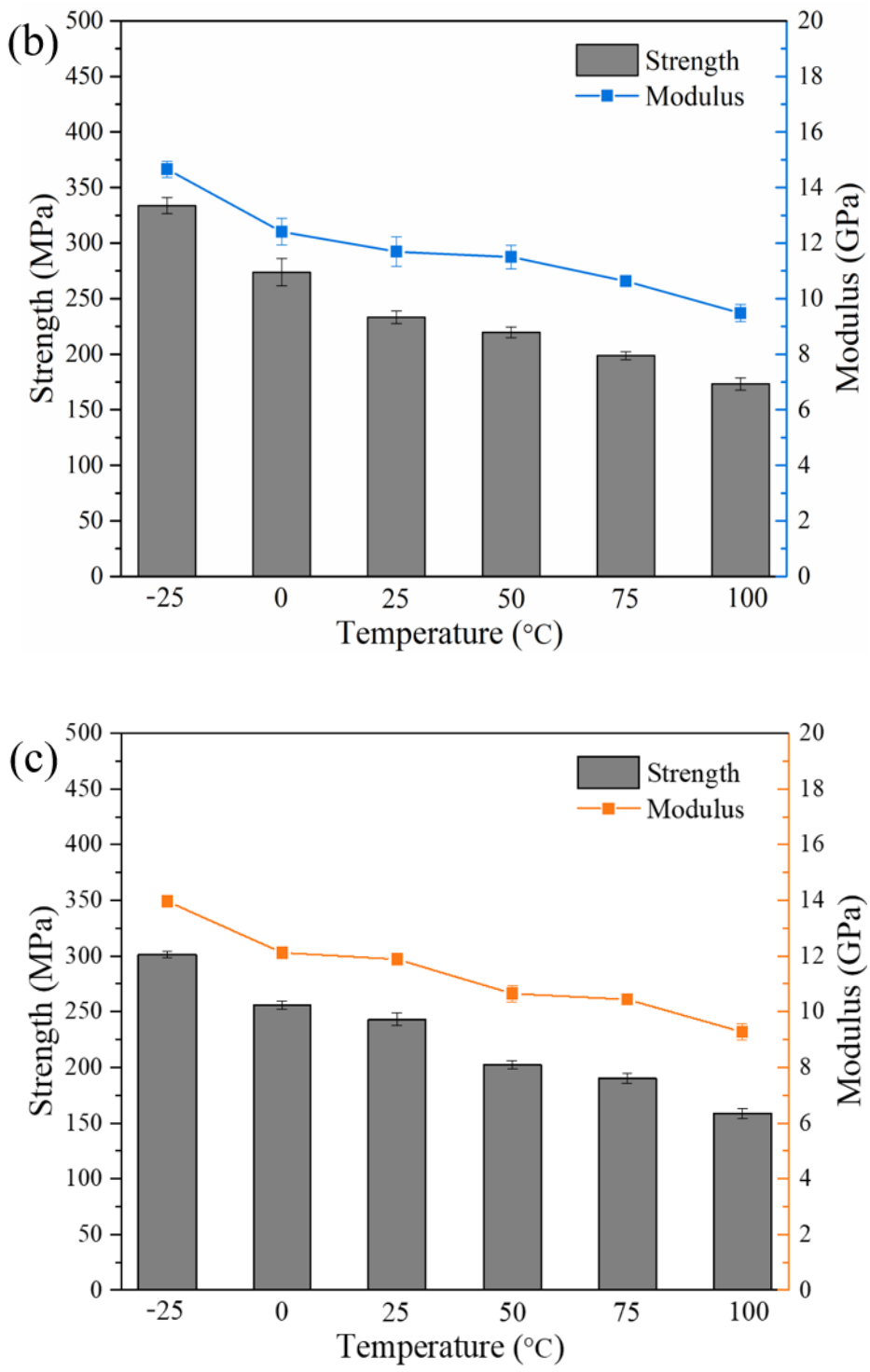

Figure 2-10 Flexural properties of CPT material with different water-absorbed states: (a) dry CPT; (b) CPT of fresh water saturated; (c) CPT of sea water saturated.

2.3.1.4 Microstructure

The fracture section of specimens after three-point bending test also indicates some evidence about the failure mechanism. The photos are shown in Figure 2-11.

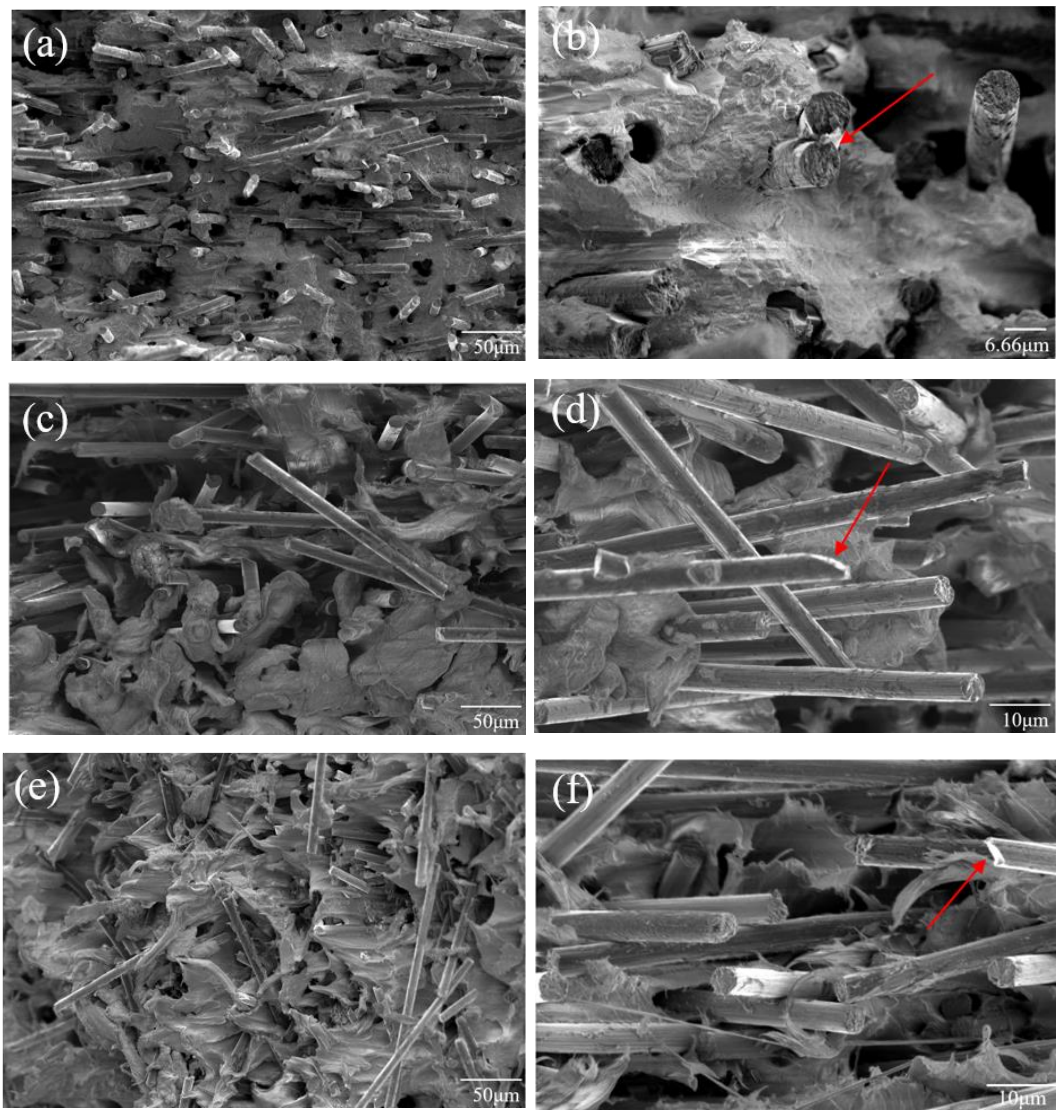

Figure 2-11 Flexural properties of CPT material after three-point bending test: (a) dry CPT at low magnification; (b) dry CPT at high magnification; (c) CPT of fresh water saturated at low magnification; (d) CPT of fresh water saturated at high magnification; (e) CPT of sea water saturated at low magnification; (f) CPT of sea water saturated at high magnification.

Dry CPT specimens broke suddenly, resulting in short fragmentation length of carbon fibers in the longitudinal direction. As Figure 2-11 (a) shows, a relatively smooth fracture surface is formed after resin fracture, which demonstrates the brittle property of dry CPT. Pull-out phenomena can also be found, but most of them are along the transverse direction. In addition, as the red arrow in Figure 2-11 (b) shows, the fracture surfaces of carbon fibers are roughly in the direction of the fiber diameter, and carbon fibers are embedded tightly by matrix. So, the interfacial interaction between fibers and resin matrix appear to be strong.

However, the CPT specimens saturated in fresh water exhibits huge difference in failure feature. After water absorption, the mobility of the polymer chain increases, leading to plasticization of the matrix. Thus, the wave-like resin can be observed in Figure 2-11 (c). Different from dry CPT, carbon fibers slip and pull out easily in the saturated CPT. Fragments of fibers and matrix can be also observed, which demonstrates the brittleness and low strength of saturated CPT. Furthermore, as the red arrow in Figure 2-11 (d) shows, the area of fracture surface of carbon fibers is larger than that of their cross section, indicating a different failure mechanism. With the increase in the load, cracks generate in carbon fibers and propagate not only along the direction of fiber diameter but also along the longitudinal direction of fibers. After the failure of the carbon fibers, cracks propagate to matrix bulk along the direction of fiber diameter, as well as the longitudinal direction of the fibers, resulting in the generation of matrix fragments and wave-like morphology. Therefore, the gaps formed by the slipping of fibers can be observed clearly. The main reason for this phenomenon is the plasticization of the matrix and the decrease in the interfacial interaction between carbon fibers and matrix caused by water absorption.

Similar to the fracture section of CPT saturated in fresh water, cloud-like resin can also be found in CPT saturated in sea water, as shown in Figure 2-11 (e), because sea water molecules can also play the role of plasticizer, which increases the fluidity and plasticity of resin polymer and makes it show better ductility under load. But pull-out phenomenon is not as serious as

CPT saturated in fresh water. So, the reason may be that the interface between fibers and matrix is stronger in sea water than in fresh water.

2.3.1.5 Droplet test

2.3.1.5.1 Interfacial adhesion

Figure 2-12 shows maximum load versus embedded lengths obtained from the droplet test. L_E is the embedded length of droplets. A least-square linear regression is adapted to identify the relationship between the load at interface debonding and embedded length, as the red line shows, which is set to pass through the origin since the maximum load is proportional to the embedded length. The blue line is the least-square linear regression of these obtained points. The parameters of linear regressions are listed in Table 2-2.

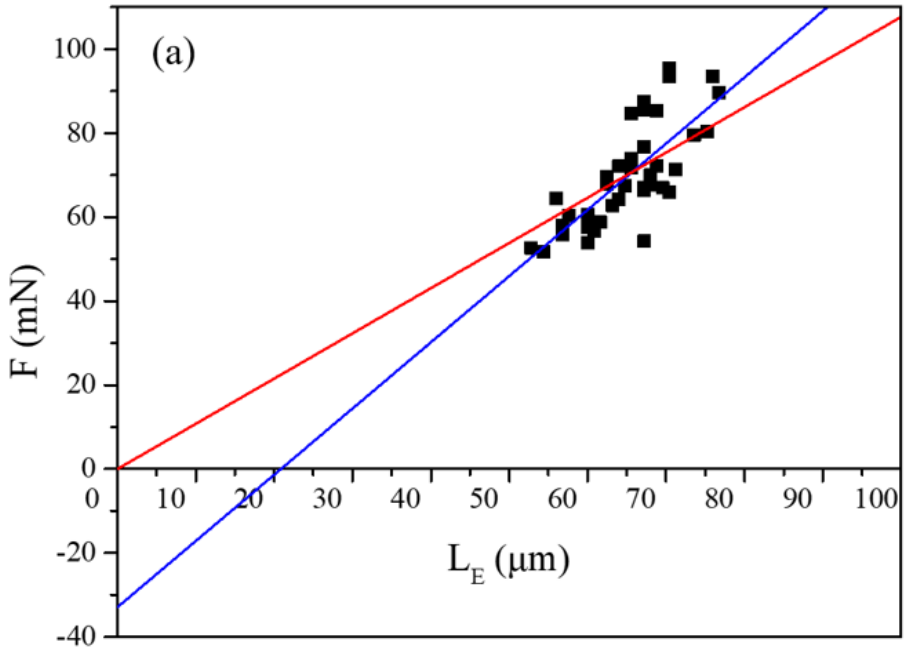

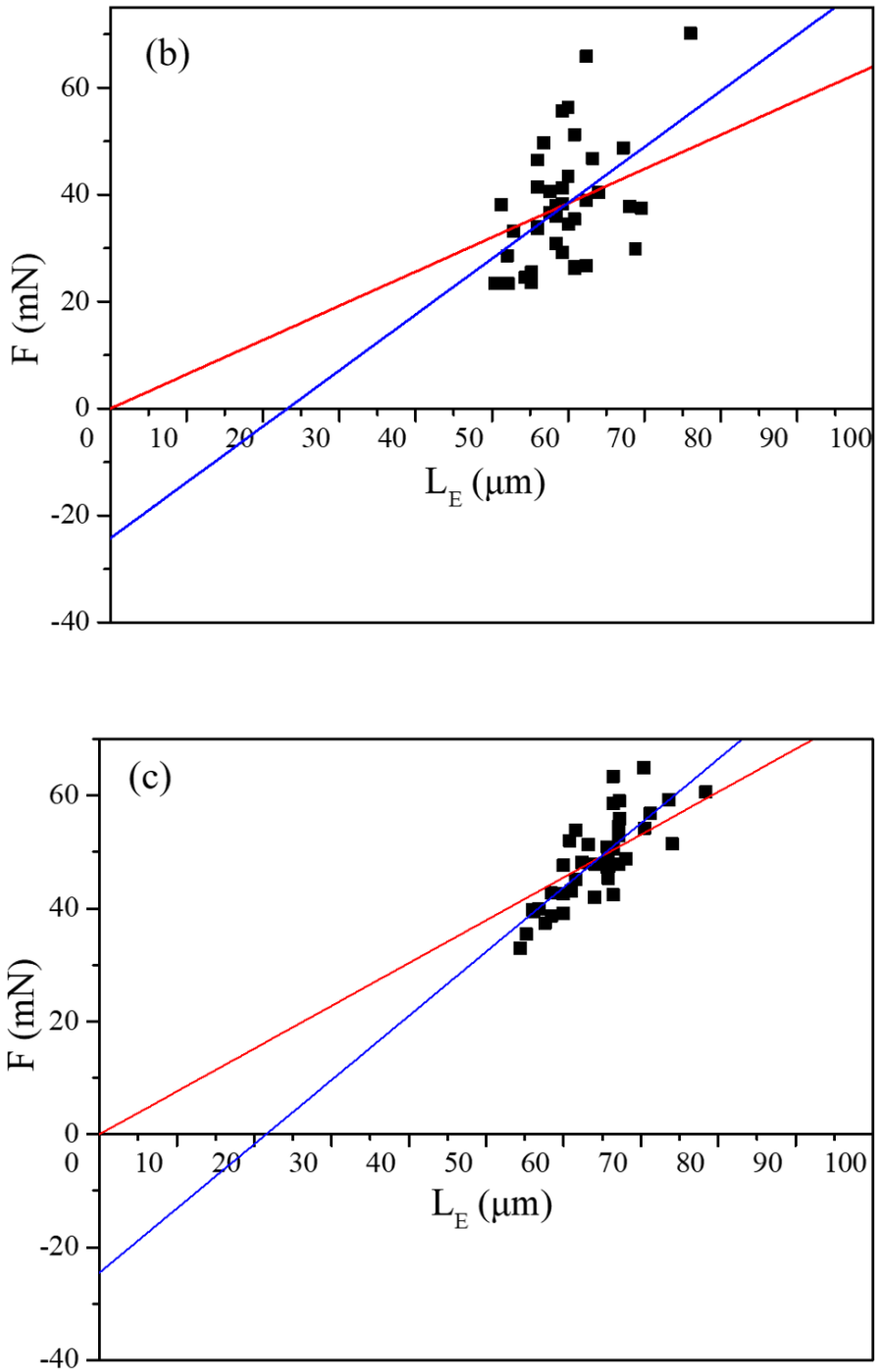

Figure 2-12 Maximum load during fiber pull-out versus embedded length for: (a) dry PA6; (b) PA6 of fresh water saturated; (c) PA6 of sea water saturated. Red lines represent least-square linear regression crossing the origin, blue lines represent least-square linear regression.

Table 2-2. Parameters of least-square linear regressions.

	Red line			Blue line		
	Slope (mN/μm)	Intercept (mN)	Adjusted R-square	Slope (mN/μm)	Intercept (mN)	Adjusted R-square
Dry PA6	1.077	0	0.9858	1.578	-32.92	0.5599
Fresh water saturated PA6	0.640	0	0.9341	1.046	-24.27	0.2224
Sea water saturated PA6	0.758	0	0.9888	1.137	-24.52	0.6214

Figure 2-13 shows IFSS values between carbon fibers and PA6 resins. The gray column is the predicted value of IFSS, calculated by using Equation 2-10. The blue column is the arithmetic mean of the 40 data points, and the emerald column is calculated by Equation 2-9, using the slope of the red line in Figure 2-12. The results show that the IFSS calculated by the three methods are similar to each other, indicating that the results obtained by droplet test are acceptable and credible. On the other hand, comparing the results before and after water absorption, fresh and sea water indeed decrease the IFSS between PA6 and carbon fibers. So, in three-point bending, weak IFSS between resin matrix and fibers in saturated specimens leads to the failure of interface first under the effects of load. So, the pull-out phenomena can be observed in the fracture sections of specimens Meanwhile, the failure mechanism mentioned in 2.3.1.4 can also be confirmed.

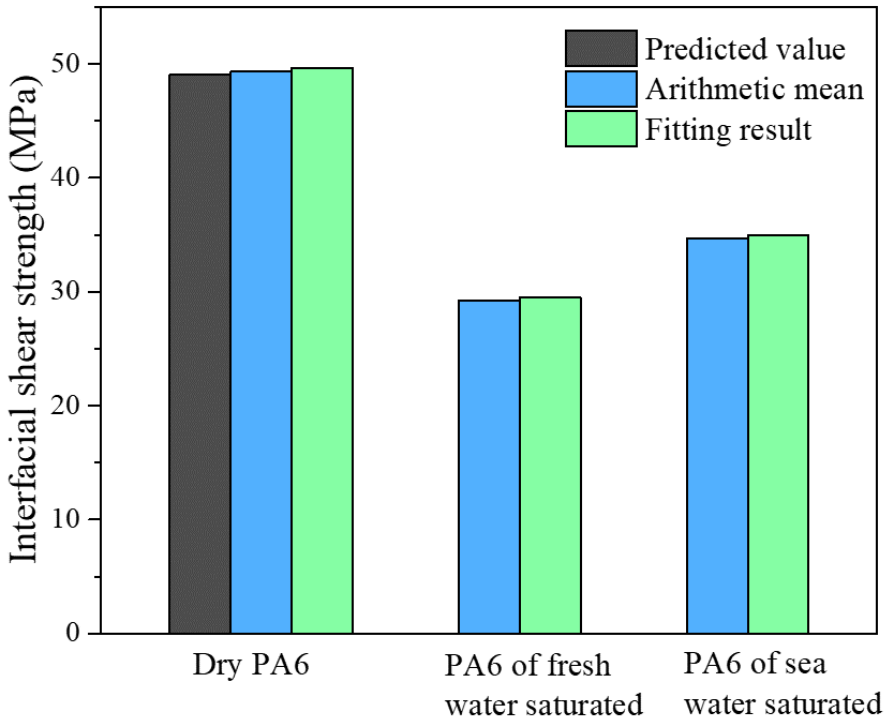

Figure 2-13 IFSS between CFs and different PA6

2.3.1.5.2 Thermal residual stress

As the blue line shows, the least-square linear regression of these points does not cross the origin. The negative intercepts may indicate the negative effect of several experimental factors such as the thermal residual stress, the thermal-oxidative degradation of the resin matrix, or the selected range of embedded length. Considering that the droplets preparation and droplet tests were performed under identical experimental conditions, the thermal residual stress is probable to take primary responsibility for the negative intercepts. Because resin shrinks during the cooling process while carbon fiber can keep its shape, the shrinkage of solid fiber and melt matrix mismatch each other. So, thermal residual stress generates in the interface. We need to check the reliability of the experimental results. The absolute value of intercept of the line fitted by least-square linear regression (the blue line shown in Figure 2-12) is considered to be the thermal residual stress.

The thermal residual stress can be calculated using Equation 2-11, assuming in axial direction, the matrix deformation is uniform [91].

$$F_r = E_f A_f \Delta T(\alpha_m - \alpha_f) \quad \text{Equation 2-11}$$

where F_r is the thermal residual stress, E_f is the elastic modulus of the fiber, A_f is the cross section area of the carbon fiber, ΔT is the temperature change from the crystallization temperature to the final temperature, and α_m and α_f are the thermal expansion coefficient of resin and fiber.

A more rigorous solution has also been proposed if the matrix deformation is non-uniform and the interface shear stress is integrated over the entire embedded length. The modified method of calculating thermal residual stress is shown as the following equations:

$$F_r = \frac{E_f A_f \Delta T(\alpha_m - \alpha_f)}{1 - 2k v_f} \quad \text{Equation 2-12}$$

$$k = \frac{\theta v_f}{1 + v_m + \theta(1 - v_f)} \quad \text{Equation 2-13}$$

$$\theta = \frac{E_m}{E_f} \quad \text{Equation 2-14}$$

where v_m and v_f are the Poisson's ratios of the resin and fiber. The F_r calculated by Equation 2-11 and 2-12 can be thought as the maximum value in the specific experiment condition [91].

Parameters used to calculate the thermal residual stress are listed in Table 2-3. Parameters of CF are provided by Toho Tenax Co. Ltd, and parameters of PA6 resin re provided by Toray Industry, Inc. The calculated thermal residual stresses are shown in Figure 2-14. Calculated value and modified value are the results calculated by Equation 2-11 and 2-12. Comparing F_r

from calculation and least-square linear regression, the experimental values are all less than the theoretical maximum value. As mentioned before, the specimens for droplet test were cooled at a constant rate from the crystallization temperature to room temperature, which could ensure sufficient crystallization of PA6 resins. Thermal residual stress can be partially removed owing to the slow cooling rate. Thus, it can be concluded that the thermal residual stress does not have significant influence on the IFSS obtained by experimental results, which means the experimental values of IFSS are acceptable.

Table 2-3 Parameters of materials used for calculating thermal residual stress.

	Elastic modulus (GPa)	Poisson's ratio	Thermal expansion coefficient ($°C^{-1}$)
CF	237	0.26	-0.74×10^{-5}
PA6	2.2	0.35	8×10^{-5}

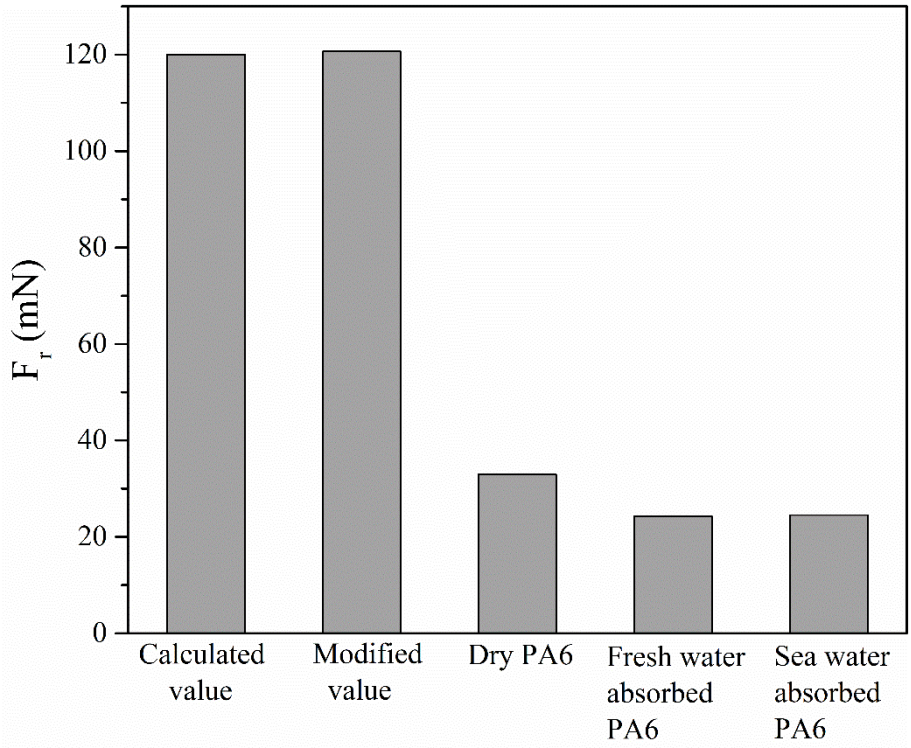

Figure 2-14 The thermal residual stress obtained by calculation and experiment

2.3.1.6 Conclusion

In this research, water absorption behavior of the CPT material in fresh water and sea water were studied. Flexural behavior of CPT in different water contents and temperatures was investigated.

To sum up, the water absorption of CPT in fresh water is higher and faster than that in sea water. The flexural properties of CPT material change from sensitive to insensitive with the increase in the water content and the difference between fresh and sea water on the flexural properties of CPT is not significant. In addition to the reduction of the properties of resin itself, the decline of IFSS is also thought to take primary responsibility for the degradation of flexural properties.

2.3.2 Cyclic water absorption-desorption

2.3.2.1 Water absorption

The water absorption process in every cycle has been monitored. The results of weight gain versus time are shown in Figure 2-15, and the results of weight gain versus the square root of time and Fick's diffusion law are shown in Figure 2-16. Cyclic water absorption-desorption properties of CPT in fresh and sea water are listed in Table 2-4.

As shown in Figure 2-16, with the increase in the cycle numbers, *W* value increased, the CPT material is intended to absorb more water in both water environment. Furthermore, *D* value in fresh and sea water after the 1st cycle are 3.59×10^{-8} m^2 h^{-1} and 3.10×10^{-8} m^2 h^{-1}, which are also mentioned in 2.3.1.1. And after the 2nd and 3rd cycle, *D* value increased to 3.64×10^{-8} m^2 h^{-1} and 3.67×10^{-8} m^2 h^{-1} in fresh water, and 3.50×10^{-8} m^2 h^{-1} and 3.59×10^{-8} m^2 h^{-1} in sea water, respectively. Obviously, the extent of the increase in *D* value after several time of cyclic water

absorption-desorption in sea water is larger than that in fresh water. The changes in the tightness of the interface bonding after water immersion may lead to this difference. As we know, water molecules can destroy the hydrogen bonds between polymer and CF, make the interface loose and create more space. After drying, because water molecules play the role of lubricant, resin and fibers that were originally bonded together may have mutual slippage. Thus, the loosened interface cannot be completely restored to the original state. Wider spacing in the interface makes it easier for water molecules to enter the interior of the specimens. So, the *D* value increased after several time of cyclic absorption-desorption.

Table 2-4. Cyclic water absorption-desorption properties of CPT and pure PA6 in fresh and sea water

		W (%)	W_c (%)	k	D ($\times 10^{-8}$ m^2 h^{-1})
Fresh water	Pure PA6	8.10	/	1.44681	5.64
	CPT (1st cycle)	5.96	6.48	0.85111	3.59
	CPT (2nd cycle)	6.17	/	0.88564	3.64
	CPT (3rd cycle)	6.24	/	0.89845	3.67
Sea water	Pure PA6	7.85	/	1.38118	5.47
	CPT (1st cycle)	5.70	6.28	0.75567	3.10
	CPT (2nd cycle)	5.92	/	0.83348	3.50
	CPT (3rd cycle)	6.06	/	0.86321	3.59

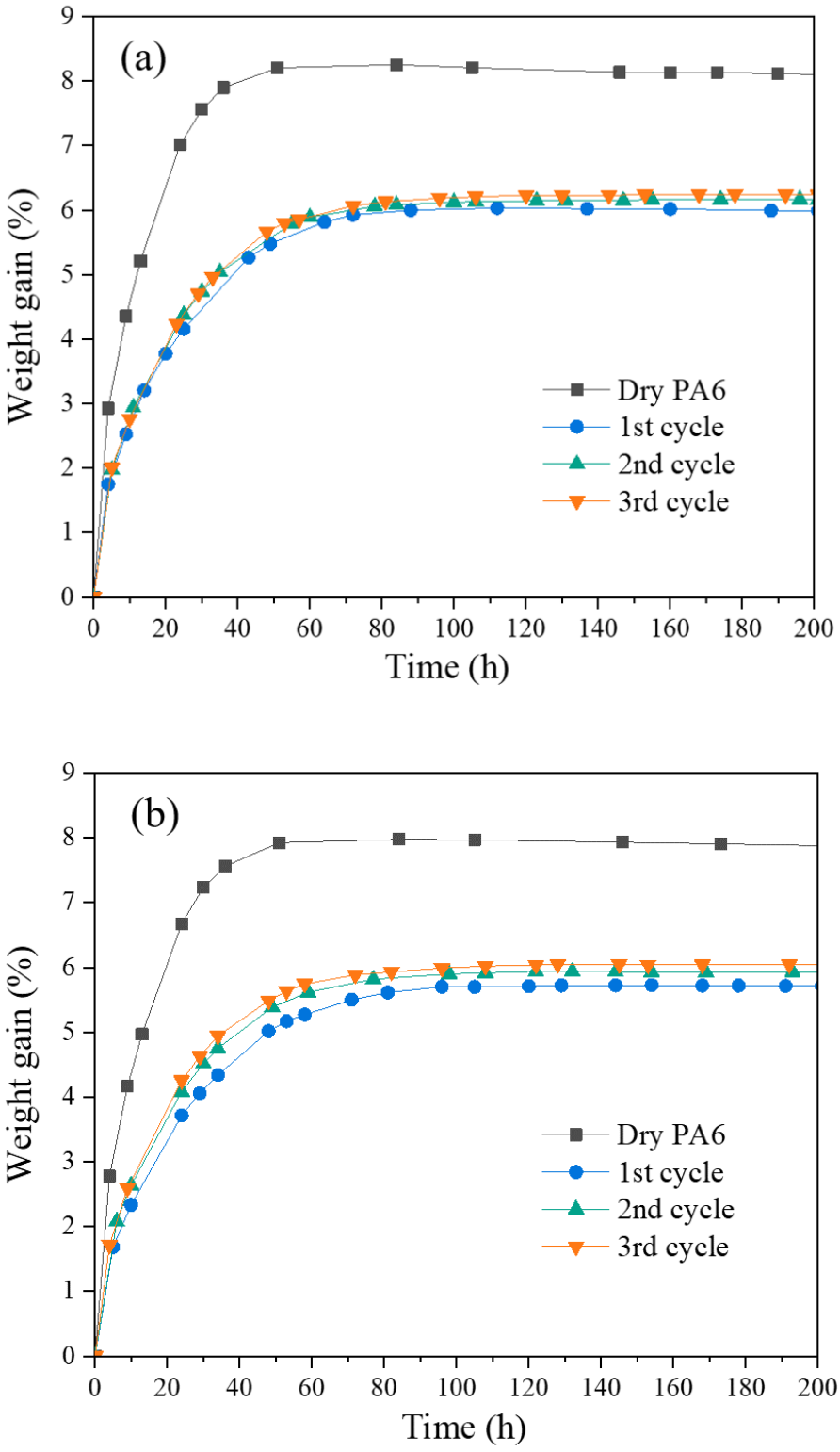

Figure 2-15 Weight gain of CPT material in three water absorption stages of cyclic water absorption-desorption test (a) in fresh water; (b) in sea water

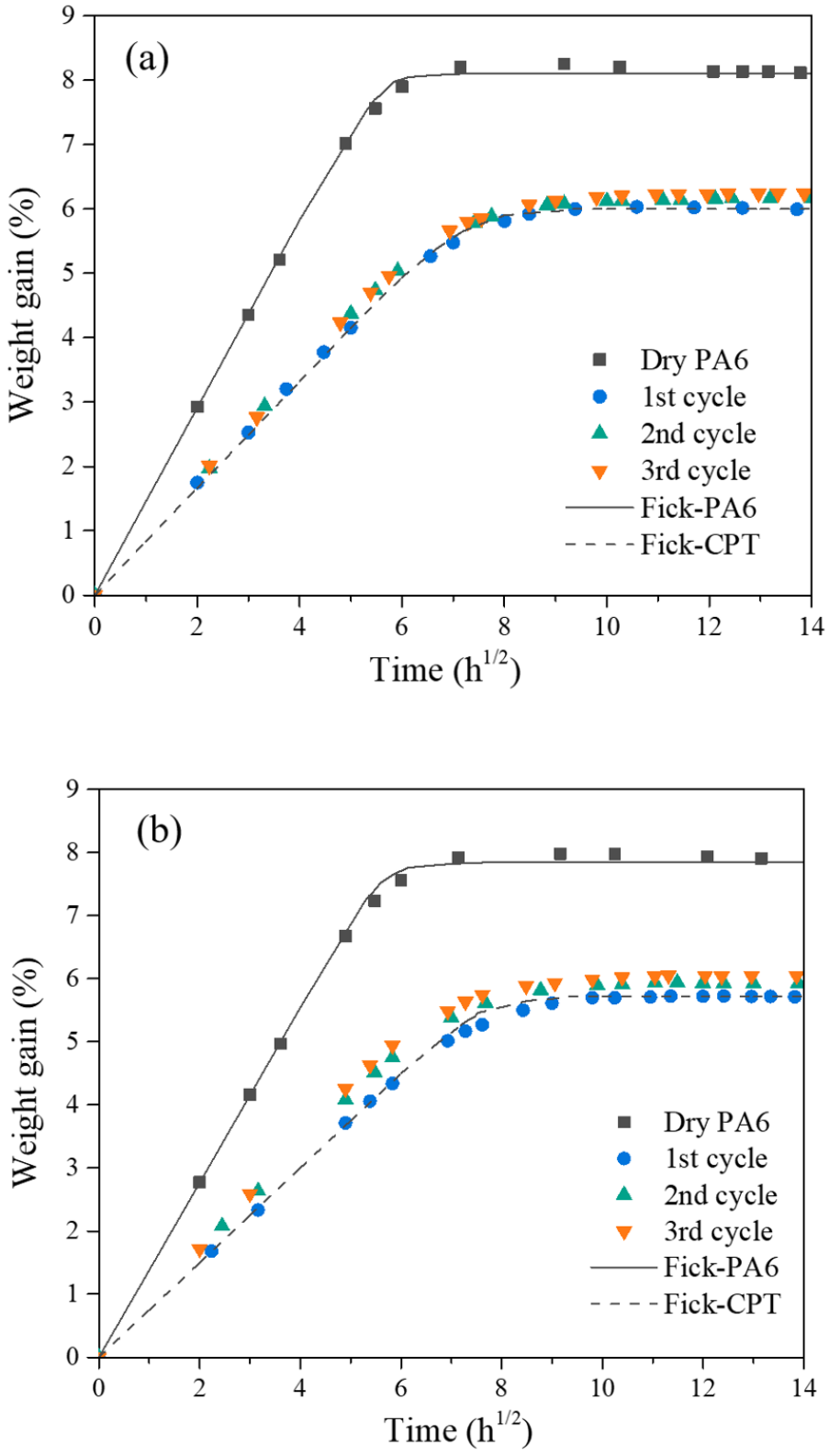

Figure 2-16 Weight gain of CPT material in three water absorption stages of cyclic water absorption-desorption test with Fick's diffusion law (a) in fresh water; (b) in sea water

However, for specimens of sea water saturated, water molecules evaporate while salt is left in the interface after drying, leading to a wilder space of interface than specimens of fresh water saturated. The next time when specimens are immersed in sea water, the interface become wider than that after the last time, so water molecules can enter the interior part along the space in the interface faster than before. So, the increase in *D* value is larger than that in fresh water.

2.3.2.2 Three-point bending test in cyclic water absorption-desorption test

The flexural properties of CPT specimens after cyclic water absorption-desorption test were studied by three-point bending. Flexural properties of CPT specimens with four different dry states in cyclic absorption-desorption test conducted in fresh and sea water are shown in Figure 2-17 and Figure 2-18, respectively.

Flexural properties decrease with the increase in the temperature, which is consistent with the result in 2.3.1.3.3. When the temperature is lower than 25 ℃, the change in the temperature has little negative effects on the flexural properties. It can be explained by the fact that the test temperature is lower than the glass transition temperature of PA6 in the CPT specimens. In same temperature, with the increase in the cycle numbers, flexural modulus decreases slowly. The same phenomenon also appeares in CPT specimens saturated in sea water. The modest reduction in the modulus indicates that the original performance of the dry CPT is basically maintained after the cyclic water absorption-desorption. However, flexural strength undergoes detectable decline when the test temperature is above 25 ℃.

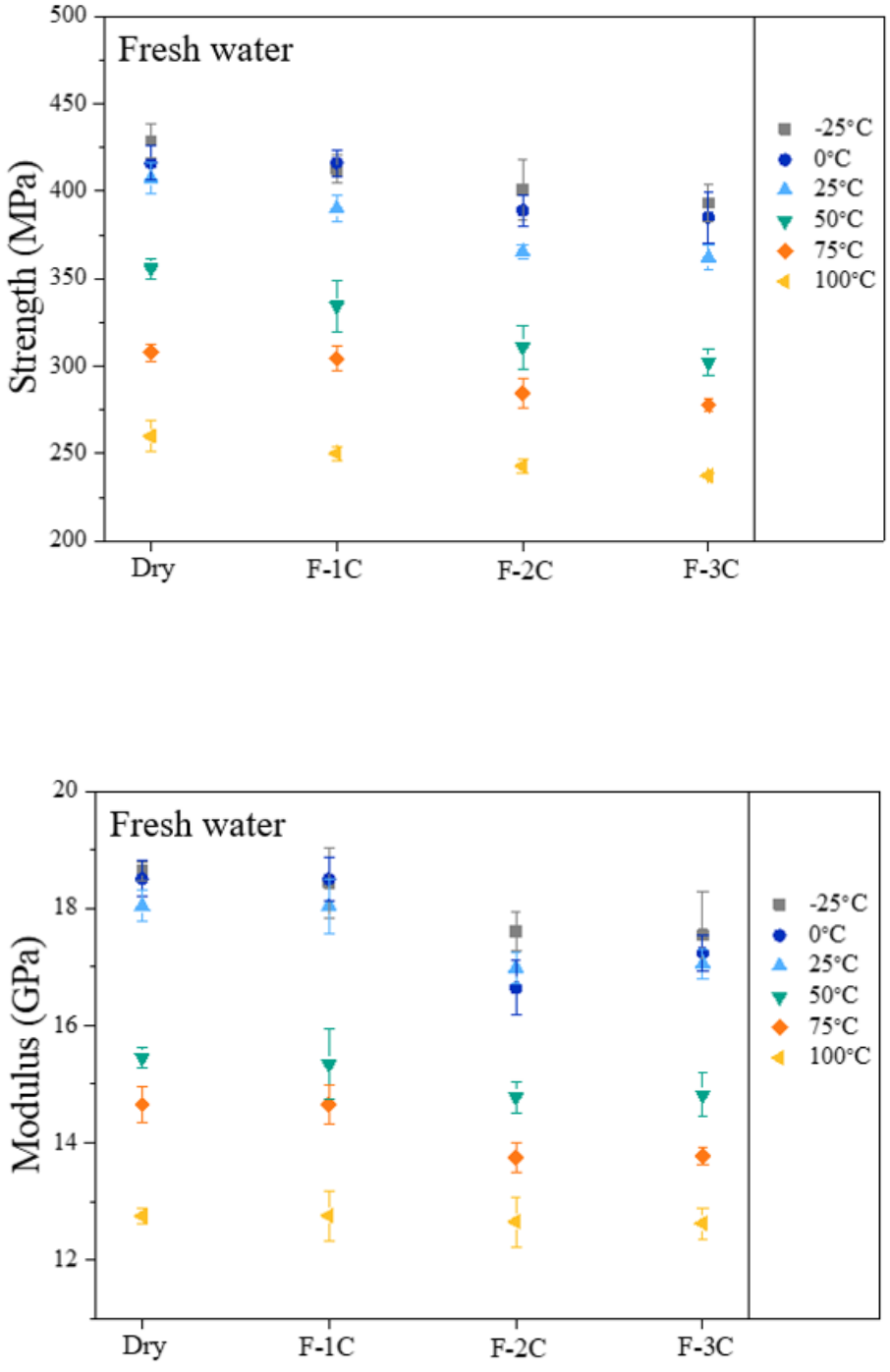

Figure 2-17 Flexural properties of CPT specimens with four different dry states in cyclic water absorption-desorption test conducted in fresh water

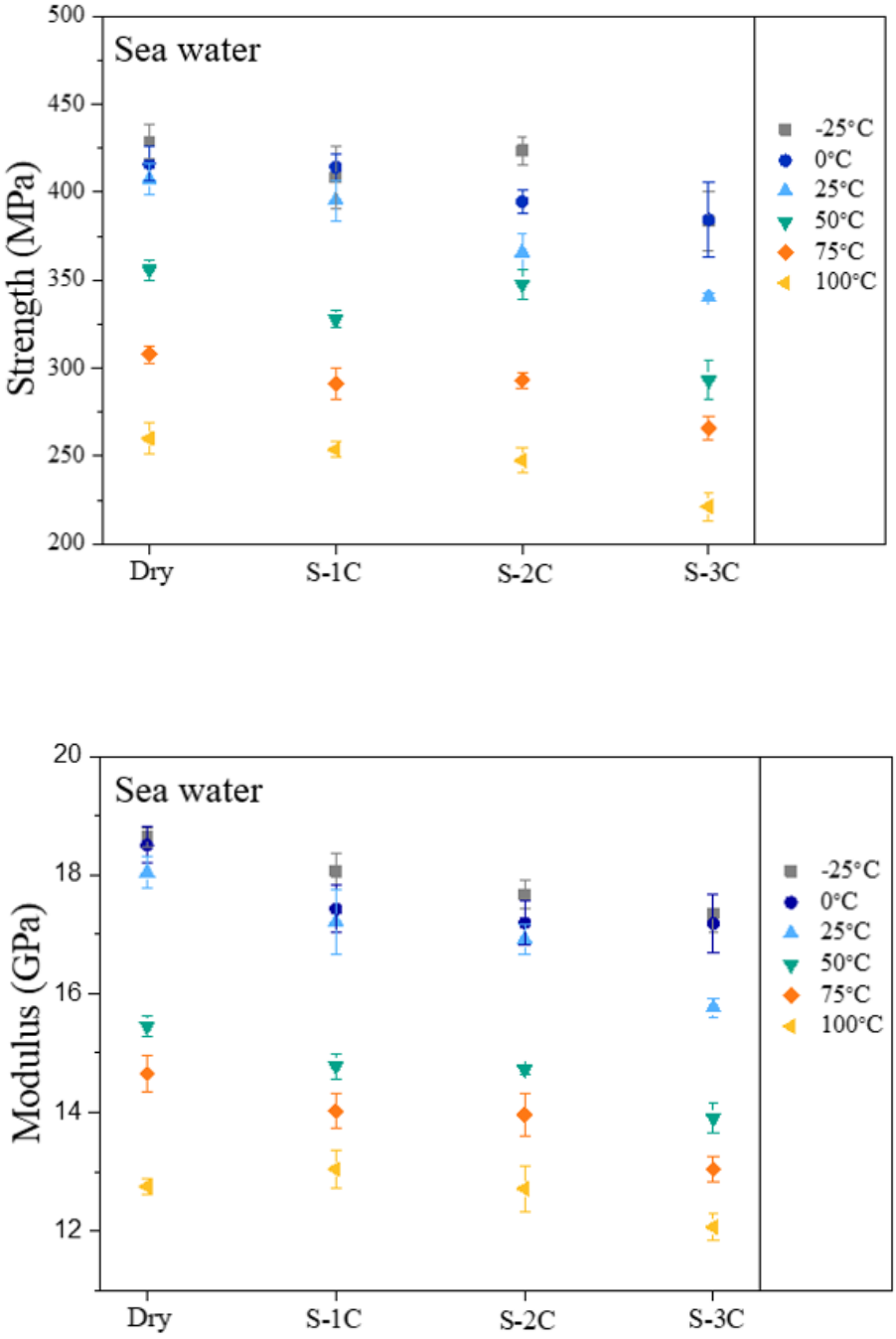

Figure 2-18 Flexural properties of CPT specimens with four different dry states in cyclic water absorption-desorption test conducted in sea water

Flexural properties of CPT specimens with three saturated states in cyclic absorption-desorption test conducted in fresh and sea water are shown in Figure 2-19 and Figure 2-20,

respectively. Different from dry states, the change in the temperature has detectable effect on the flexural properties of CPT when the temperature is lower than 25 ℃. The results reflect the change in the thermodynamic properties of the resin after absorbing water.

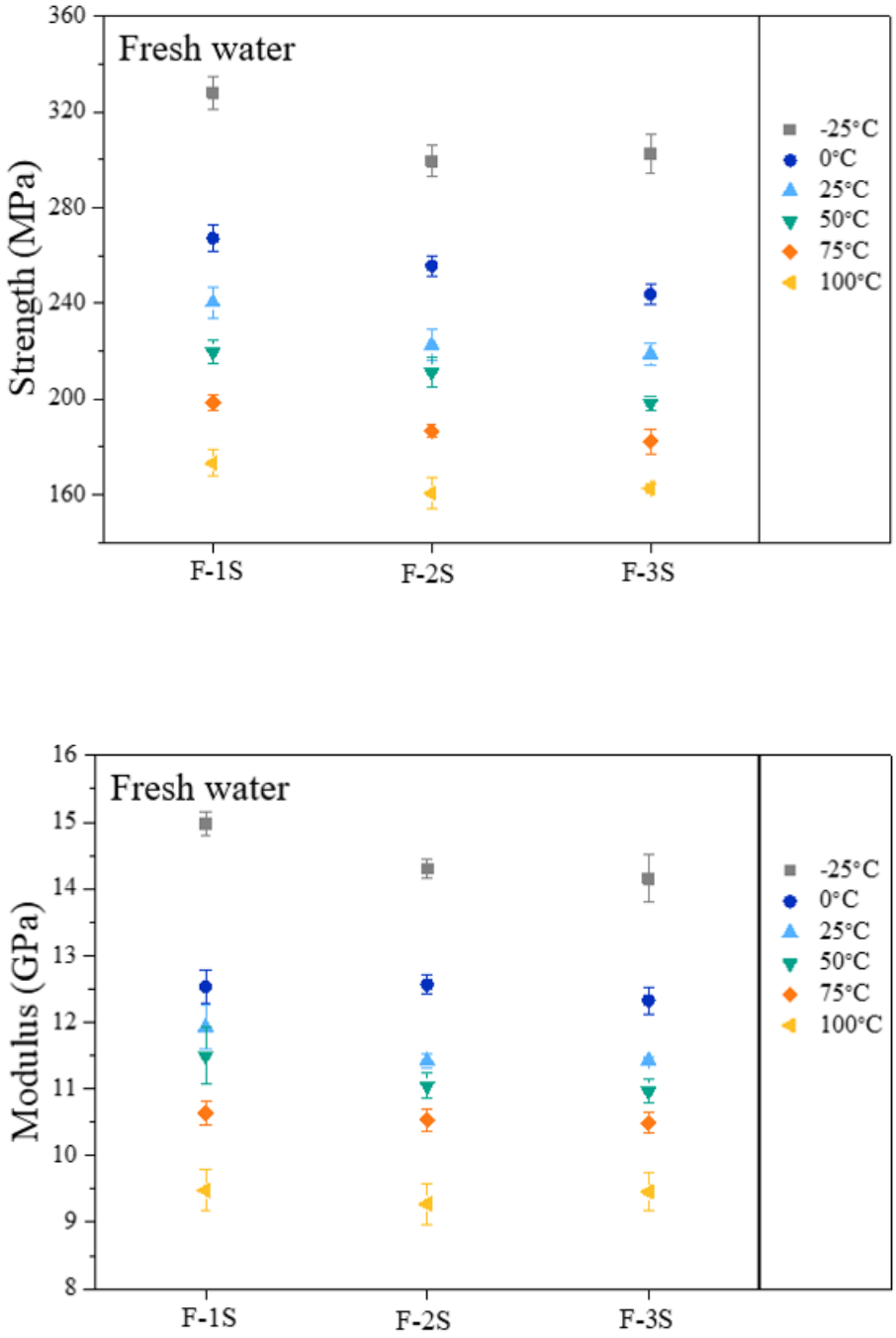

Figure 2-19 Flexural properties of CPT specimens with three saturated states in cyclic water absorption-desorption test conducted in fresh water

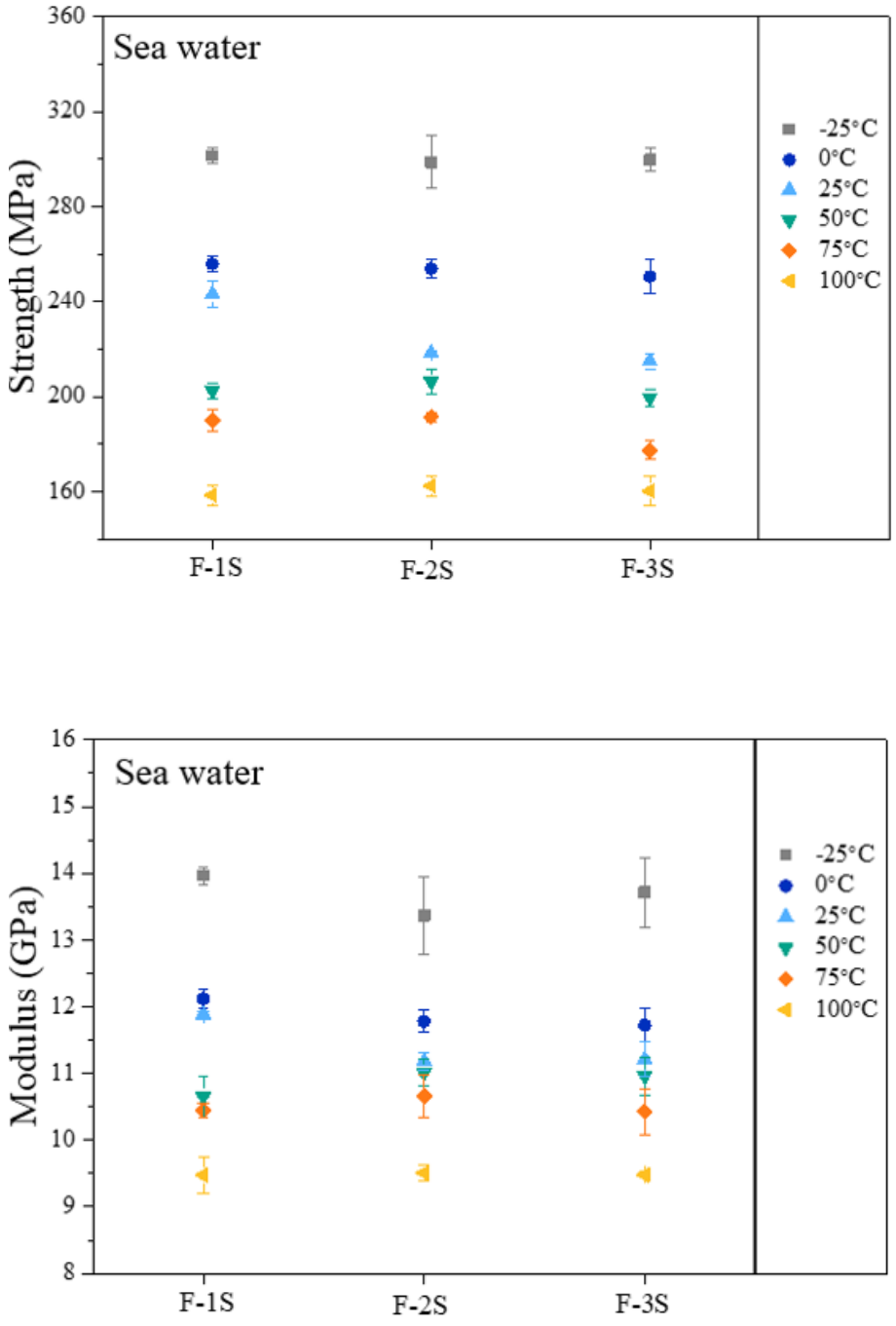

Figure 2-20 Flexural properties of CPT specimens with three saturated states in cyclic water absorption-desorption test conducted in sea water

2.3.2.3 Conclusion

In this research, cyclic water absorption-desorption behavior of CPT material was studied. Three cycles of water absorption-desorption test were conducted. Flexural properties of CPT after each cycle were investigated. In short, CPT material performed similar behavior in fresh and sea water in cyclic water absorption-desorption. Wider interface provides easier access for water molecules entering the inner part. So, the water absorption process is accelerated to a certain extent. However, the water absorption-desorption has a little impact on the flexural properties. Therefore, CPT material can maintain stable mechanical properties in the environment with changing humidity.

2.4 Summary

In this study, the flexural properties of CPT material after fresh and sea water immersion were studied. Effects of water absorption are proven to have significant influence on the performance of CPT specimens, making materials reduce their performance to some extent depending on the condition of the specimens.

Water absorption has small influence on the flexural property of CPT composites at lower temperature, whereas it can accelerate the mechanical degradation at higher temperature. The difference in the influence between fresh and sea water was proved to have less impact on the flexural properties of CPT material. Micro-observation tests demonstrate more pull-out and fracture of fibers in broken specimens, revealing the different failure mechanism of CPT material before and after fresh and sea water absorption. The calculation from droplet test provides a theoretical basis for the decline of flexural properties of CPT material.

Besides, properties of CPT material after cyclic water absorption-desorption were also investigated. CPT material can almost keep its original state after several times of water absorption-desorption, indicating that this material is suitable to be used in the environment with volatile humidity. For further research, properties of CPT after more cycles should be analyzed.

This study also points out the direction for future research. Improving the waterproof ability of CPT material is the key to determine its further application in marine field.

Chapter 3. Analysis of the influence of long-term aging in fresh and sea water on the performance of CPT material

3.1 Introduction

Depending on the purpose of products, some products should be used in water environment for a long time like ferries, propellers and water sports equipment. In the long-term use, CPT materials may have different performance with short-term aging. Besides, in some coastal region, the influence of sea wind should not be neglected. So, long-term aging in fresh and sea water should be studied. High temperature was used to accelerate the aging process [92-95]. Effects of long-term exposure of moisture conditions on the performance of CPT will be discussed.

3.2 Material and experiments

3.2.1 Material

CPT specimens were prepared by the same method described in 1.6.1 and 2.2.1.

3.2.2 Experiments

3.2.2.1 Long-term aging test

Dry CPT specimens were immersed in fresh and sea water at 70 ℃, respectively. High temperature was employed to accelerate the aging process. After a certain period of time, a group of specimens were taken out from water and their properties were studied. The time interval was set at 1 month. The aging test lasted basically for 6 months.

3.2.2.2 Barcol hardness test

The Barcol hardness of the specimens was tested by Barcol hardness impressor (GYZJ934-I, Barber–Colman Co.) according to the standard JIS K 7051. Ten valid values were taken in each group. In actual use, “HBI-A” is added before the measured hardness value.

3.2.2.3 Micromorphological analysis

The surface of the specimens, after long-term aging in water, was observed by a microscope (VHX-1000, KEYENCE Co.). The surface morphology of specimens was studied by a 3D laser scanning microscope (VK-X250, KEYENCE Co.). The roughness of surface (S_a) is a roughness evaluation parameter based on a regional morphology, which is defined as:

$$S_a = \frac{1}{NM}\sum_{i=1}^{N}\sum_{j=1}^{M}|Z_{ij}| \qquad \text{Equation 3-1}$$

where Z is the distance from the point on the contour of the object surface area to the reference plane, N and M are the sampling points in two directions perpendicular to each other in the evaluation area. [96].

3.2.2.4 Differential scanning calorimetry test

The differential scanning calorimetry (DSC) test was conducted on the specimens after aging, to clarify whether the crystallization behavior and other thermodynamic properties were affected by the long-term aging. The DSC program is shown in Figure 3-1.

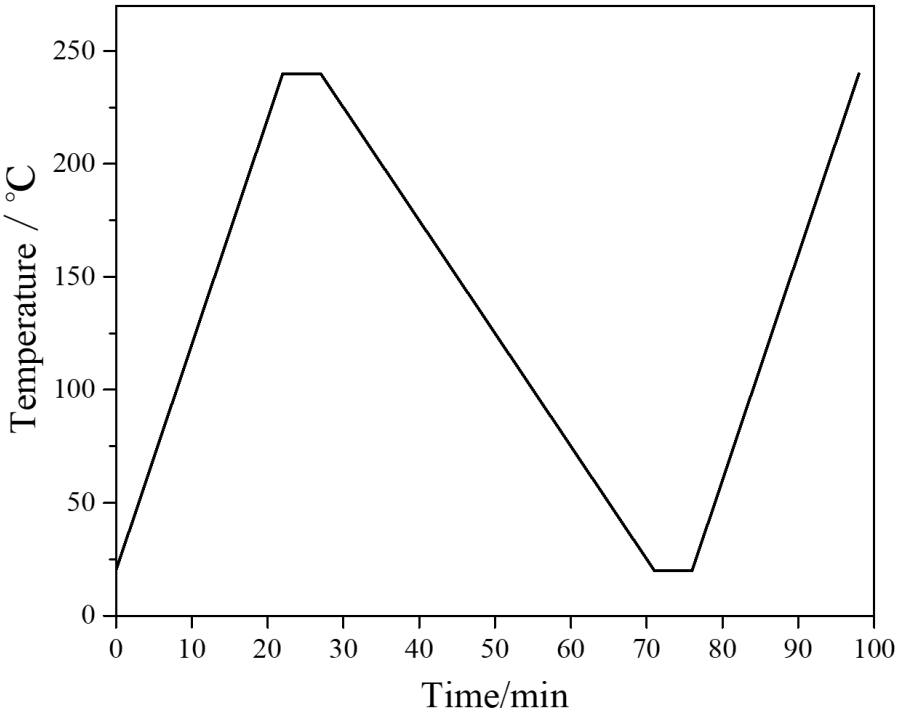

Figure 3-1 DSC program for measuring the thermodynamic properties of aged CPT

Nitrogen was chosen as the purge gas and protective gas in DSC test. The weight of the

specimen was controlled between 2-10 mg. Each group of the aging specimens were tested three times. First of all, the specimen was put into a special aluminum crucible for DSC and weighed. Then, the weighed specimen was put into the furnace of DSC machine. The furnace was closed, and the heating program was started to reach the standby temperature, which was set at 20 ℃. The test was started when the temperature of furnace was stable at 20 ℃.

There were five steps in DSC program. The first step was the heating step, the furnace was heated until 240 ℃ with a heating rate of 10 ℃·min^{-1}. Then, the furnace was kept in 240 ℃ for 5 minutes. After that, the furnace was cooled down until 20 ℃ with a cooling rate of 5 ℃·min^{-1}. Similarly, a thermostatic time of 5min was added in 20 ℃. Finally, the furnace was heated to 240 ℃ with a heating rate of 10 ℃·min^{-1} again. The furnace cooled down naturally after the fifth step.

3.2.2.5 Fourier-transform infrared test

The Fourier-transform infrared spectrum (FTIR) test was conducted by a Fourier transform infrared spectrometer (FT/IR-660 Plus, JASCO Co.). The surface of the aging specimens was studied. The sample chamber was in vacuum during the test. The light source used was a high-brightness ceramic light source.

3.2.2.6 Three-point bending test

The three-point bending test was conducted to determine the flexural properties of the CPT specimens after the long-term aging tests. A universal testing machine (AUTOGRAPH AGXplus, Shimadzu Co.) was used. The span of the supporters (L) was determined by the thickness of specimens. The ratio of the span to the thickness was 16:1. The bending load point radius was 5 mm. A thermostatic chamber was used to control the ambient temperature

for the duration of the test and a thermometer was used to monitor the real-time temperature of the specimens. The test was conducted at 25 ℃. Five specimens were tested in each group. The load speed was 1 mm·min^{-1}. The schematic of the set-up for the three-point test is shown as Figure 3-2. Equation 2-7 and 2-8 were used to calculate the strength and modulus.

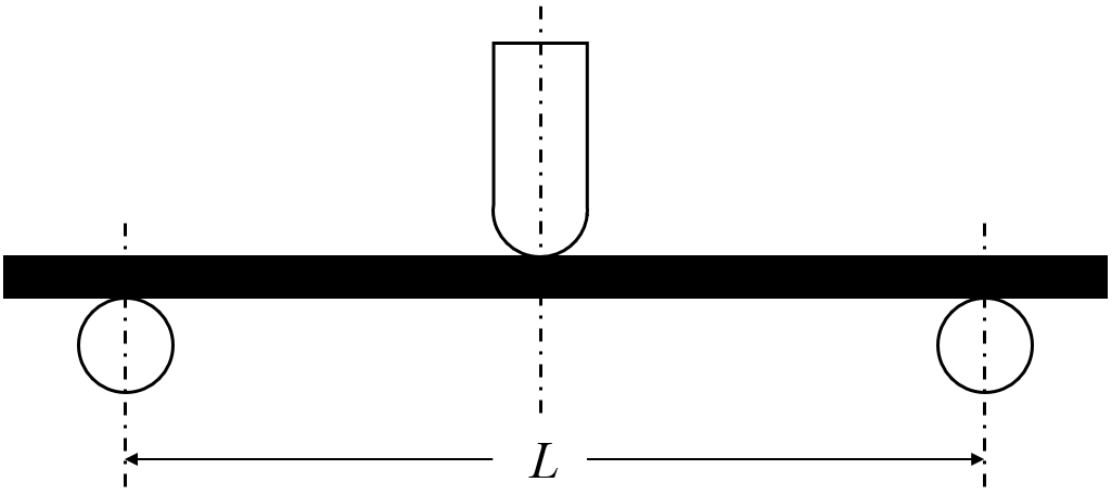

Figure 3-2 Setting of three-point bending test

3.3 Results and discussions

3.3.1 Barcol hardness test

The results of the Barcol hardness of the specimens are shown in Figure 3-3. As mentioned in chapter 2, the Barcol hardness of dry specimens is HBI-A 55, and that of saturated specimens in fresh and sea water are HBI-A 36 and HBI-A 37, respectively.

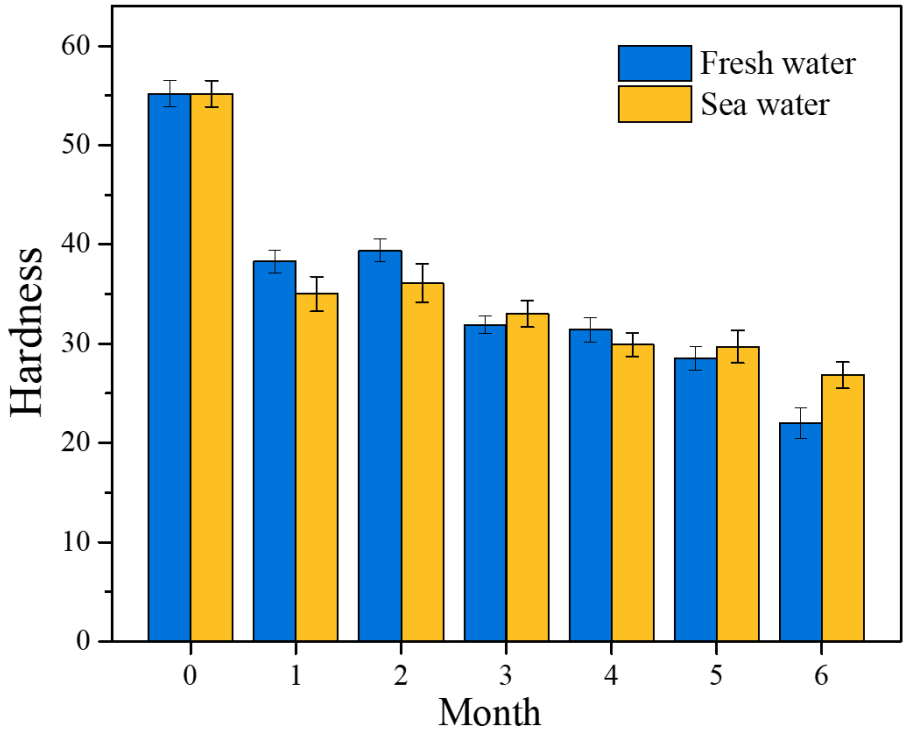

Figure 3-3 Barcol hardness of CPT material after long-term aging

When the aging time is not long, specimens aged in fresh water show higher hardness than specimens aged in sea water. The hardness of both specimens decreases with the increase in the aging time. When the aging time increases to 5 months, the hardness of specimens aged in fresh water obtains a larger decrease than the specimens aged in sea water. That is to say, the hardness of the specimens aged in sea water decreases steadily during the aging process, while that in fresh water decreases rapidly after 5-months aging. Compared with dry

specimens, the hardness decreases by about 60% and 50% in fresh water and sea water after 6-months aging, respectively. The results may be due to several reasons.

3.3.2 Micromorphology

The surface morphology can show the effects of long-term aging on material directly and the roughness of the specimen can be used to evaluate the degree of aging and degradation on the specimens more intuitively. Roughness results can be investigated by 3D laser scanning microscope. The micrograph and 3D laser scanning of the surface of a dry specimen is shown in Figure 3-4, and specimens aged in fresh and sea water are shown in Figure 3-5 and 3-6, respectively. Fifteen different areas on the specimen surface were used as evaluation areas to test the roughness, and the reported roughness is the average value of these 15 results. The roughness of a dry CPT material is 2.24 μm.

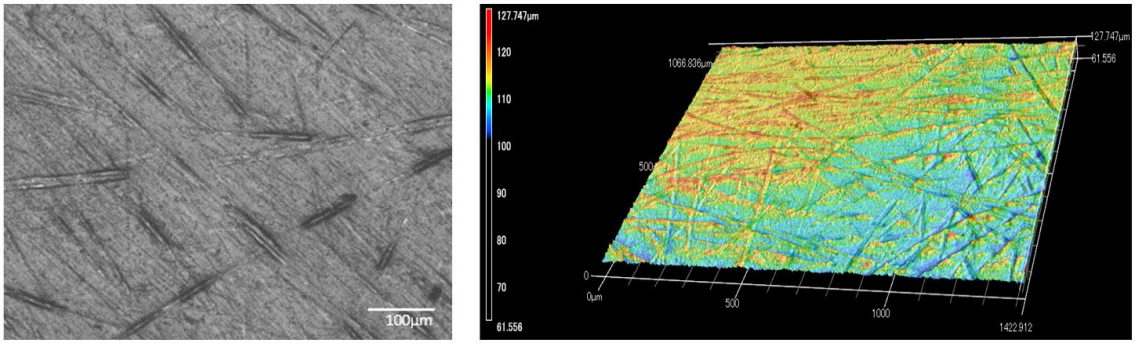

Figure 3-4 Micrograph and 3D laser scanning morphology of dry CPT specimen

For CPT specimens aged in fresh water, we can find that with the increase in the aging time, the changes in the surface happens according to Figure 3-5. When the aging time is less than 2 months, the exfoliation of resin appears near fibers, and with the extension of the aging time, more fibers which are originally covered inside gradually expose to exterior environment, indicating that resin decomposes and exfoliates under the attack of hot water.

But the results of 3D laser scanning do not show much difference.

When the aging time is extended to 3 months, more detectable phenomenon can be found, as Figure 3-5 (c) shows. Compared to (b), CF framework near the surface is completely exposed to the exterior in (c). The scale range also increases with the increase in the aging time. Because CFs are not thought to be corroded by water, the increasing range should be caused by the resin exfoliation.

With aging time extended to 4, 5 and 6 months, more profound changes in the surface can be observed. As shown in (d) and (e), cracks generate on the surface and propagate to the inner part of specimen. After 6-months aging, not only the resin, but also a layer of the matrix exfoliates from the matrix bulk. So even pores can also be observed near the surface area. The frameworks of CF appeared clearly in 3D laser scanning photos, showing that with the aging process, the surface resin exfoliates under the hydrothermal effects.

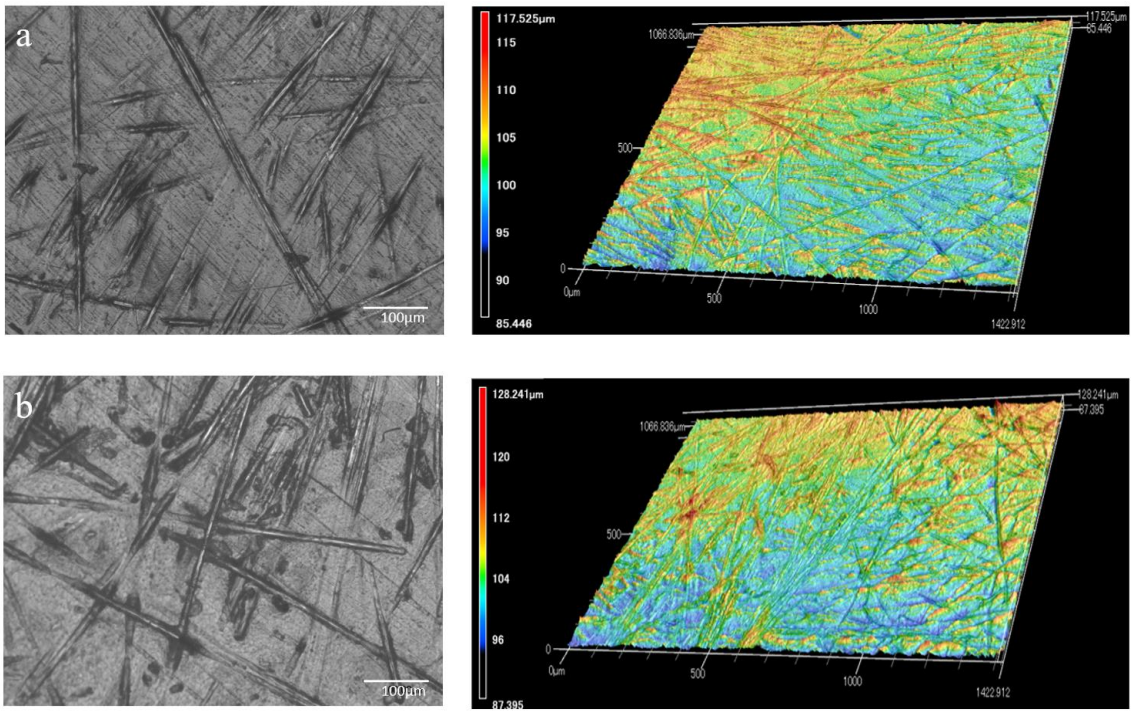

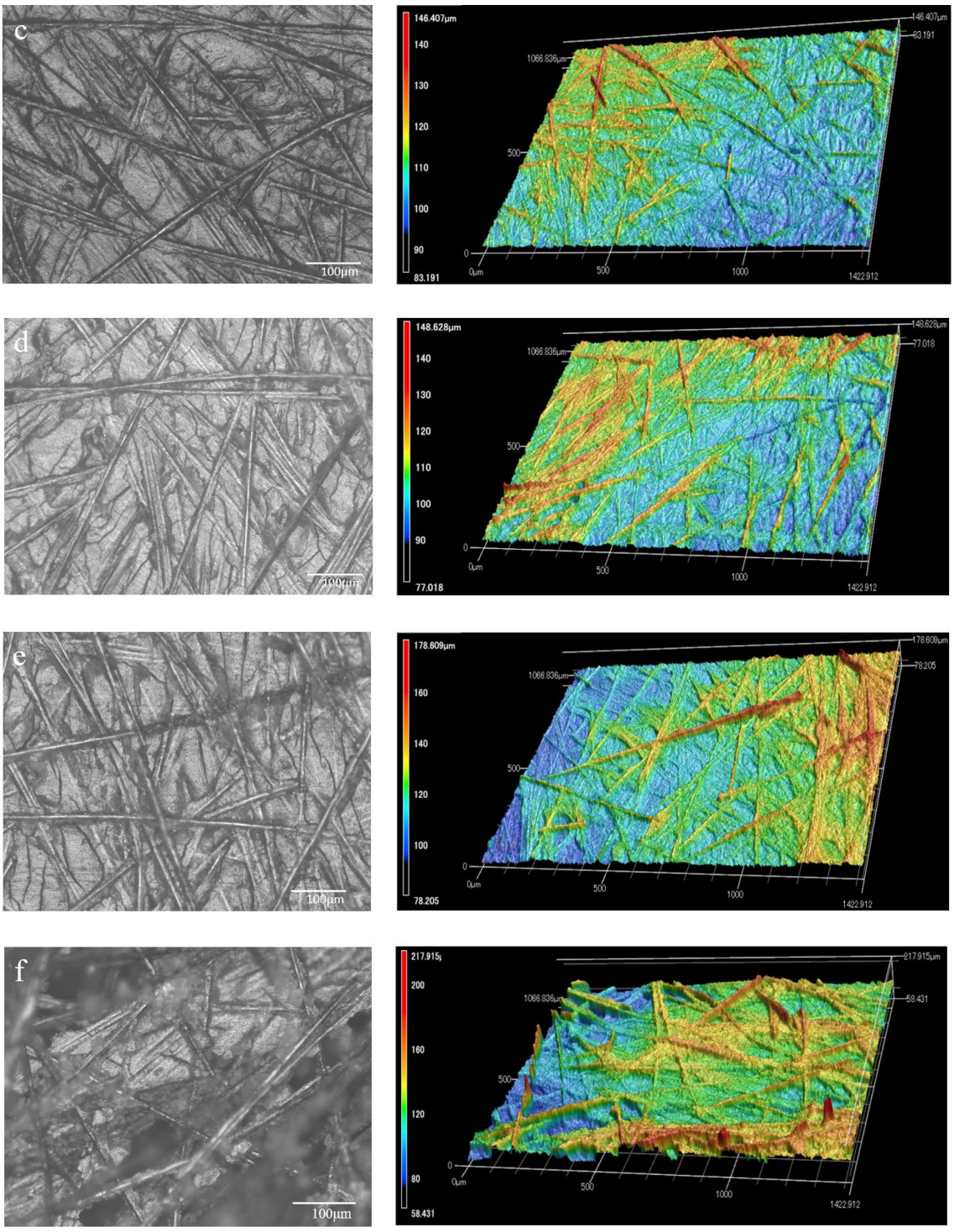

Figure 3-5 Micrograph and 3D laser scanning morphology of CPT specimens aged in fresh water after: (a) 1 month; (b) 2 months; (c) 3 months; (d) 4 months; (e) 5 months; (f) 6 months.

However, for CPT specimens aged in sea water, different results from that in fresh water can be detected. With the increase in the aging time, surface morphology changed slowly. Even when the aging time is extended to 6 months, the degradation and exfoliation of resin is not as serious as that in fresh water.

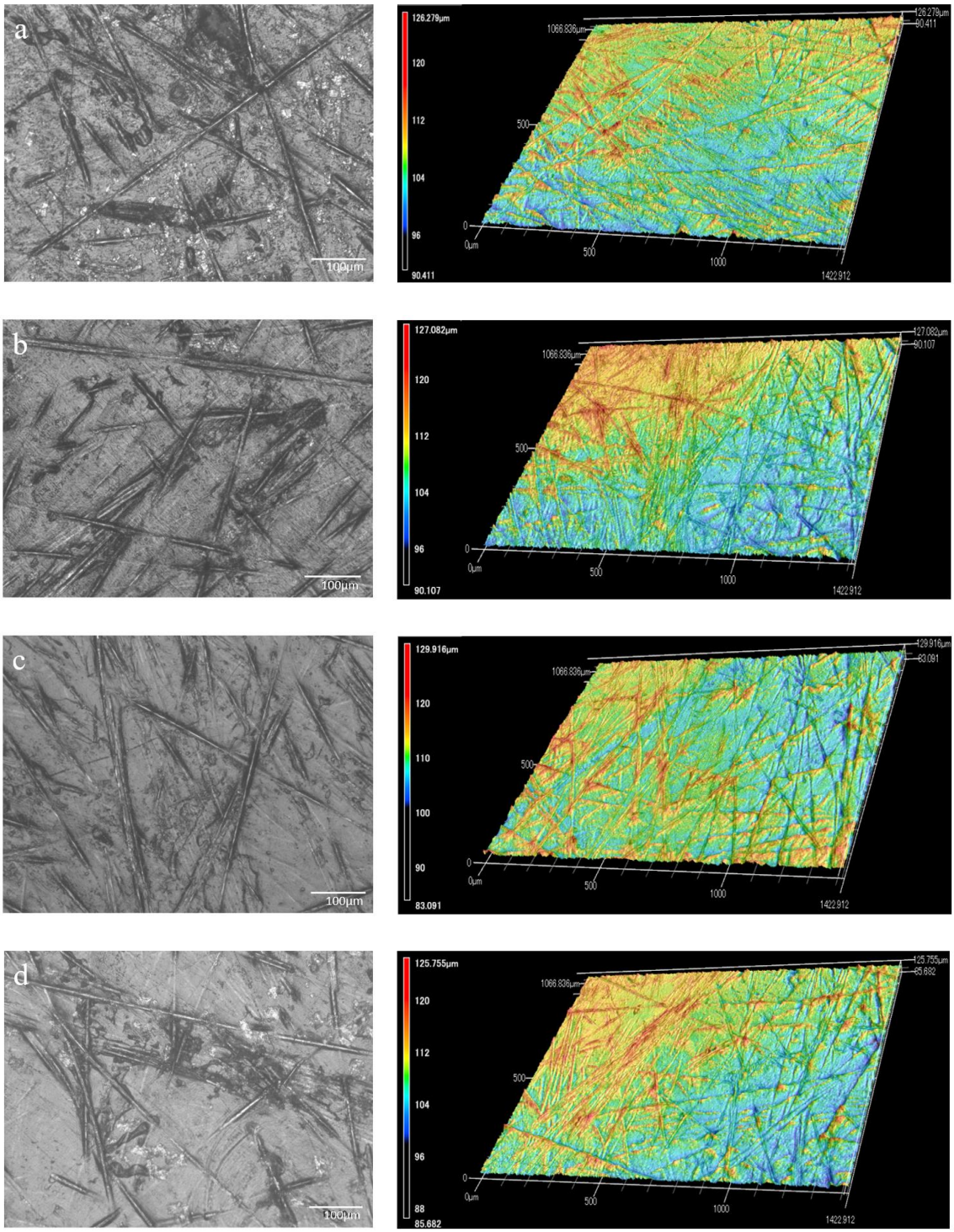

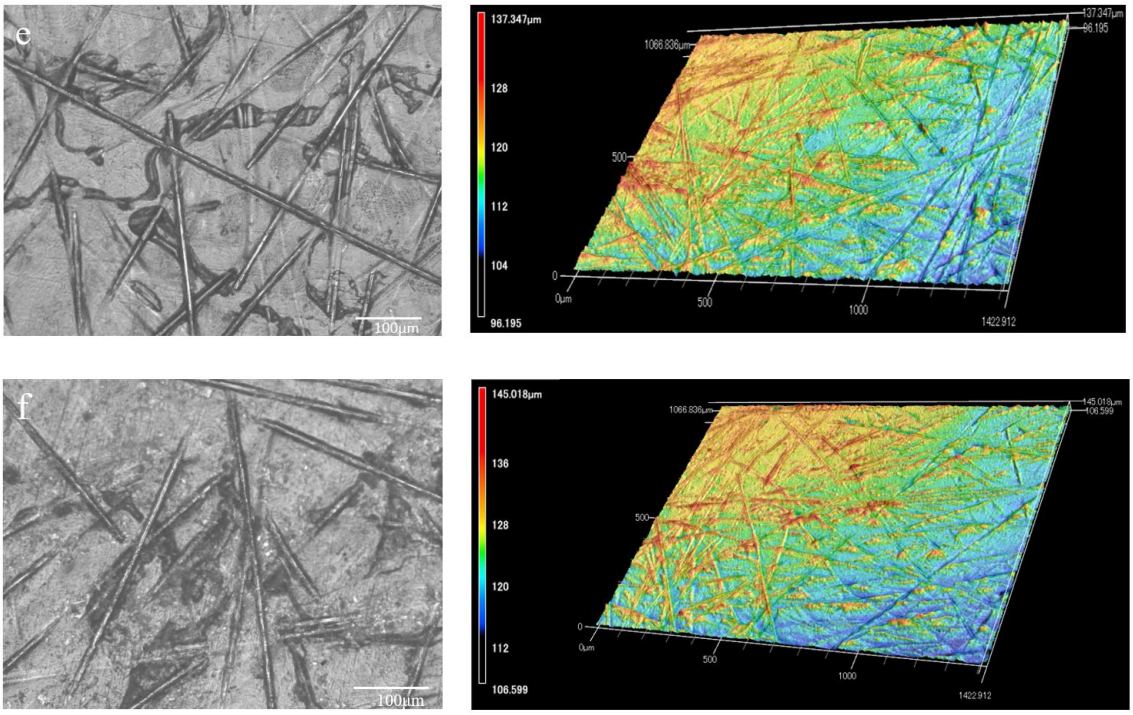

Figure 3-6 Micrograph and 3D laser scanning morphology of CPT specimens aged in sea water after: (a) 1 month; (b) 2 months; (c) 3 months; (d) 4 months; (e) 5 months; (f) 6 months.

Because of the various surface morphology, materials have different performance in Barcol hardness test. When the surface of the material is damaged, cracks occur and propagate, finally lead to matrix exfoliation from the matrix bulk, as the cracks and pores existing in Figure 3-5 (f). For this reason, the CPT specimen aged for 6 months in fresh water is more likely to be compressed like a sponge in Barcol hardness test. So, the hardness of CPT specimens aged for 6 months in fresh water decreased most significantly.

The results of roughness of these aged specimens were shown in Figure 3-7. The roughness of CPT aged in fresh water increases sharply after 4 months. The roughness after aging for 6 months is about 6 times of that of the dry specimen. But the roughness of specimens aged in sea water is relatively stable. So, CPT material may have better resistance to sea water than

fresh water in long-term use.

PA6 resin is weak to acid, because acid ions can neutralize some carboxyl and amino groups and accelerate the reaction equilibrium of amide bond breaking. But PA6 is alkali and salt solvent resistant. Generally, sea water is weakly alkaline due to the hydrolysis of weak acid anions. The pH value of sea water has little change, generally about 8.0. Therefore, the aging of CPT material in fresh water is more serious than that in sea water.

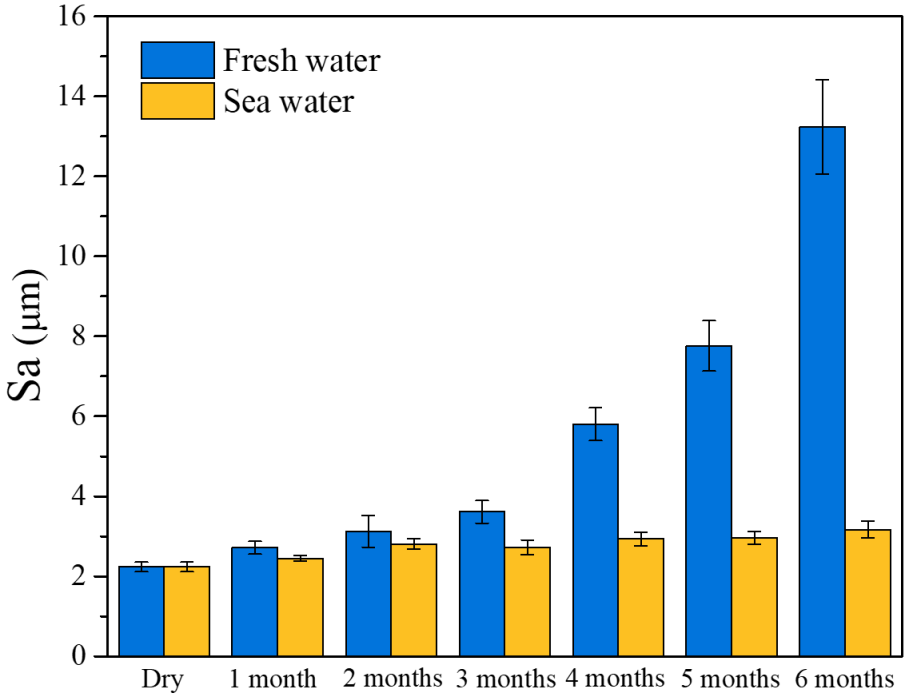

Figure 3-7 Surface roughness of CPT specimens after long-term aging

3.3.3 Differential scanning calorimetry analysis

Another reason for the decrease in the hardness may be the change in the crystal form. So, DSC test was employed to study the thermodynamic and crystallization behavior of CPT material after long-term aging. Usually, crystallization improves the tensile and flexural strength of plastics. Crystallinity (X_c) is used to express the proportion of crystallized area in

polymer. X_c can be calculated by Equation 3-2:

$$X_C(\%) = \frac{\Delta H_m}{(1-\lambda)\Delta H_m^0} \times 100 \qquad \text{Equation 3-2}$$

where ΔH_m is the melting enthalpy of specimens, which can be obtained from DSC result, ΔH_m^0 is the enthalpy value of melting 100 % crystalline form of PA6 ($\Delta H_m^0 = 240\ \mathrm{J \cdot g^{-1}}$ [97]), and λ is the mass fraction of CF, which is 28.2% is CPT material.

The results of thermodynamic properties are summarized in Table 3-1 and 3-2. T_o is the onset melting temperature, T_e is the end melting temperature and T_p is peak melting temperature. These parameters are helpful to judge the crystallinity and crystallization behavior of materials.

For dry CPT material, T_o is 185.4 °C, T_e is 237.0 °C, T_p is 225.6 °C, and $\triangle H_m$ is 45.15 J·g^{-1}. So, the calculated X_c is 26.21%. As shown in the table, with the increase in the aging time, X_c of specimens decreased by about 15.5% and 11.4% in fresh and sea water, respectively.

Table 3-1 DSC results of CPT specimens aged in fresh water

	T_0 (°C)	T_e (°C)	T_p (°C)	$\triangle H_m$ (J·g^{-1})	X_c (%)
1 month	183.7	237.0	225.9	46.59	27.04
2 months	184.8	236.0	224.8	47.06	27.31
3 months	182.1	235.5	222.2	47.03	27.30
4 months	180.4	232.7	222.3	47.05	27.31
5 months	171.2	231.5	221.5	42.82	24.85
6 months	168.9	231.0	220.1	39.34	22.83

Table 3-2 DSC results of CPT specimens aged in sea water

	T_0 (°C)	T_e (°C)	T_p (°C)	$\triangle H_m$ (J·g^{-1})	X_c (%)
1 month	187.2	236.8	226.7	42.38	24.60
2 months	187.2	235.5	225.6	41.85	24.29
3 months	186.2	235.1	225.7	41.56	24.12
4 months	186	234.2	224	40.06	23.25
5 months	184.2	230.4	222.8	37.62	21.84
6 months	178.2	230.0	221.9	37.54	21.79

Another important result is the changes in the T_o, T_e, and T_p. The three temperatures move towards low temperature after aging. For CPT specimens aged in fresh water, compared to dry specimens, T_o decreases by about 16 °C, and T_e decreases by about 6 °C after 6-months aging. T_p also decreases by about 6 °C, indicating that a different crystal form is formed during the aging process. Similarly, for CPT specimens aged in sea water, T_o decreases by about 9° C, T_e decreases by about 7 °C and T_p decreases by about 4 °C after 6-months aging, which are less than the values in fresh water.

The changes in the three temperatures can also be found in DSC figure. The DSC curves of the aged CPT specimens in fresh and sea water are shown in Figure 3-8 and 3-9, respectively. The positive direction of Y axis represents exothermic process.

In fresh-water aging, the melting peak become wider as the aging time increased. And the onset and end melt temperature also move towards low temperatures. However, at the same time, the intension of the melting peak around 220 ℃ decreases. Besides a small peak appears around 200 °C when the aging time is extended to 4 months, and the intension of this peak gradually become larger with the increase of aging time. Generally, PA6 resin has 2 crystal forms, namely α and γ-crystal. The content of the two crystal forms is mainly affected by processing conditions and additives. PA6 is easy to show α-crystal structure when crystallized

or compressed at high temperature, while it is easy to form γ-crystal structure when crystallized or injected at low temperature. PA6 in different crystal forms has different mechanical properties. α-crystal is favorable for improving the strength, while the γ-crystal can improve the toughness. Because CPT specimens were made by compression molding at high temperature, most of the crystal form of PA6 should be α-crystal, which has a higher melting peak around 220 ℃. But the peak melting temperature of γ-crystal is lower than α-crystal, which is around 200 ℃. Therefore, γ-crystal is softer and less stable than α-crystal. The crystal form of PA6 in CPT is α-crystal when the specimens were just immersed in water. But during the aging process, α-crystal gradually transfers into γ-crystal. So, the melting peak become wider, and a lower peak appears [40].

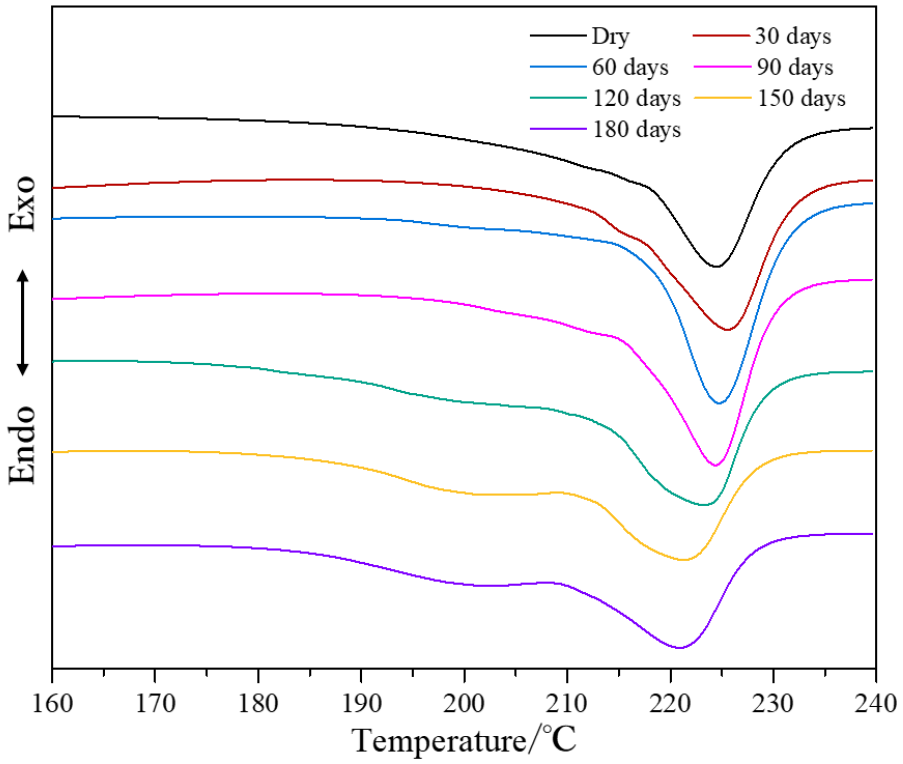

Figure 3-8 DSC curves of CPT aged in fresh water with a heating rate of 10 K·min^{-1} under different aging time

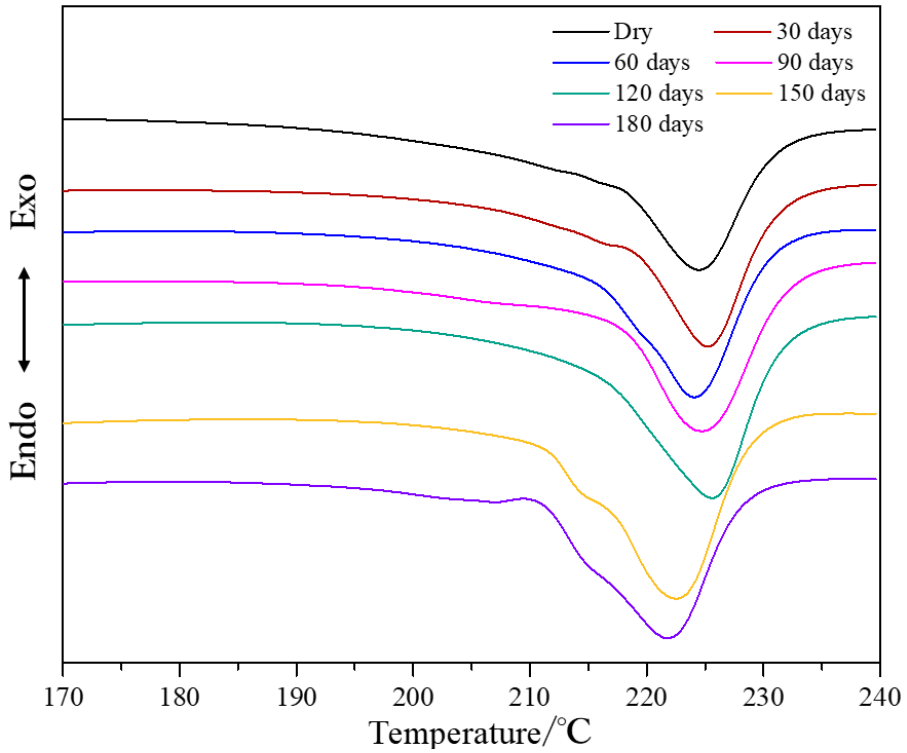

Figure 3-9 DSC curves of CPT aged in sea water with a heating rate of 10 K·min^{-1} under different aging time

In sea water, the melting peak is not as wide as that in fresh water. But the decrease in the onset and end melting temperature can also be found. A small peak also appeared in 207 ℃ only on the curve of specimens aged for 6 months. The intension of the peak is also less than that in fresh water. In conclusion, long-term exposure to water molecules leads to the transfer of crystal form of PA6 resin, but it is not as serious as in fresh water.

Thus, the long-term aging in water environment negatively affects the thermodynamic properties of CPT material. The crystal form of PA6 changes under the action of water from the harder crystal form to the softer crystal form. So it is one reason that the hardness of CPT material decreases after long-term aging.

3.3.4 Fourier-transform infrared analysis

In order to investigate the possible chemical reactions of PA6 resin during the aging process, FTIR test was conducted. Specimens aged for 2,4 and 6 months in fresh and sea water are taken as example, as shown in Figure 3-10 and 3-11.

Some peaks of aged CPT material are shown in Figure 3-10. Table 3-3 summarizes the detailed information of the assignment of IR bands for CPT material [58, 60]. The stretching and deformation vibration of C=O, C-N, and C-C-N structure in amide bond indicate the chemical structure of PA6. According to Figure 3-11, the peak intensity of the absorption related to most bands evolved progressively after ageing. During long-term aging, the peaks rise similarly for both water media.

Table 3-3 Typical peaks of PA6 in Figure 3-10

IR Band (cm^{-1})	**Assignment [58,60]**
3290	Hydrogen-bonded N-H stretching vibration in the crystalline phase
2930	Asymmetric CH2 stretching vibration
2850, 2049	Symmetric CH2 stretching vibration
1634	C = O,C-N stretching & C-C-N deformation vibration
1537	N-H in plane bending & C-N, C-C stretching vibration
1261	Amide III

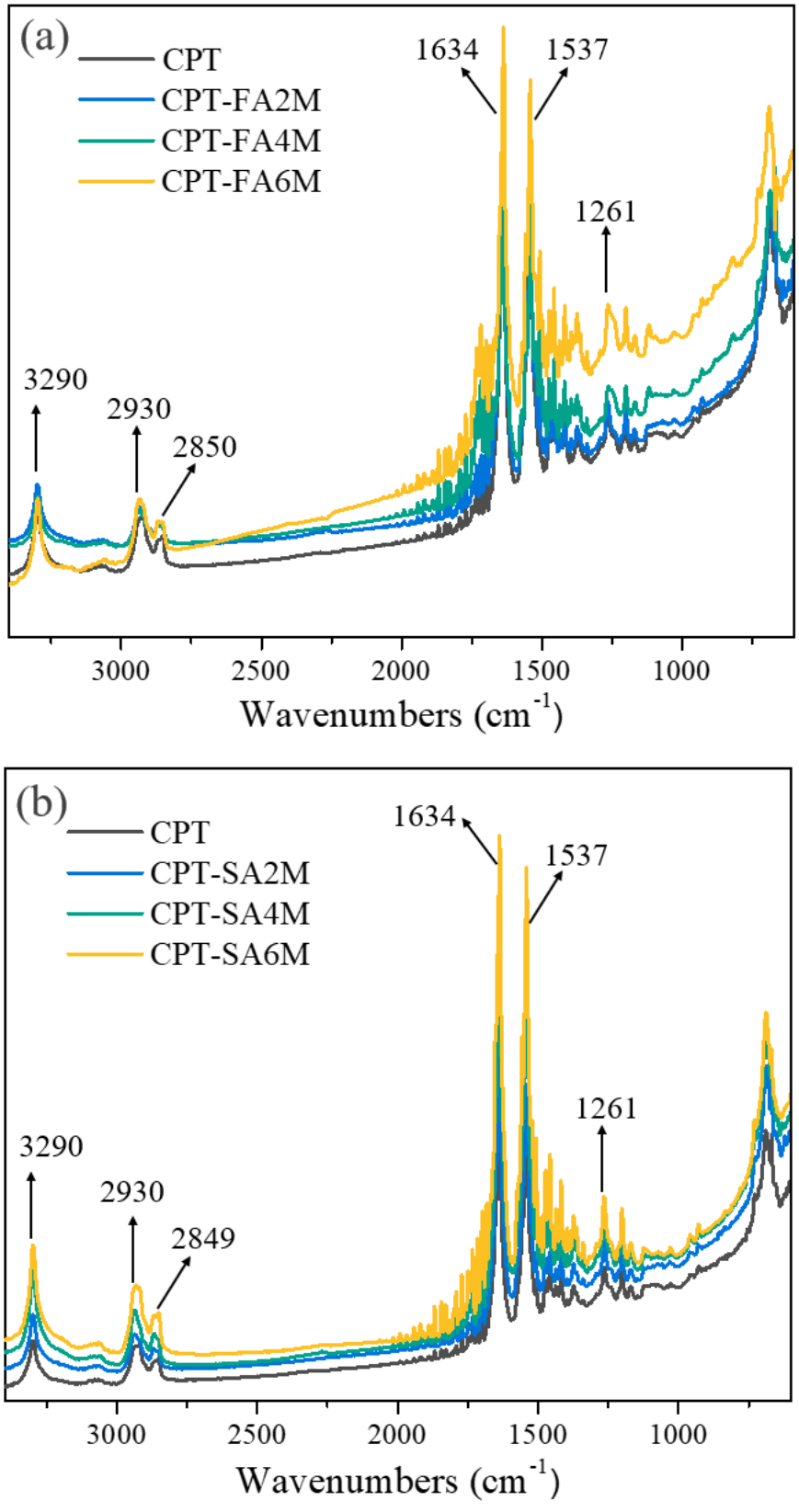

Figure 3-10 FTIR of CPT aged in (a) fresh water; (b) sea water

Generally, wavenumber between 1700 cm^{-1} and 1760 cm^{-1} is the typical area for carbonyl structure. So, the FTIR result in the carbonyl area are shown in Figure 3-11. As we can see from the figure, when the aging time increases, the intensity of three marked peaks increases, indicating the generation and increase in the three structures in PA6. The information of the three peaks are shown in Table 3-4 [58, 60]. Chemical structures of the three peaks are shown in Figure 3-12. Peak in 1749 cm^{-1} has been attributed to the formation of aliphatic carboxyl group, peak in 1735 cm^{-1} has been related to the formation of ester group, and peak in 1718 cm^{-1} has shown the relationship with the formation of ketone group. The appearance of these peaks suggests the degradation of the CPT materials occurs owing to the long-term aging exposure. In addition, comparing the spectra of CPT aged in fresh and sea water, the higher the three peaks are and the larger the absorption area is, the more fracture polymer chain happens. So, more PA6 decomposed in fresh water than in sea water. The FTIR results are consistent with the micromorphology of surface and surface roughness mentioned in 3.3.2.

Table 3-4 Three marked peaks in Figure 3-11

IR Band (cm^{-1})	**Assignment [58,60]**
1749	Aliphatic carboxyl group
1735	Ester group
1718	Ketone group

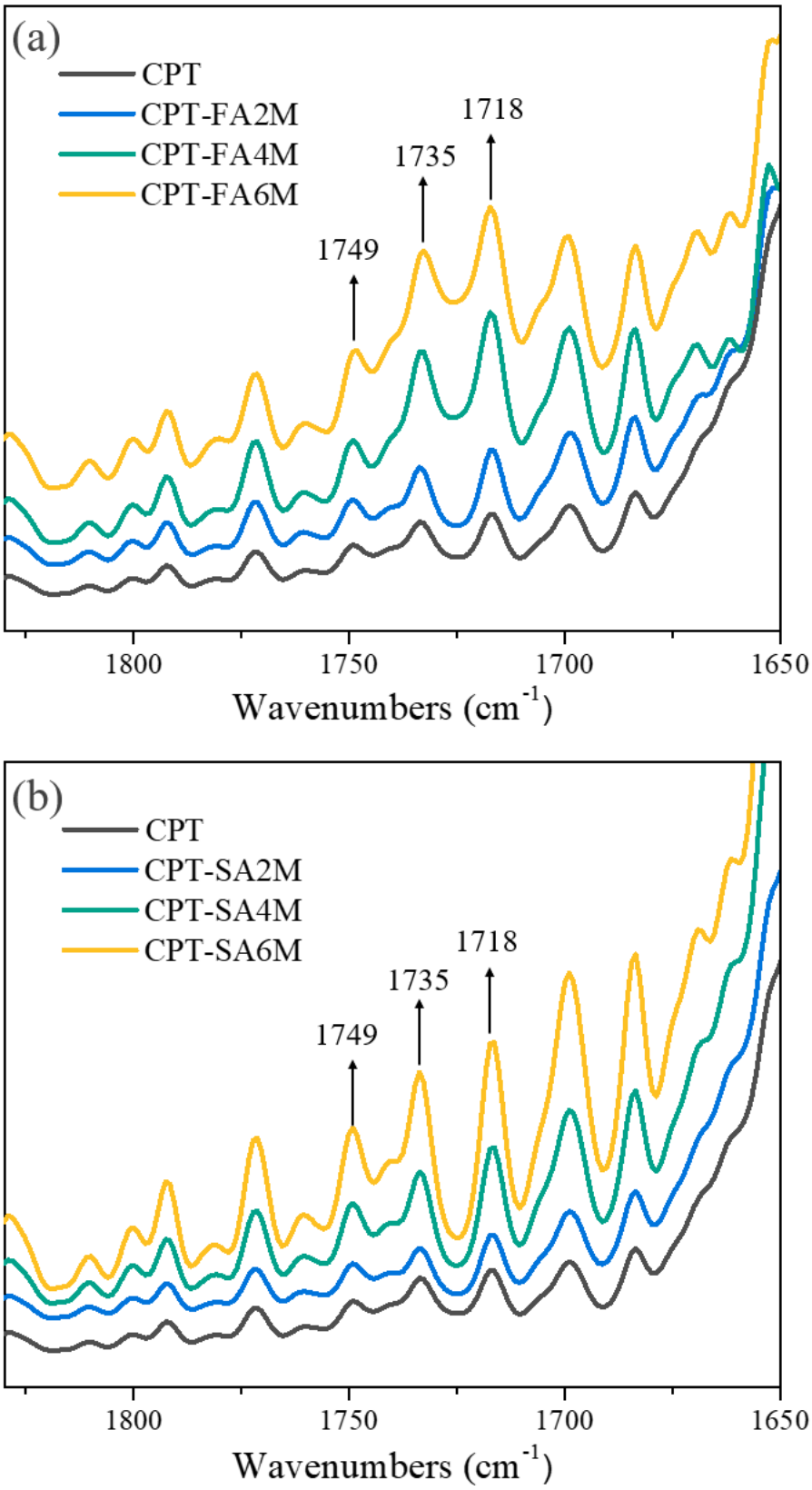

Figure 3-11 FTIR in the carbonyl area of CPT aged in (a) fresh water; (b) sea water

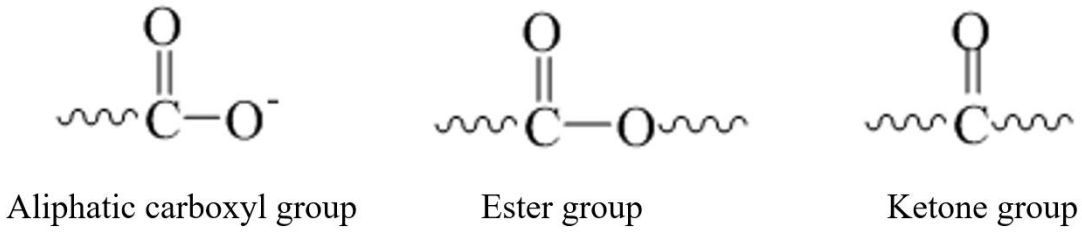

Figure 3-12 Chemical structures of the three peaks in Figure 3-11

During the long-term aging exposure, the amide bond (- CONH -) of PA6 resin is converted to carboxylate (- COOM), as shown in Figure 3-13 [38]. Hot water molecules attacked amide bonds in PA6, causing hydrolysis of the structure, indicating that the functional groups mentioned in Table 3-4 are generated in this process. The result proves the scission of polymer main chain of PA6 in CPT material during the long-term aging exposure.

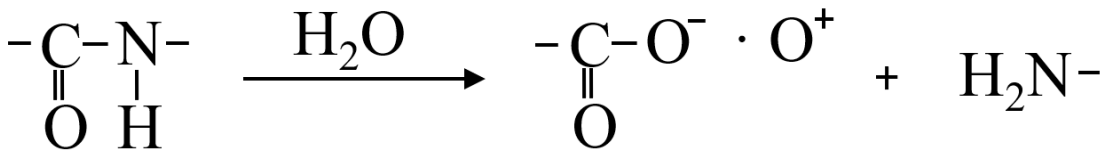

Figure 3-13 Possible degradation reaction of PA6 during long-term aging process [38]

The degradation reaction of the main chain of PA6 resin mentioned above results in the decrease of the average molecular weight of polymer, which leads to the decrease in the mechanical properties of resin.

3.3.5 Three-point bending test

3.3.5.1 Experimental results

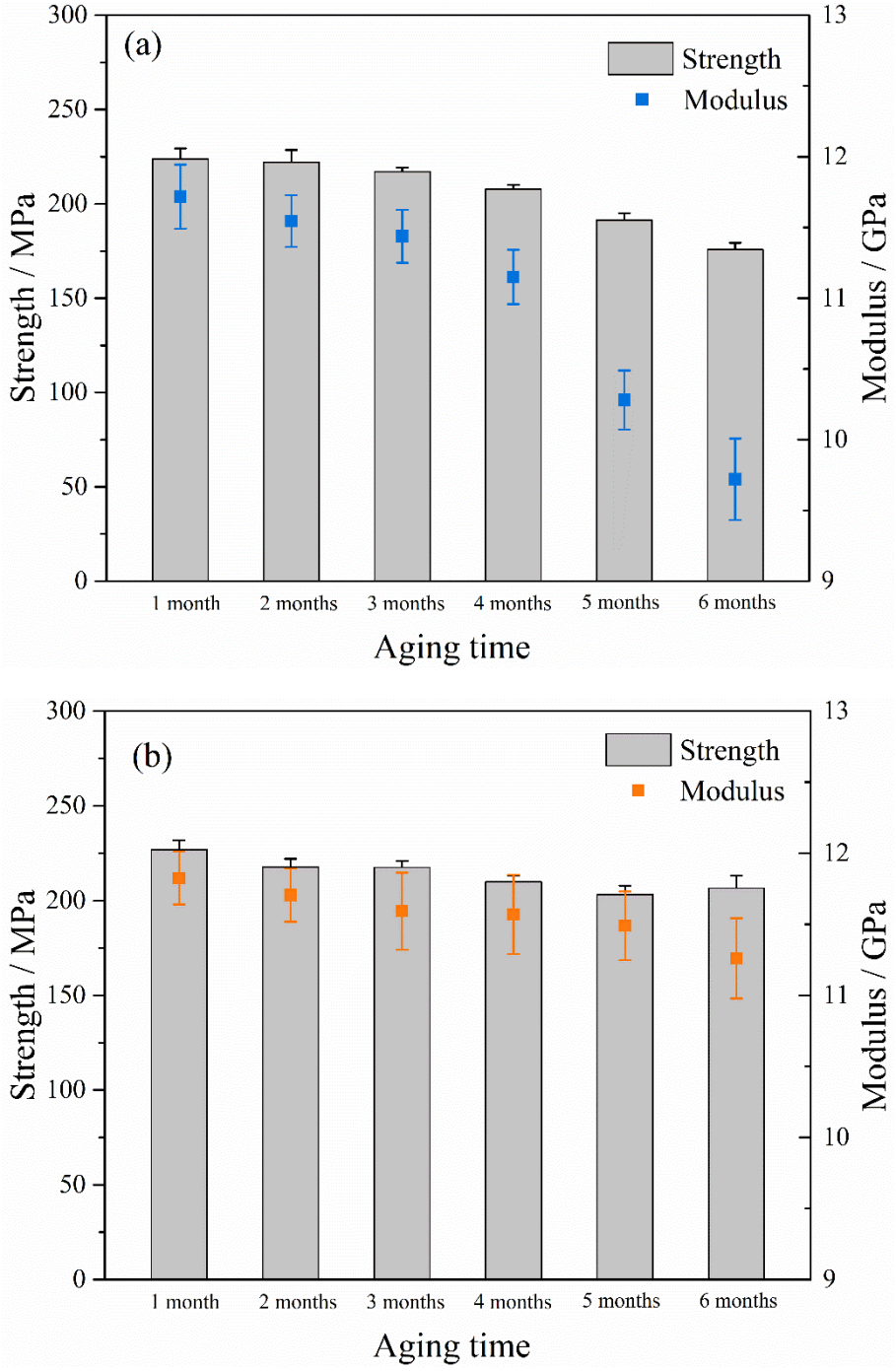

Figure 3-14 Flexural properties of CPT specimens after long-term aging: (a) in fresh water, (b) in sea water.

The mechanical properties of aged CPT material were also investigated by three-point

bending test. Relative results are shown in Figure 3-14. The flexural strength and modulus of CPT in fresh water keep stable in the first three months of aging but began to slowly decrease from the fourth month, and finally a detectable decrease can be found from the fifth month. The modulus after 6-month aging decreases by about 17% compared with the modulus at the first month of aging. However, in sea water, the flexural strength almost maintains stable value. The flexural modulus declines slowly during the whole aging process. The difference in the decrease in the hardness, the different surface morphology and chemical structures of resin between CPT material aged in fresh and sea water shows consistency with the results of three-point bending test.

3.3.5.2 Rule of Mixture (RoM) and Factor *C*

3.3.5.2.1 Rule of Mixture (RoM)

In order to describe the difference between fresh and sea water better, rule of mixture (RoM) is employed to analyze the changes in flexural properties. The well-known RoM is a practically analytical method to predict the mechanical properties of fiber reinforced composite material. It is used to predict the upper- and lower-bound on various properties of unidirectional and continuous fibers reinforced composite materials. The RoM states that the property in the direction along fibers may be as high as Equation 3-3 shows:

$$E_c = E_f V_f + E_m V_m \qquad \text{Equation 3-3}$$

E_f and E_m are the mechanical properties of fibers and resin, and V_f and V_m are the volume fraction of the fibers and resin, respectively. The schematic diagram of the representative volume element(RVE) in the RoM is shown in Figure 3-15 [98].

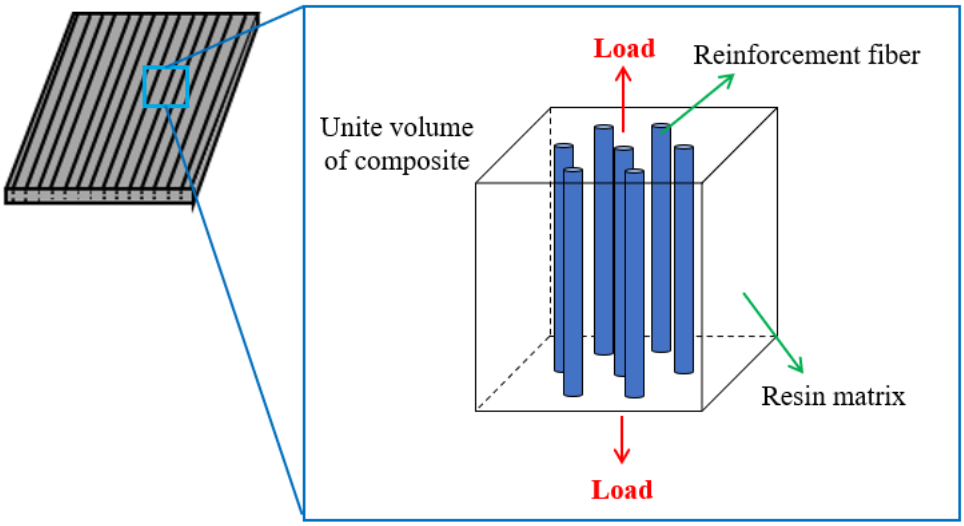

Figure 3-15 Representative volume element in unidirectional fiber reinforced composite [98]

However, the RoM is based on unidirectional fiber reinforced composite material. There are several assumptions that are preconditions to use this theory. First, the constituent volume fraction in the representative volume element are assumed to be the same as those in the actual composite. Second, the perfect bonding at the interface is assumed. Finally, the fiber and matrix materials are assumed to be linearly elastic and homogeneous.

3.3.5.2.2 Factor *C* and modified Rule of Mixture (MRoM)

The RoM only applies to unidirectional and continuous fibers reinforced composite. However, in discontinuous fiber reinforced composite system, such as the CPT material, the fiber orientation and continuity are not as perfect as the assumptions mentioned above, as Figure 3-16 [98] shows. Thus, the RoM is not suitable to predict the mechanical properties of discontinuous fiber reinforced composite system unless the theory is modified.

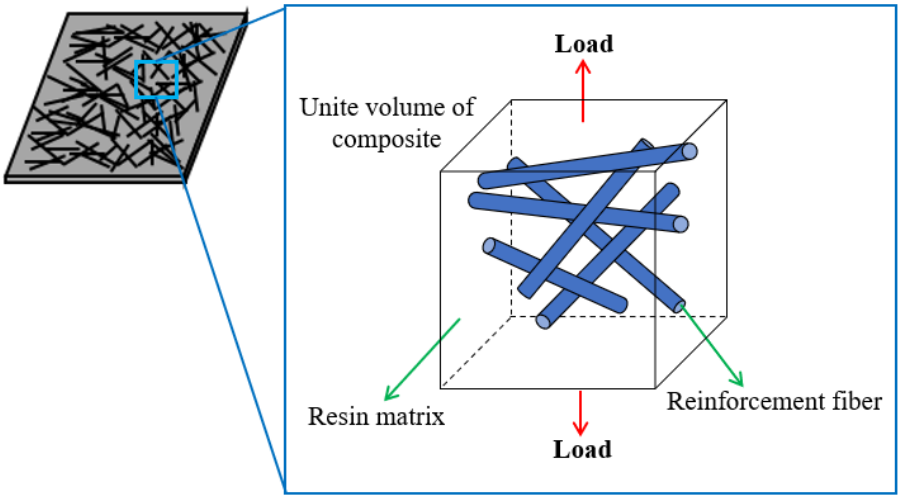

Figure 3-16 Representative volume element in discontinuous fiber reinforced composite [98]

Because the reinforcement efficiency in actual composite manufacturing is not as promising as assumed, a new factor, *C* is introduced to the RoM, and the modified RoM (MRoM) is as shown in Equation 3-4.

$$E_c = C_1 C_2 E_f V_f + E_m V_m \qquad \text{Equation 3-4}$$

Here, C_1 represents the factor for fiber orientation distribution (FOD), and C_2 is the factor for fiber length distribution (FLD). The experimental results will be used to determine the factors *C* in CPT material. Usually, C_1 and C_2 can be estimated by empirical equations, and related to the critical length of fibers.

In general, CPT material is in-plane isotropic, so C_1 can be estimated by the empirical equation as shown in Equation 3-5.

$$C_1 \approx \frac{1}{\pi} \qquad \text{Equation 3-5}$$

3.3.5.2.3 Critical length and Kelly Tyson model

The factor C_2 represents the FLD in discontinuous fiber reinforced composite system. In order to calculate the value of C_2, the critical length of fibers should be discussed, because fibers longer than the critical length and shorter than the critical length have different effects on C_2 value, as Equation 3-6 shows.

$$C_2 = \sum_{L_i=L_{min}}^{L_c} \frac{L_i}{2L_c} + \sum_{L_i=L_c}^{L_{max}} (1 - \frac{L_c}{2L_i}) \qquad \text{Equation 3-6}$$

where L_i is the fiber length in a given FLD, and L_c is the critical length of fibers [99].

On the other hand, a famous Kelly-Tyson model is applied to calculate the IFSS of composites by considering the influence of fiber length. Assuming the shear stress is constant along fiber direction, the IFSS can be determined through Kelly-Tyson model. So, according to Kelly-Tyson model, L_c can be calculated by the following equation:

$$L_c = \frac{\sigma_f d}{2\tau} \qquad \text{Equation 3-7}$$

where σ_f is the ultimate fiber strength at a critical length and can be calculated by Equation 3-8.

$$\sigma_f = \sigma_0 \left(\frac{L_0}{L_c}\right)^{\frac{1}{m}} \Gamma(1 + \frac{1}{m}) \qquad \text{Equation 3-8}$$

L_0 is the reference gauge length for volume correction, Γ is the gamma function, σ_0 is the scale parameter (characteristic stress) and m is the Weibull modulus, which is also known as the shape parameter of the distribution [100].

The critical length can be calculated by Kelly Tyson model. The parameters used for calculation are summarized in Table 3-5, which come from some relative researches [100, 101]. The IFSS results come from the droplet test mentioned in chapter 2.

Table 3-5 Parameters for Kelly-Tyson model [100, 101]

Gamma function Γ	Reference gauge length L_0 (mm)	Weibull modulus m	Scale parameter σ_0 (MPa)	IFSS σ (MPa)		
				Dry	Fresh water	Sea water
0.92414	10	5.6	4920	49.68	29.25	34.97

So, the critical length of carbon fibers in dry, fresh water saturated, and sea water saturated CPT specimens can be estimated by using Equation 3-7 and 3-8. The results are listed in Table 3-6. It can be seen from the results that after water absorption, the critical length of carbon fibers in CPT increases, and the L_c value in fresh water is larger than that in sea water, indicating a weaker interfacial stress in fresh water.

Table 3-6 Critical length of carbon fibers in dry, fresh water saturated, and sea water saturated CPT specimens

	Dry	Fresh water	Sea water
Critical length L_c (mm)	0.5330	0.8354	0.7179

The length of carbon fibers in CPT is 6mm, which is larger than the critical length calculated above. And the FLD can be neglected because CPT is a commercial product with a stable property. So, for simple calculation, Equation 3-6 can be simplified to:

$$C_2 = 1 - \frac{L_c}{2L_i} \qquad \text{Equation 3-9}$$

L_i is the fiber length, which is 6 mm.

3.3.5.2.4 Description of the flexural properties after long-term aging by MRoM

The values of C_1 and C_2 are calculated by Equation 3-5 and 3-9. So, the E and σ of CPT specimens after long-term aging are estimated by MRoM as Equation 3-4 shows. Table 3-7 gives the value of C_1 and C_2 and the calculated results of flexural modulus and strength. The reduction of E_c and σ_c are the ratio of the value of this property reduced compared to the dried specimens.

Table 3-7 C_1 and C_2 and the calculated results of flexural modulus and strength by MRoM

	Dry	Fresh water	Sea water
L_c (mm)	0.5330	0.8354	0.7179
C_1	0.3183	0.3183	0.3183
C_2	0.9556	0.9304	0.9402
E_c (GPa)	16.18	15.80	15.95
Reduction of E_c	/	2.35%	1.44%
σ_c (MPa)	267.9	260.9	263.6
Reduction of σ_c	/	2.64%	1.61%

Meanwhile, the retention ratio is also defined as the ratio of the mechanical property of the aged specimens at different aging time to that of the unaged specimens. Figure 3-17 shows the retention ratio of the flexural modulus and strength of specimens aged in fresh water and sea water. In the figure, the difference in decreasing trends can be more easily found. After 4 months aging, the changing trends of the two groups of specimens became different. Comparing the results, the reduction ratio, calculated by MRoM is smaller than that shown in Figure 3-17. So, the decline in flexural properties is not only caused by the decrease in the IFSS, which is proved by MRoM, but the degradation of resin also plays an important role in

the degradation. This result is also proved by surface morphology and FTIR.

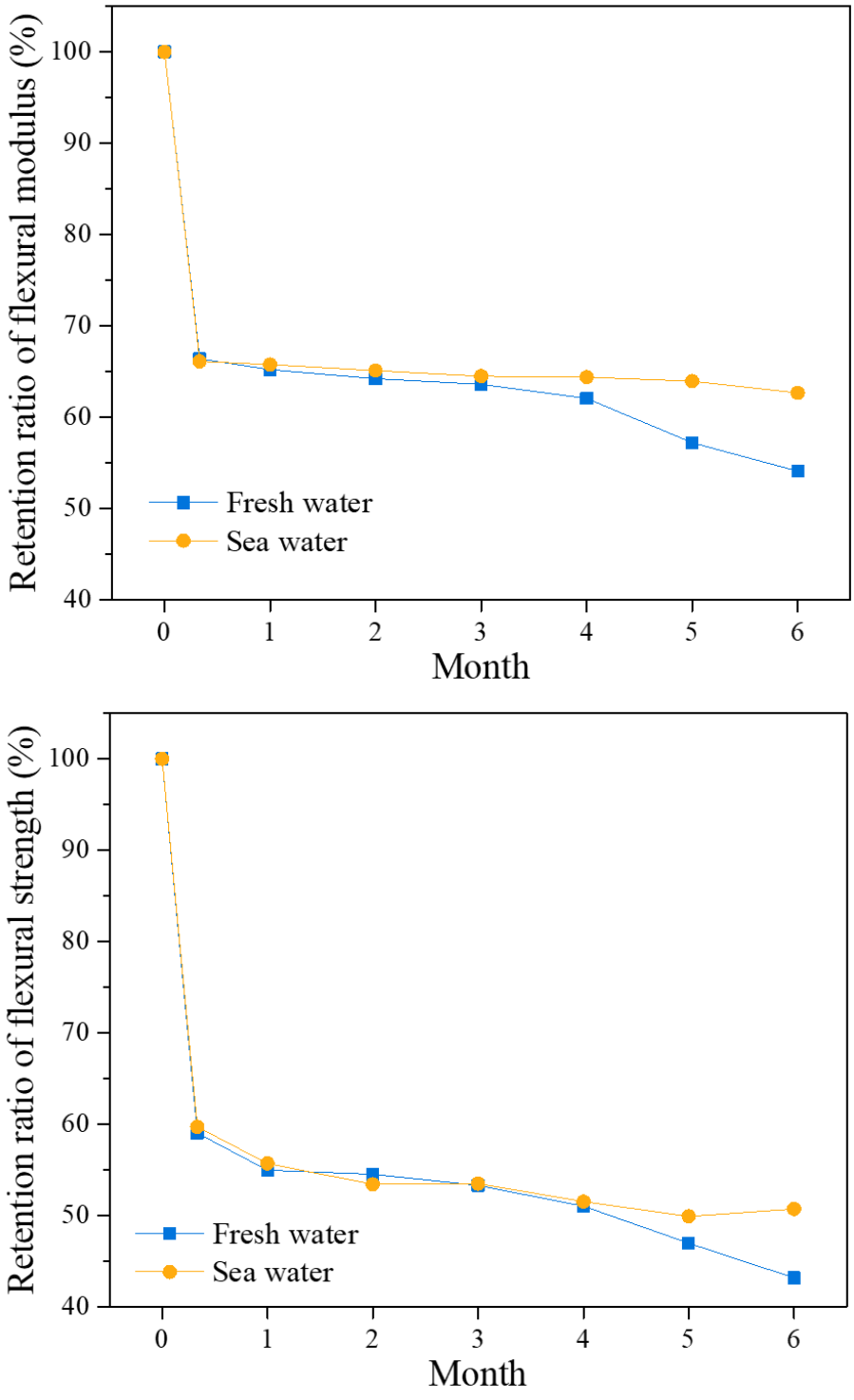

Figure 3-17 The retention ratio of the flexural modulus and strength of specimens aged in fresh water and sea water

3.3.6 Conclusion

In this research, the performance of CPT material after long-term aging in fresh and sea water was investigated.

To sum up, the hardness of CPT specimens aged in fresh water is lower than that in sea water after 6-month aging. The crystal form of PA6 resin in CPT material partly changes from α-crystal to γ-crystal, resulting in the decline of thermodynamic properties. In addition, the resin on the surface of specimens began to decompose after aging in water, and the aging is more severe in fresh water than in sea water. The MRoM was employed and the results is consistent with the results mentioned above.

3.4 Summary

In this study, the effects of the long-term aging in fresh and sea water environment were researched. The long-term aging is proven to have significant effects on the performance of CPT specimens. When other test conditions remain unchanged, the performance of CPT specimens depends on the length of aging time.

The long-term aging in water environment negatively affects the properties of resin matrix of CPT material. Some of the PA6 crystal in CPT material transfers from a α-crystal form to a γ-crystal form, and the degree of crystallinity of PA6 decreases with the long-term aging, leading to a lower melting temperature and lower hardness of CPT material. And CPT aged in fresh water has more γ-crystal form after 6-month aging than that in sea water. Besides, PA6 resin decomposes and the polymer chains tend to break with the increase in the aging time, in both water environment. However, fresh water has more serious influence on polymer chain scission than sea water, indicating a better resistance of CPT material to sea water than to fresh water.

Furthermore, the modified rules of mixture are established. The estimated results indicate that the decline of the flexural properties of CPT after long-term aging is not only affected by the decrease in IFSS, but also mainly influenced by the decrease in the strength of resin after degradation. Therefore, the degradation of PA6 resin in CPT material for a long-term use needs to be considered and prevented.

This study also provides guidance for future use of this material in water rich environment for a long period. And the application related to sea water can be further developed.

Chapter 4. Analysis of the effects of thermo-oxidative aging on the performance of CPT material

4.1 Introduction

Contrary to the previous discussion on the influence of water environment, the effects that will be discussed in this chapter is about fire. In 2019, several huge fire disasters occurred in the world. Among the representative ones, the six-month-long mountain fires in Australia have had a profound impact on local ecology and global climate. The fire in Notre Dame de Paris has caused irreparable damage to human culture and art. Back to Japan, the fire in Shurijo Castle has brought great loss to Japanese traditional culture. And the vicious arson crime that was committed in Kyoto animation company even killed over 30 people.

Thus, in order to deal with fire disasters more properly, it is necessary to increase the speed

of response to fires. New materials for fire disaster rescue are also required. Fire-fighting equipment used at this stage includes fire engines, fire-fighting robots, unmanned aerial vehicle, etc. From the perspective of convenience, mobility and flexibility, fire-fighting tools calls for a low weight, good water and thermo-oxidative resistance.

For fire-fighting equipment, usually two types exist. First is the fire robot that directly do deep into the fire site for fire-fighting and rescue. Another type includes the unmanned aerial vehicle or remote water gun robot, which are used for monitoring the real time development of fire and remote fire control by water spray. Because this type of fire-fighting equipment has medium distance to the fire sites, the ambient temperature of the equipment is not very high, so, the use of resin matrix composites has become possible. As discussed in former chapters, CPT material shows relatively low weight, acceptable mechanical properties and some other advantages that the short, semi-long carbon fiber reinforced plastics have. So, the research objective in this chapter is the effect of thermo-oxidation on the mechanical properties of CPT material.

4.2 Material and experiments

4.2.1 Material

CPT plates were prepared by the same method described in 1.6.1. The thickness of plates was controlled in 2 mm. CPT specimens were cut with a dimension of 40 mm×10 mm×2 mm using a diamond disc cutter. Then, the cut specimens were kept in a vacuum oven at 90℃ until the weight change was below 0.01% before the tests.

4.2.2 Experiments

4.2.2.1 Thermo-oxidative aging test

The thermo-oxidative aging test was carried out on a box-type electric furnace in air for a total of 100 hours. The photo of the furnace and the schematic of the inner part are shown in Figure 4-1 and 4-2, respectively.

The test temperatures were chosen as 140 ℃, 160 ℃, 180 ℃ and 200 ℃. The atmosphere was air. Specimens were put into ceramic crucibles separately. The furnace was preheated to the specified temperature first, and these crucibles were placed at the bottom of the furnace. The aging test lasted for 100 hours in each temperature. Specimens were aged at a certain temperature for 20 hours and then naturally cooled in the furnace, which is defined as one cycle. The test lasted typically for 5 cycles in total. Flexural properties of these aged CPT specimens were tested after every cycle.

Figure 4-1 The photo of the box-type electric furnace

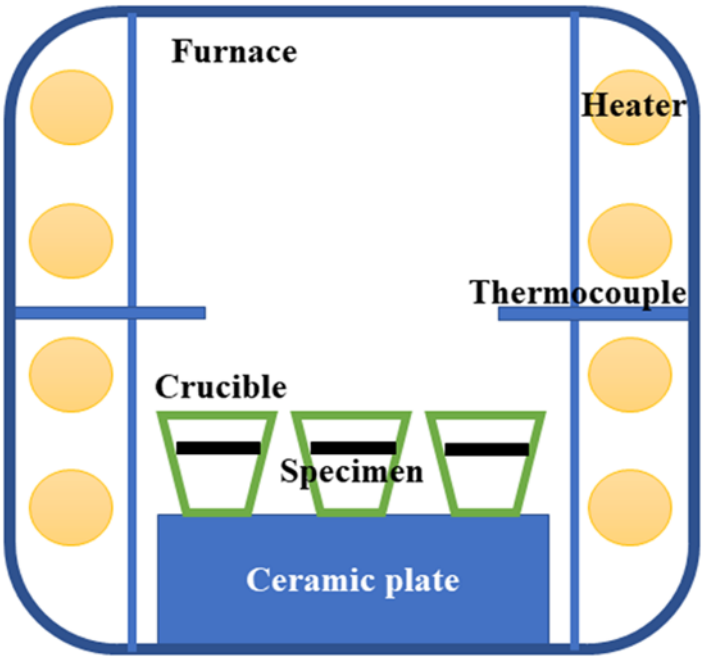

Figure 4-2 The schematic of the inner part of the furnace

4.2.2.2 Three-point bending test

The three-point bending test was conducted to determine the flexural properties of the CPT specimens after the thermo-oxidative aging test. A universal testing machine (AUTOGRAPH S-X 0.5 kN, Shimadzu Co.) was used. The span of the supporters (L) was determined by the thickness of specimens. The ratio of the span to the thickness was 16:1. The bending load point radius was 3mm. A thermostatic chamber was used to control the ambient temperature for the duration of the test and a thermometer was used to monitor the real-time temperature of specimens. The test was conducted at 25 ℃. Five specimens were tested in each group. The load speed was 1 mm·min^{-1}. The schematic of the set-up for the three-point test is shown in Figure 4-3. Equation 2-7 and 2-8 are used to calculate the strength and modulus.

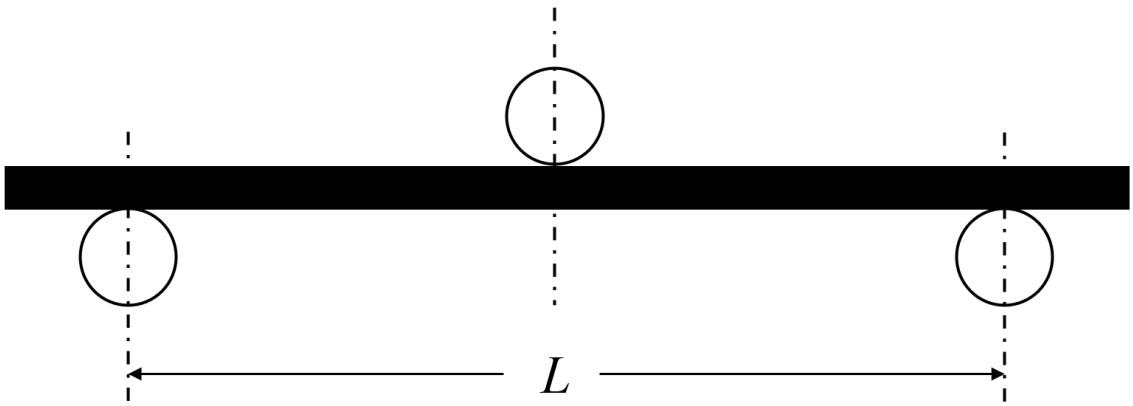

Figure 4-3 Setting of three-point bending test

4.2.2.3 Micromorphological analysis

The surface of the specimens, after the thermo-oxidative aging test, was observed by a microscope (VHX-1000, KEYENCE Co.). The fracture surface of the specimens after the three-point bending test was observed by a scanning electron microscope (VE-8800, KEYENCE Co.). The surface morphology of specimens was studied by a 3D laser scanning microscopy (VK-X250, KEYENCE Co.).

4.3 Results and discussions

4.3.1 Thermo-oxidative aging

4.3.1.1 Weight loss

The weight of the tested specimen was measured at each time interval. The whole oxidation weight loss of these specimens in unit area was calculated, respectively. The results are shown in Figure 4-4. Because specimens aged at 200 ℃ broke and could not keep their shape at the first 10 hours of the aging process, the evaluation of the effects of 200 ℃ aging on the mechanical properties of CPT material was suspended in this research. Therefore, it can be concluded that the limit use temperature of CPT at thermo-oxidative condition should be below 180 ℃.

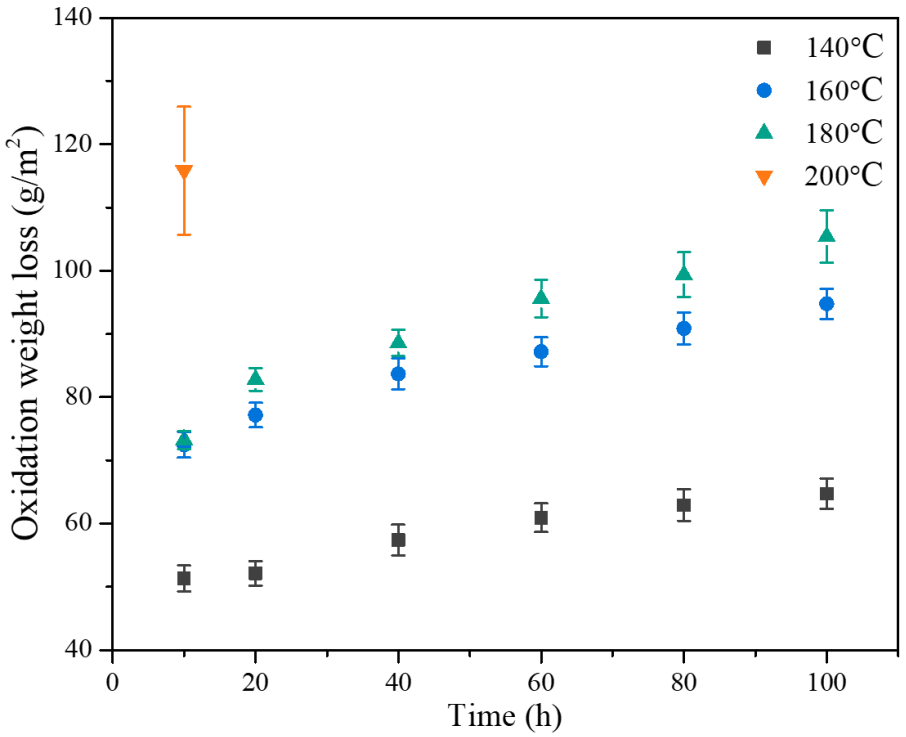

Figure 4-4 The weight loss of CPT material during thermo-oxidative aging

As the figure shows, the weight loss of the CPT specimens gradually increases during the thermo-oxidative process. In the first 10 hours, the weight loss of the specimens oxidized at 160 ℃ and 180 ℃ is similar. Then, with the increase in the time, the weight loss at 180 ℃ become higher than that at 160 ℃, but the trends are similar. So, the higher thermo-oxidative temperature, the more degradation of the CPT material have, and the degradation mechanism should be the same.

Besides, the CPT specimens aged at 140 ℃ has lower weight loss than that at 160 ℃ and 180 ℃. And the trend of the increase is much slower than that at higher temperatures. So, the mechanism of thermo-oxidation among the three chosen temperatures may be different.

The weight loss of CPT specimens at each time interval in thermo-oxidative aging test are shown in Figure 4-5. The results also prove the results in Figure 4-4. At the first 10 hours, the CPT aged at 140 ℃ has a lower weight loss, while the CPT aged in higher temperatures has higher weight loss, and the difference between 160 ℃ and 180 ℃ is small.

Along with the thermo-oxidative aging test, the weight loss at each time interval begins to decrease, and finally maintain a stable value, indicating that the degradation of the CPT material is relieved after the initial stage, and CPT can maintain a relatively stable state after aging for 100 hours. The critical time of the three groups of specimens are all 40 hours according to Figure 4-5. Therefore, the first 40 hours after application at high temperature is the main stage of degradation of CPT material. In order to expand the field of application of CPT materials, special attention should be paid to the first 40 hours.

Furthermore, since the weight loss of all three groups of specimens decreases to a small value, and specimens also keep its shape after aging for 100 hours, it can be inferred that the weight loss of CPT is less than that of pure PA6 resin. It may be due to the carbon fiber framework exposed on the specimen surface can prevent the exterior atmosphere contacting the inner

part of CPT and relieve the thermo-oxidative effect. Thus, this result indicates a good thermo-oxidative resistance of CPT material, which needs more experiments to verify.

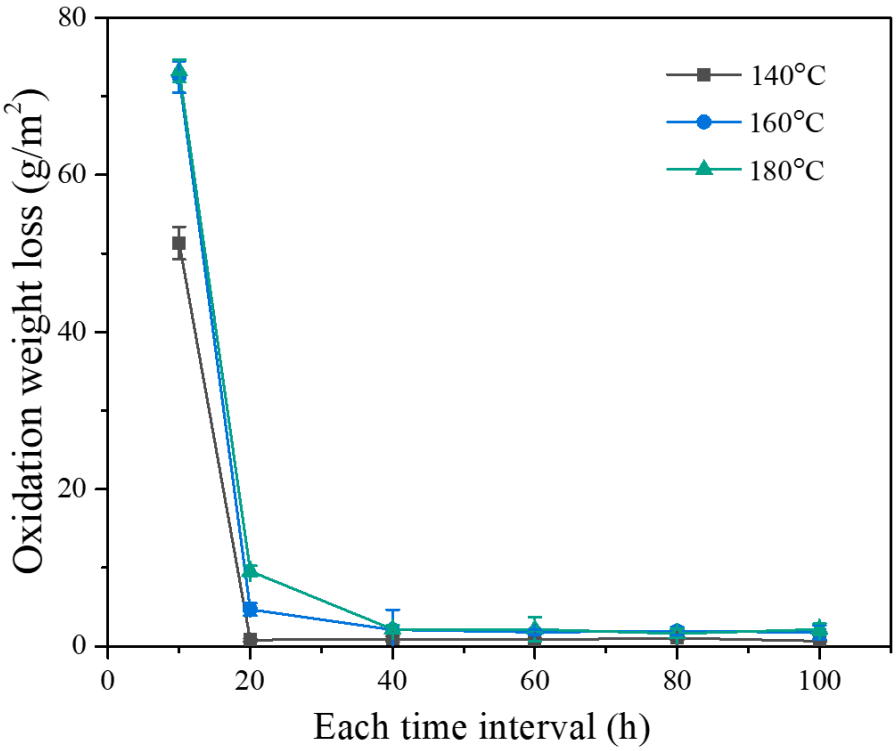

Figure 4-5 The weight loss of CPT material at each time interval in thermo-oxidative aging test

4.3.1.2 Oxidation rate

The oxidation rate of CPT specimens should be studied because it can provide detailed information for the degradation process. The relation between oxidation loss of CPT specimens aged at 140 ℃, 160 ℃ and 180 ℃ and time are shown in Figure 4-6. The data were fitted by least-square linear regressions, and the parameters are summarized in Table 4-1. The slope of the fitted line is regarded as the oxidation rate.

With the increase in the aging temperature, the oxidation rate of CPT specimens gradually increases. From the 20th hour of aging, the oxidation rates are gradually stable, and the weight loss shows a linear trend, as Figure 4-6 shows. In addition, it can be seen that the CPT has a relatively low oxidation rate after used several hours in high temperature. The increased aging time does not change the oxidation rate. Thus, the CPT material may have great thermo-oxidative resistance. CPT material with high mechanical property and low weight shows the potential for the application in thermo-oxidative environment.

Table 4-1. Parameters of least-square linear regressions.

	Slope ($g \cdot h^{-1} \cdot m^{-2}$)	**Intercept**	**Adjusted R-square**
140°C	0.1657	50.02	0.9940
160°C	0.2131	74.06	0.9730
180°C	0.2836	77.28	0.9142

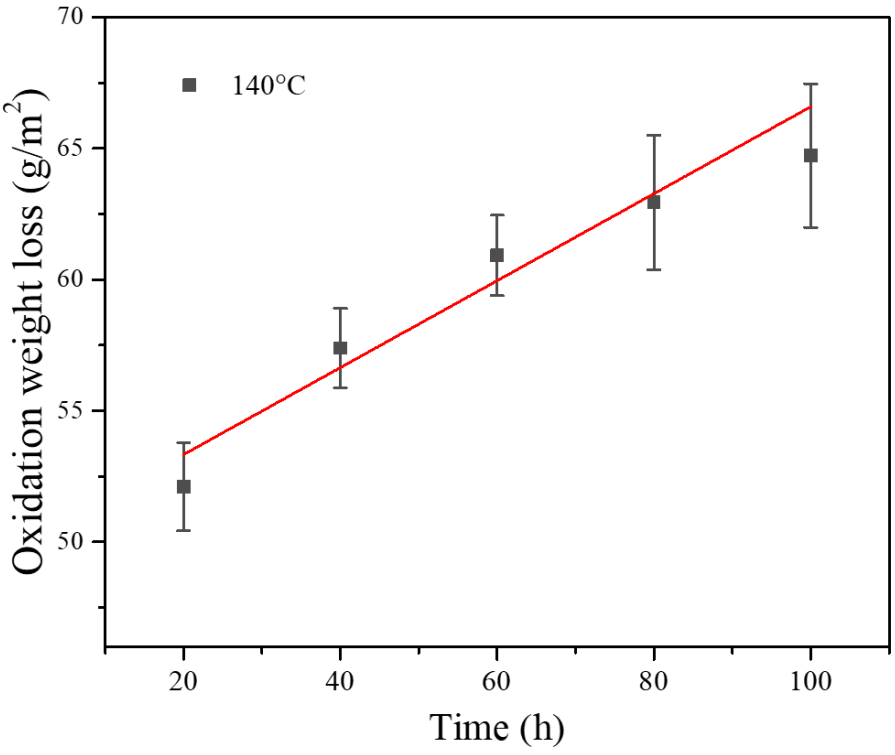

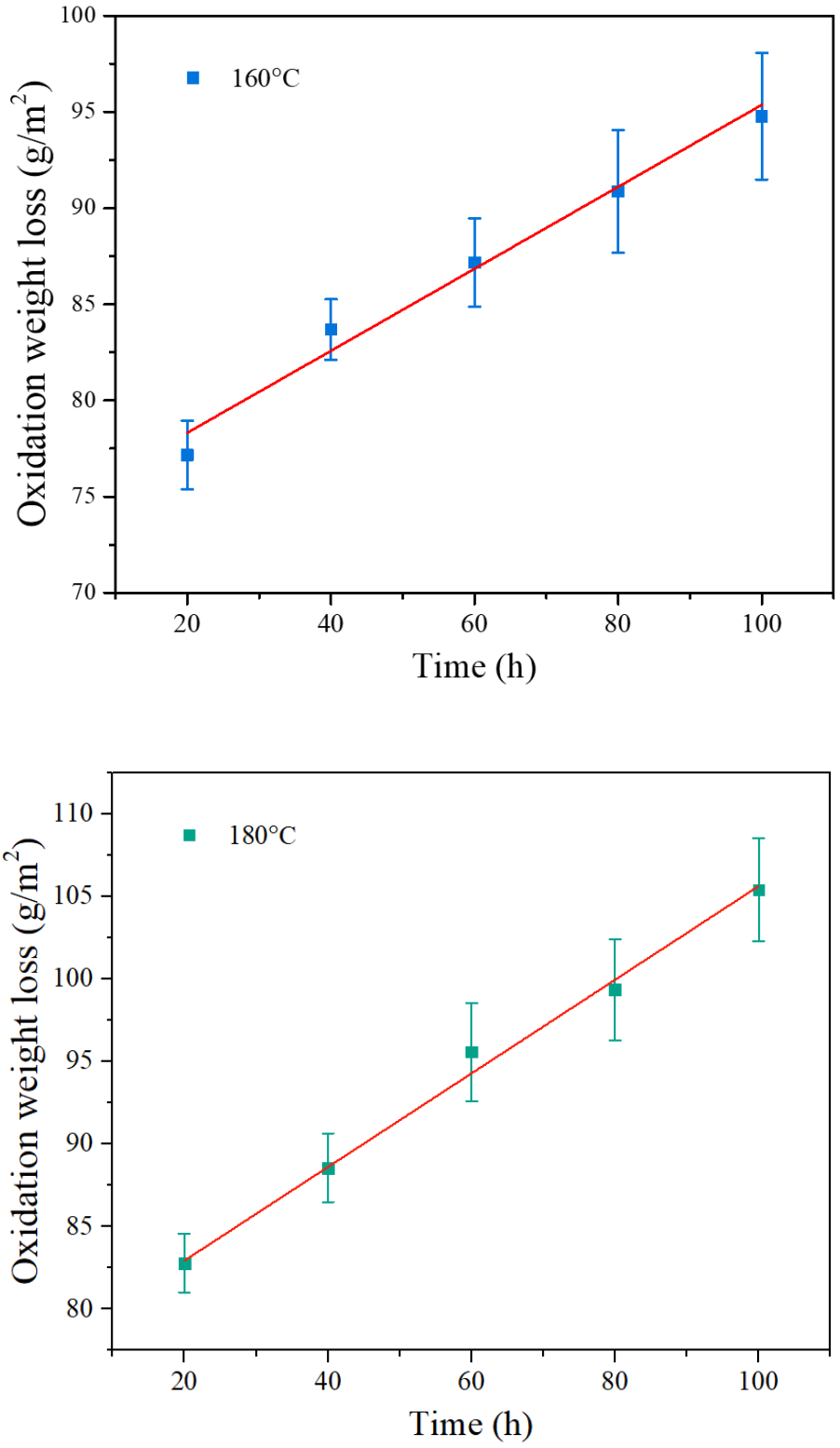

Figure 4-6 The oxidation rate of CPT aged at 140 ℃, 160 ℃ and 180 ℃

4.3.2 Three-point bending test

Similarly, three-point bending test was used to evaluate the effects of thermo-oxidative aging on the properties of CPT material. Relative results are summarized in Figure 4-7. At different aging temperatures, the flexural properties are reduced to different degrees. At 140 ℃, 160 ℃ and 180 ℃, the reduction ratio of flexural strength after aged are 8%, 13% and 17%, respectively, and the reduction ratio of flexural modulus are 2%, 4% and 12%, respectively. The change in the modulus at 140 ℃ and 160 ℃ are close to each other. Compared to the virgin specimen, there is almost no reduction in modulus. The decrease in the strength is also acceptable after thermo-oxidative aging. So, it can be concluded that specimens aged at 140 ℃ and 160 ℃ could maintain acceptable mechanical properties. However, after aged at 180 ℃, a large amount of resin on the surface decomposes. When specimens are under load, carbon fibers are easy to slip and exfoliate from the matrix bulk without the cohesion effect of resin. And this can lead to specimen failure.

Furthermore, the moduli increase at the first 20 hours, when the specimens are aged at 140 ℃, 160 ℃. This can be induced by the so-called thermal embrittlement mechanism, which is induced by the cold crystallization of resin [102]. Cold crystallization occurs when resin is heated, and the temperature is below the melting point. The resin crystallizes and the process is exothermic. Figure 4-8 shows the heating process of CPT in DSC. The area between the two red dotted lines should be the area where the cold crystallization occurs. As we can see, 140℃ and 160℃ are in this area while 180℃ is not. So, the X_c of PA6 increases at the initial stage when the aging temperature were 140 ℃ and 160 ℃. At the initial stage of aging, the positive effects of crystallization are stronger than the negative effects of resin decomposition in 140℃ and 160℃, while it is contrary at 180℃. With the increase of aging time, the decompose of resin gradually dominate, so the moduli gradually decrease.

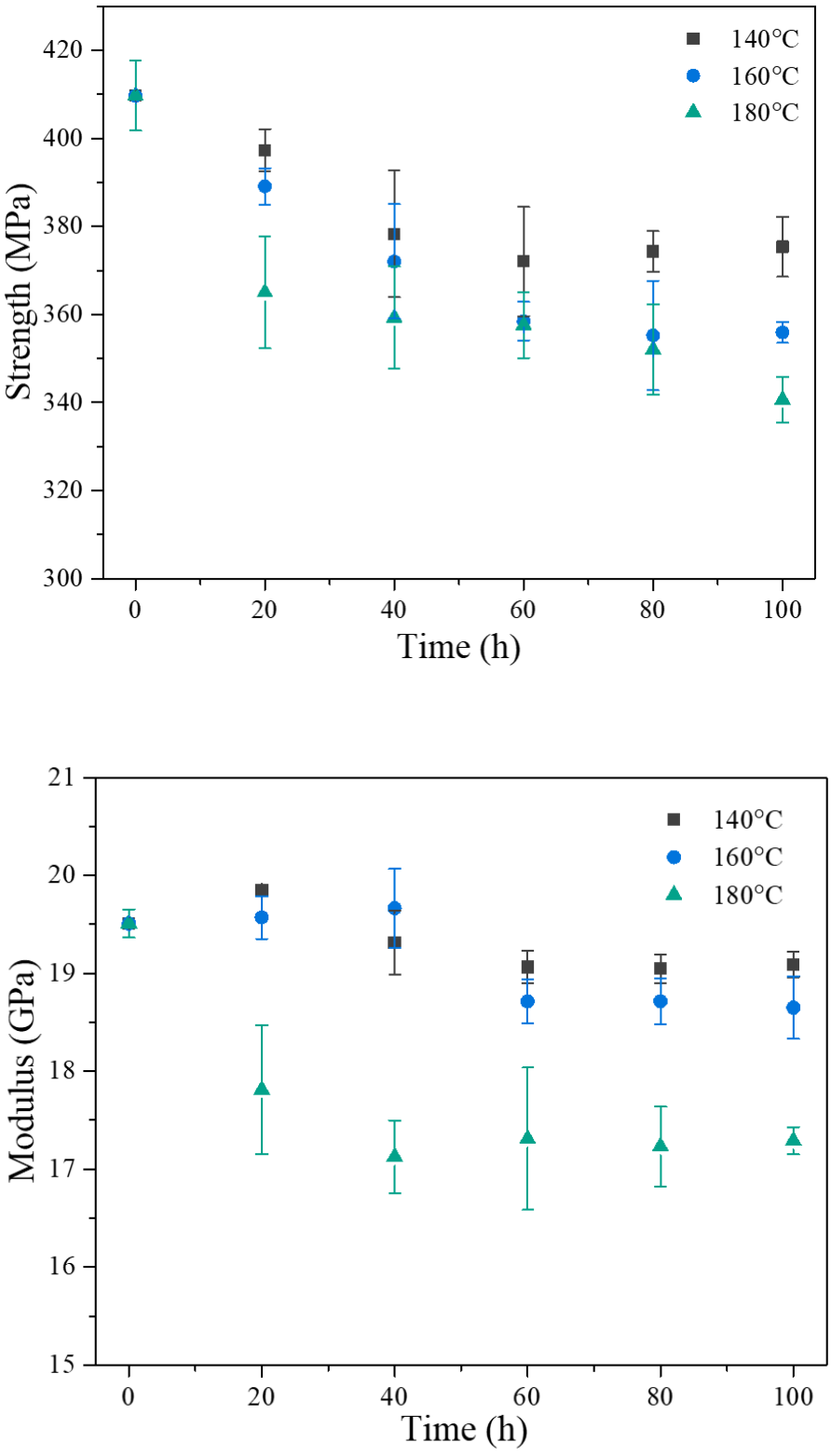

Figure 4-7 Flexural properties in 140 ℃, 160 ℃ and 180 ℃ at each time interval

Compared to published researches as mentioned in 1.4.4, more than 90% retention ratio of the mechanical properties proves that CPT material has the potential to be applied in some areas where high temperature resistance is required.

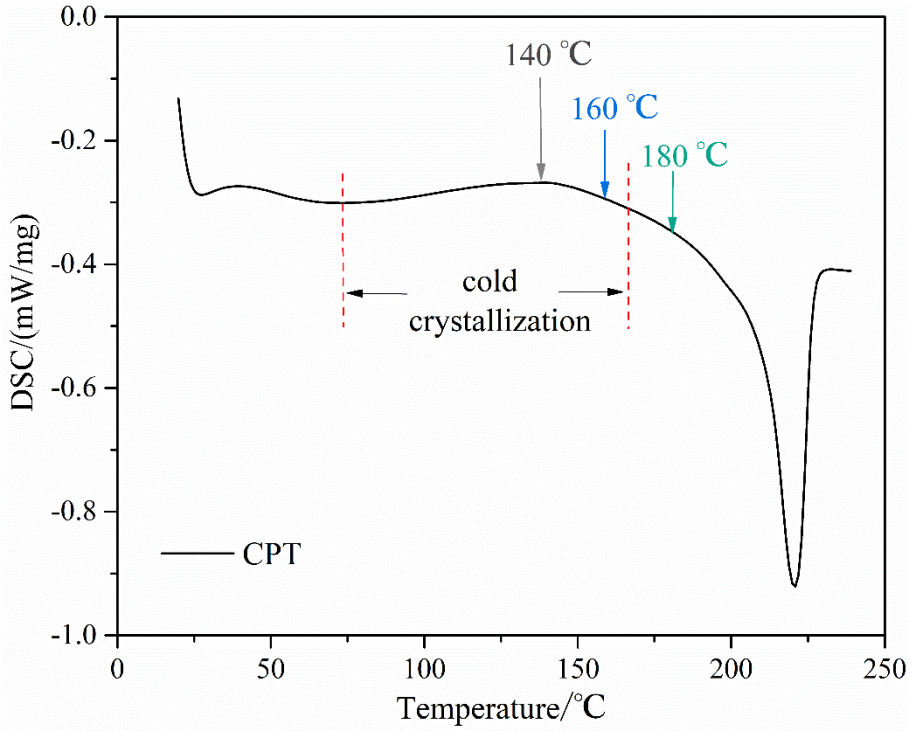

Figure 4-8 The heating curve of CPT in differential scanning calorimetry test

4.3.3 Micromorphology

4.3.3.1 Surface of specimens

4.3.3.1.1 SEM photos

In order to determine the effects of thermo-oxidative aging on CPT materials, the morphology of specimens after 100 hours aging at different temperatures was investigated. The SEM photos of the surface of these specimens are shown in Figure 4-9.

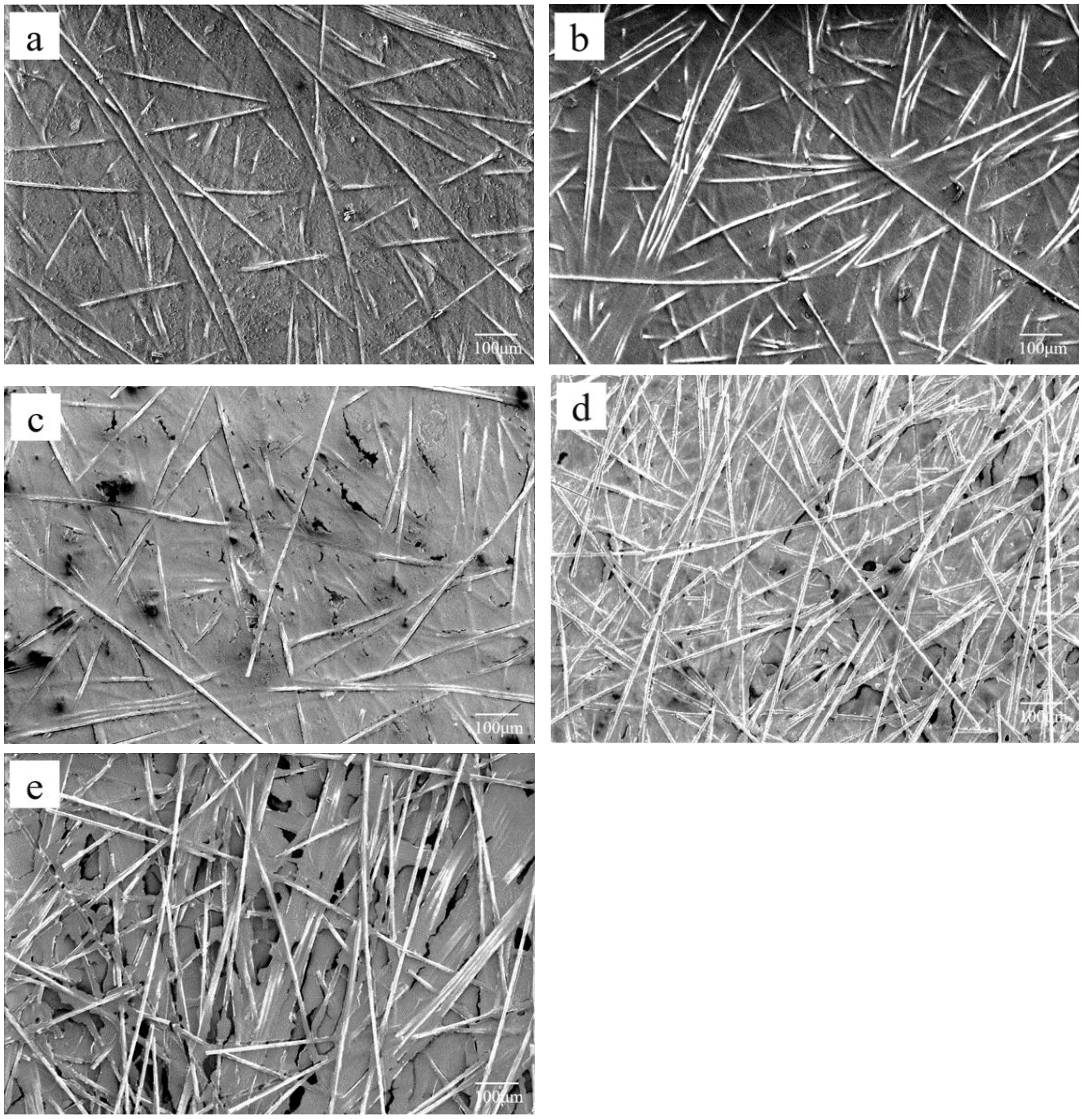

Figure 4-9. SEM photos of the surface of the aged CPT specimens: (a) virgin CPT; (b) at 140 ℃; (c) at 160 ℃; (d) at 180 ℃; (e) at 200 ℃

The virgin specimen shows flat, smooth and faultless surface. CPT aged at 140℃ shows similar surface morphology to virgin specimen, whereas many pores and cracks exhibit on the surface when the aging temperature is over 160 ℃ . It is caused by the decomposition of resin matrix during the thermo-oxidative process. With the increasing in the aging temperature, carbon fiber frameworks are gradually exposed on the surface. However, carbon fibers almost keep their shapes and structures under the effects of thermo-oxidization. As

mentioned in 4.3.1, CPT material may exhibit some thermo-oxidative resistance due to the existence of carbon fibers, acting as a reinforcement. The exposed carbon fiber may play an important role as oxidation-resistant coating in CPT and delay the oxidative degradation process.

As Figure 4-9 (c) shows, most of the cracks and pores and fault appears near fibers. Thus, it can be inferred that the degradation of resin matrix is likely to be generated from the interface of fiber and matrix, and propagate to the matrix bulk when the aging temperature is high enough or the aging time is extended.

4.3.3.1.2 3D laser scanning

Apart from SEM, 3D laser scanning was also employed for the study of micromorphology of aged specimens. The 3D photos of these specimens after 100 hours aging are shown in Figure 4-10.

It can be seen from the results that with the increase in the aging temperature, cracks and pores appear and gradually develop into gullies and pits. After degradation of the resin matrix covering the surface, carbon fibers are exposed to the surface, and form a framework, as the SEM photo shows in Figure 4-9. Furthermore, the concave and convex degree of the surface also increase. The original flat surface become pitted owing to the degradation of resin matrix.

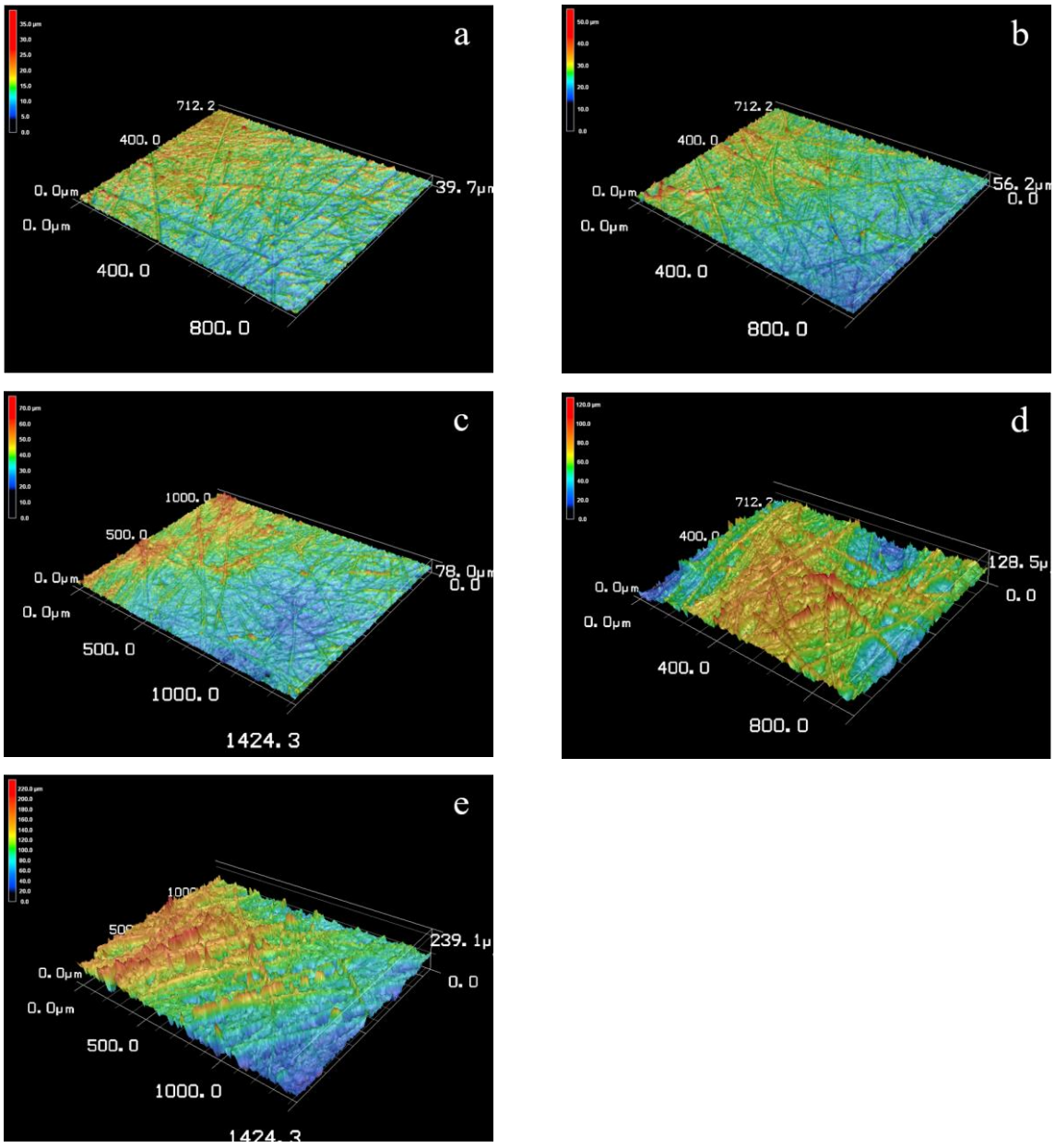

Figure 4-10 3D surface morphology of aged CPT specimens: (a) virgin CPT; (b) at 140 ℃; (c) at 160 ℃; (d) at 180 ℃; (e) at 200 ℃

The surface roughness results were also provided by the 3D laser scanning microscopy and shown in Figure 4-11. The roughness results also prove the results obtained from microscopic observation. When the aging temperature was below 160 ℃, the surface roughness increases slowly. This result accords with Figure 4-9 (a), (b) and (c). But once the aging temperature

was set above 180 ℃, the roughness of CPT surface rose rapidly. The roughness at 180 ℃ is more than twice that at 160 ℃. As Figure 4-10 (c) and (d) show, the surface of the specimens become uneven, which is formed by the remaining carbon fiber framework and the formation of cavities after the pyrolysis of PA6 resin.

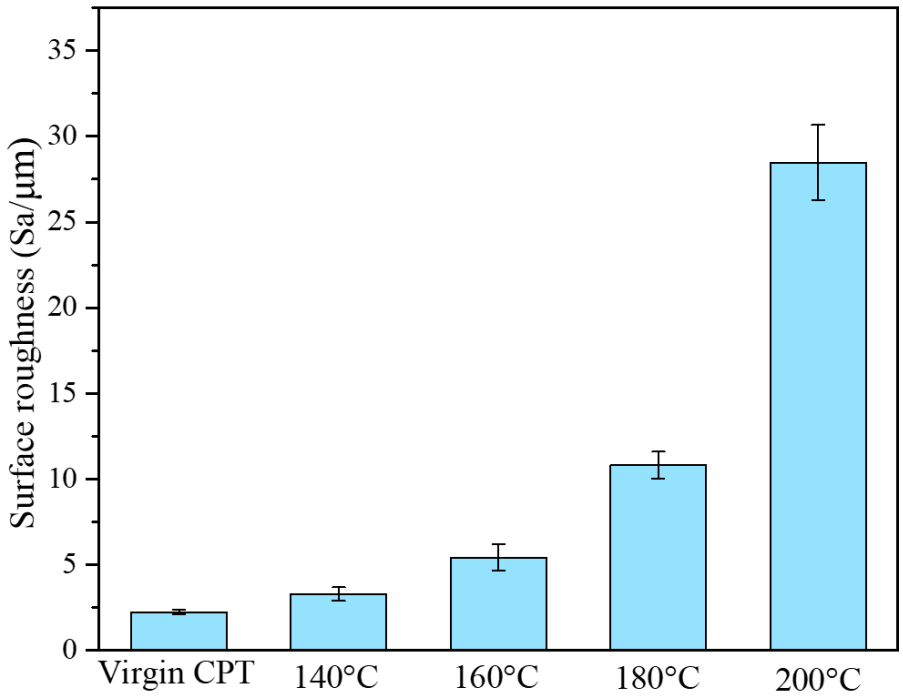

Figure 4-11 Surface roughness of CPT specimens after thermo-oxidative aging

4.3.3.2 Fracture surface

The morphology of specimens after three-point bending test was observed by SEM. Photos of the fracture surface in low magnification and the tensile side of specimens in high magnification are shown in Figure 4-12.

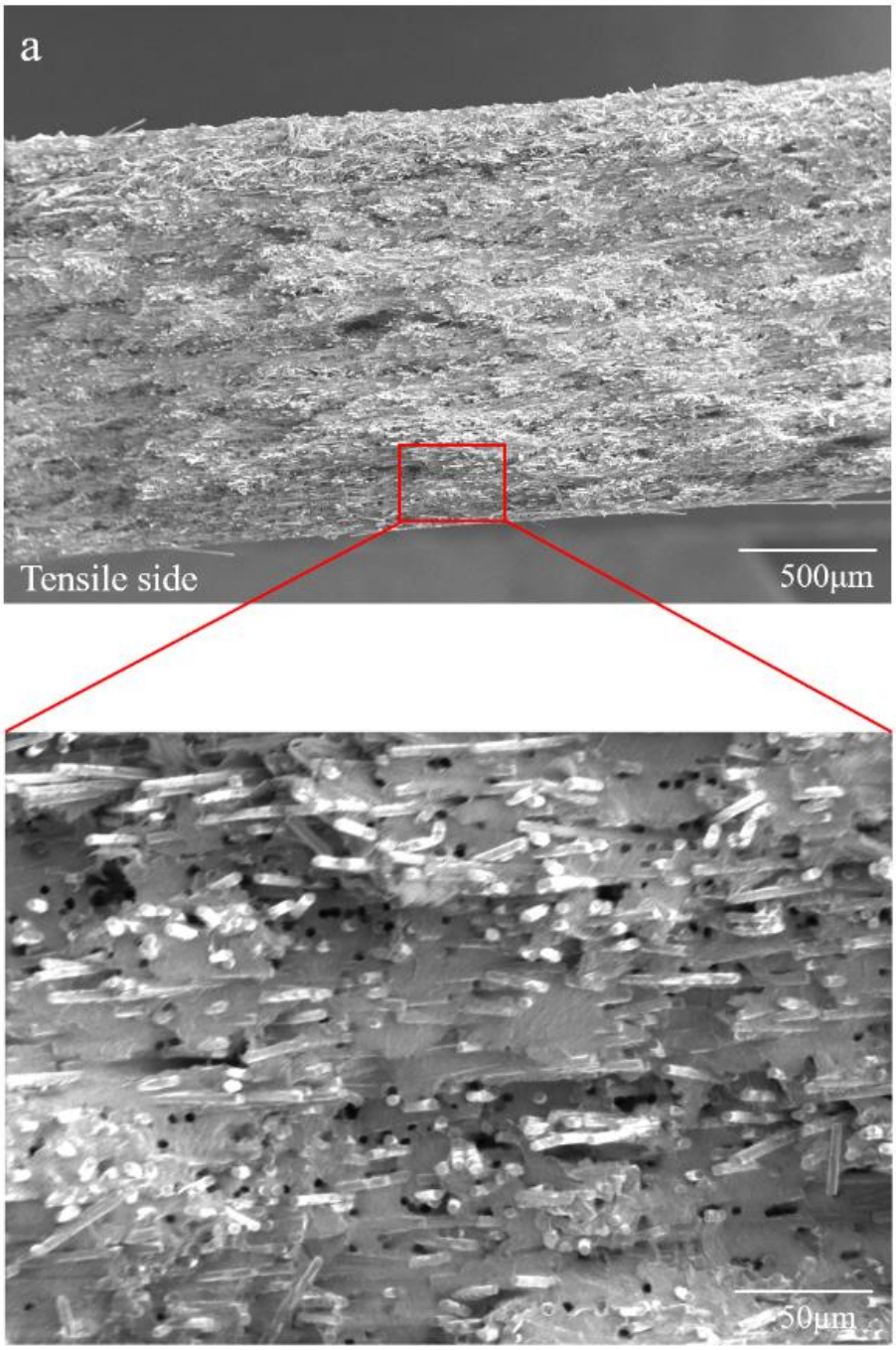
a
Tensile side
500μm
50μm

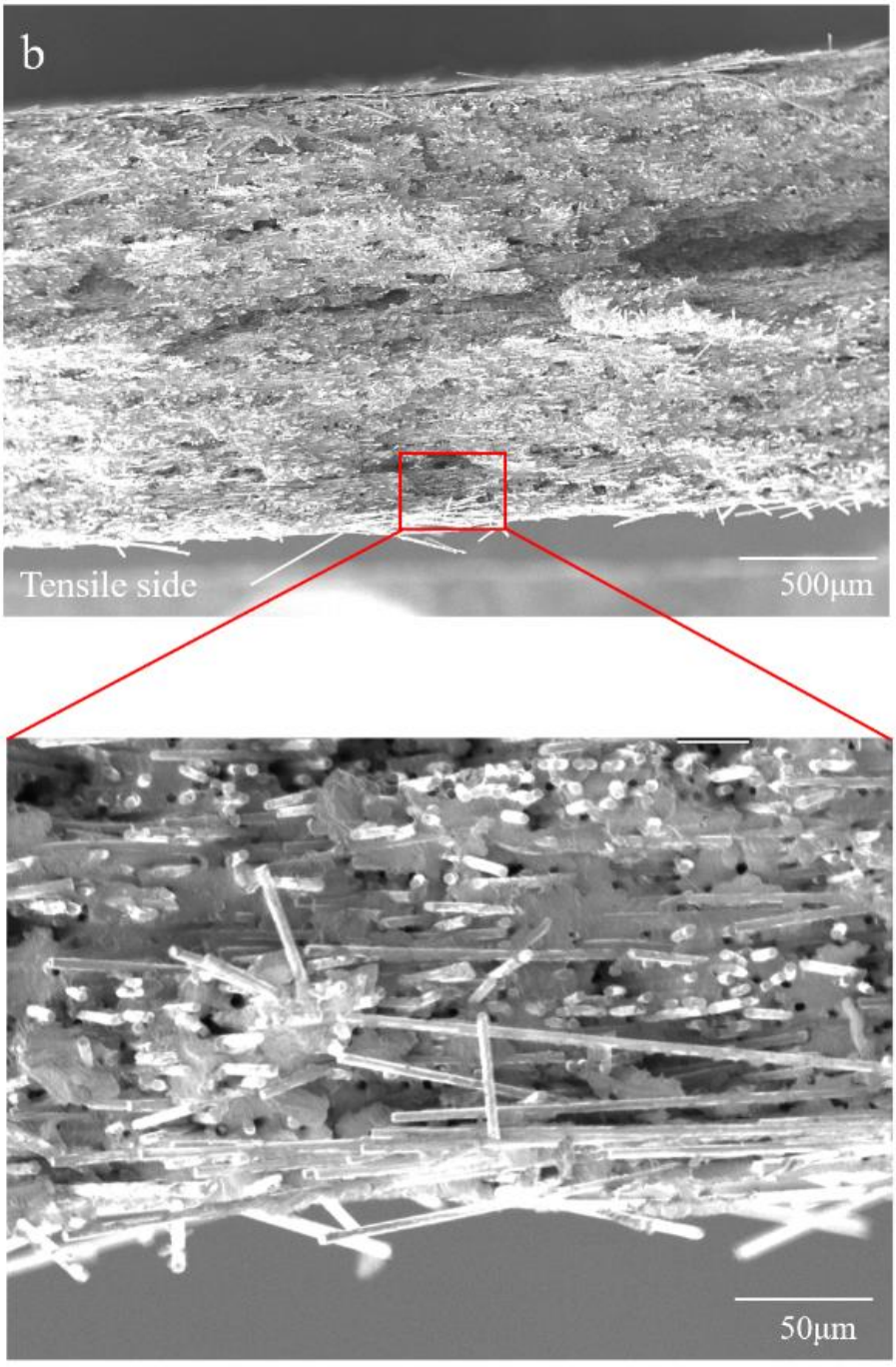
b
Tensile side
500μm
50μm

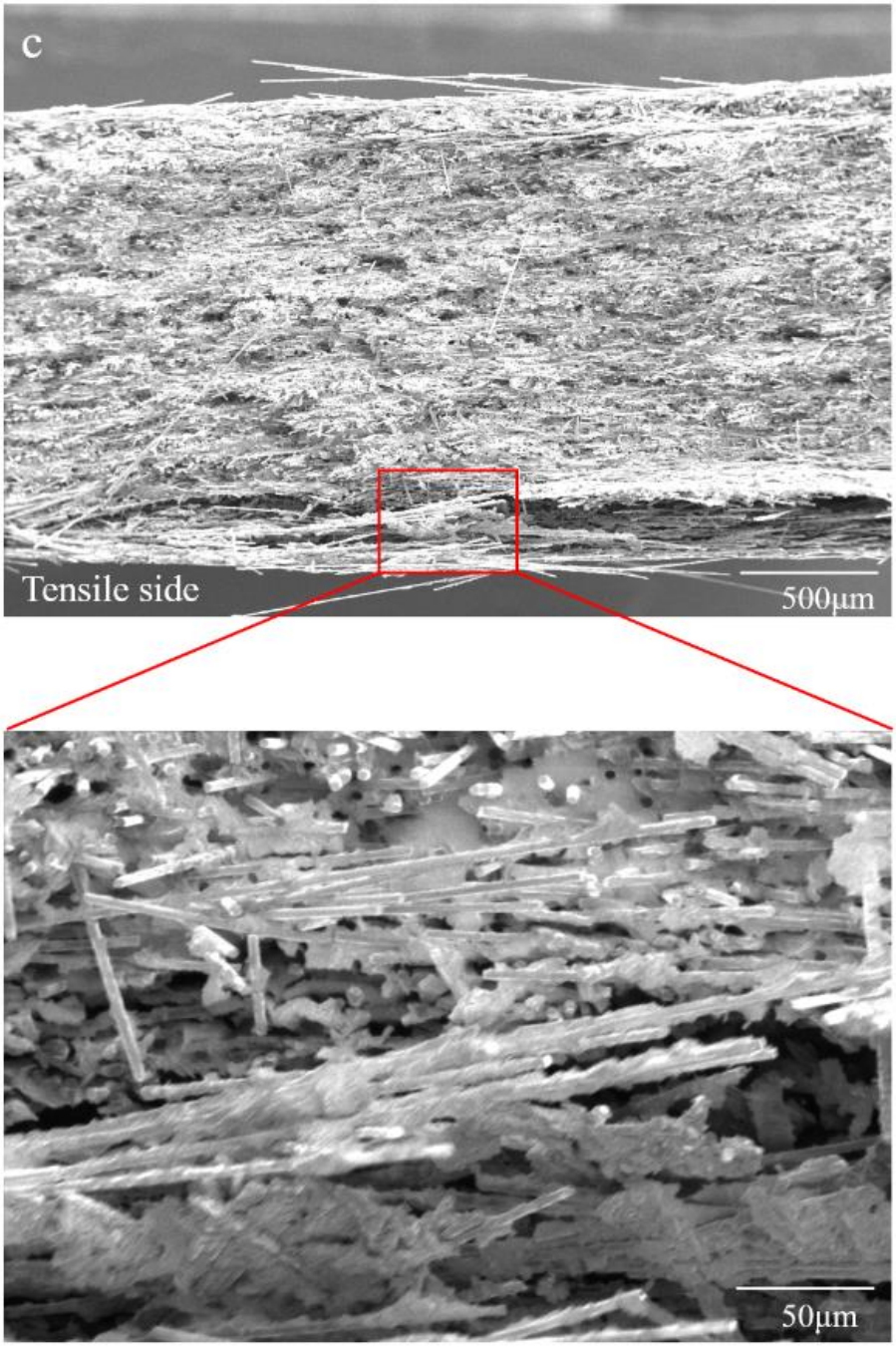

Figure 4-12 SEM photos of the fracture surface of the aged CPT specimens after three-point bending test: (a) at 140 ℃; (b) at 160 ℃; (c) at 180 ℃

When the aging temperature was 140 ℃, the fracture surface was flat and neat. On the tensile side, most of the fibers were well covered by resin matrix, with only several fibers exposed to the surface, which is consistent with Figure 4-9 (b).

For the specimens aged at 160 ℃, the carbon fiber framework is exposed to the surface, as Figure 4-9 (c) shows. Although more resin decomposes on the surface of specimen, the resin matrix in the inner part of specimen almost keeps its morphology. On the tensile sides, due to the degradation of resin, carbon fibers are exfoliated from the matrix bulk under the action of load.

At 180 ℃, the fracture surface is not as flat as the specimens aged at 140 ℃ and 160 ℃. More pull-out phenomenon appears than that at low temperatures. It indicates that the thermo-oxidative effect may have penetrated into the inner part of specimens at such a high temperature. Because of the serious thermo-oxidative effect, more exfoliation of fibers on the tensile side appears compared to low temperatures. In addition, thermo-oxidative corrosion on the surface is so severe that fibers not only on the tensile side but also the compressive side are exfoliated from the matrix bulk. Cracks and pores also intrude into the inner part of specimen but concentrate on the area only a few hundred microns close to the surface.

4.3.3.3 Oxidative layer

The schematic illustration of the thermo-oxidized specimen during three-point bending test is shown in Figure 4-13. The blue part represents the oxidation region. The yellow part is the affected area under the load on the compressive side, and the green part is the affected area under the load on the tensile side. Under the thermo-oxidative effect, carbon fibers in the oxidative region were exposed to exterior. The larger the oxidative region is, the more serious the exposure phenomenon becomes. Because more resin decomposed at high temperature, fibers lose their connecting medium, which make them easy to slide from their original

positions. So, under the action of load, the fibers without resin connection are easy to be exfoliated from the matrix bulk, and the cavities left generate cracks which can extend to the interior of the specimen, thus leading to the specimen failure.

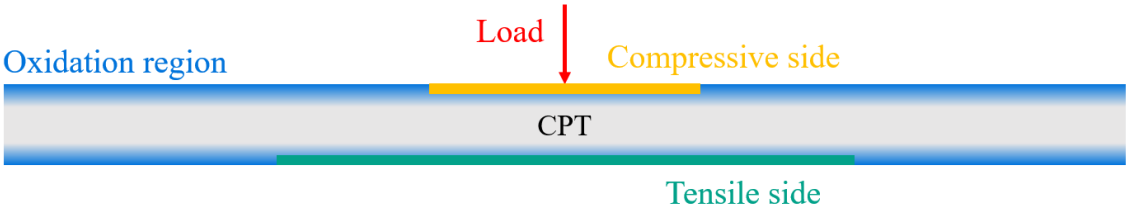

Figure 4-13 Schematic illustration of the aged specimen in three-point bending test

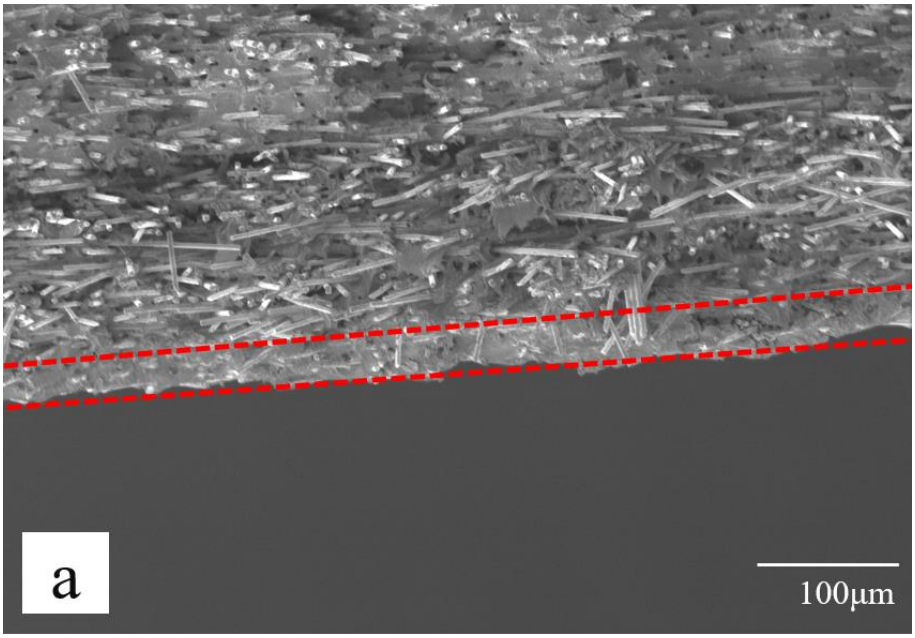

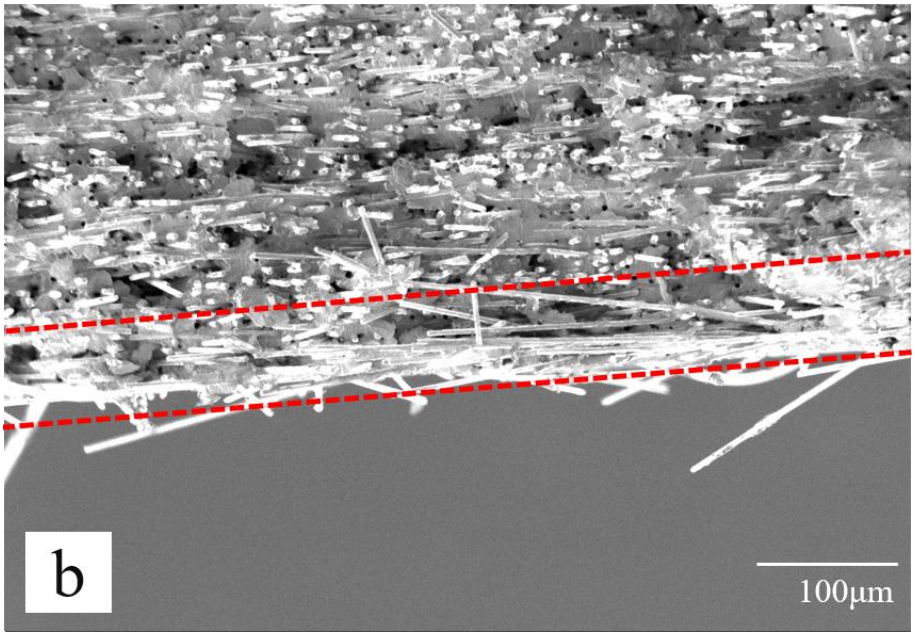

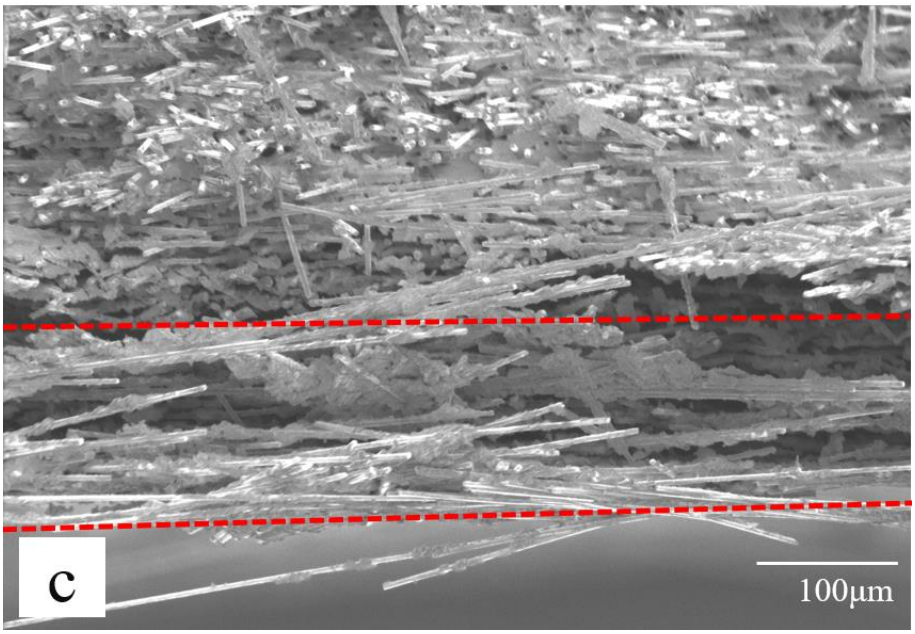

Figure 4-14 The oxidation layer of aged specimens: (a) at 140 ℃; (b) at 160 ℃; (c) at 180 ℃

Furthermore, the higher the aging temperature is, the thicker the oxidative layer on the surface of the specimen is, as shown in the area marked by the red lines in Figure 4-14. Thus, there are more pores and damages in three-point bending test. After resin decomposes, stress

concentration generates at the original interface of fibers and matrix. Since cracks on the surface has been caused owning to thermo-oxidation, the stress concentration accelerates the generation and propagation of these cracks, leading to the failure of the specimen. The thicker the oxidative region is and the more cracks and pores the specimens have, the more decline the mechanical properties are.

Based on the above results, it can be concluded that the highest application temperature of CPT material should be 160 ℃, because the decomposition of the resin in 180℃ is so serious that the CPT material cannot show a good performance in mechanical properties. CPT material can meet the need of 100 hours application below 160 ℃. So, CPT is not suitable for fire rescue, which is close to fire, but can be used in remote fire-fighting equipment which has moderate distance from the fire site.

4.3.4 Thermo-oxidative resistance

If we focus on the inner part the oxidation concentrated near the surface, it is found that the inner part was protected from oxidation effect. So, the thermo-oxidative resistance is found of CPT material, which has been proposed in 4.3.1.

The schematic diagram of the mechanism of thermo-oxidative resistance is proposed and shown in Figure 4-15. The figure shows the changes in CPT specimens that happen during the aging process. When the aging starts, PA6 resin on the specimen surface is oxidized. The oxidized PA6 formed a film that covers on the specimen surface, as Figure 4-15 (2) shows. With the development of thermo-oxidative process, PA6 resin begin to decompose and some carbon fibers are left and exposed to surface, which form a framework structure. Some pores and cracks appear near the carbon fiber framework, which is shown in Figure 4-15 (3). Gases generate owning to the decomposition of PA6 and gather in these pores, and it is hard for

these gases to escape into the surrounding air because of the carbon fiber framework.

Finally, cracks and pores gradually increase and connect into pieces, which is still protected by the fiber framework, as the light blue area in Figure 4-15 (4) shows. Gases generate during the aging process also gather together because of the cracks and pores connect together. However, due to the influence of fiber framework, these gas oxidation products are shrouded inside, concentrate on the surface area and do not escape. Thanks to the fiber framework, it is difficult for the external oxygen to enter into the internal part and continue to react with resin inside, so the fiber framework existing in CPT material can relieve the oxidative effect during aging process.

Therefore, within a certain thermo-oxidative time, CPT material can maintain good thermo-oxidative resistance.

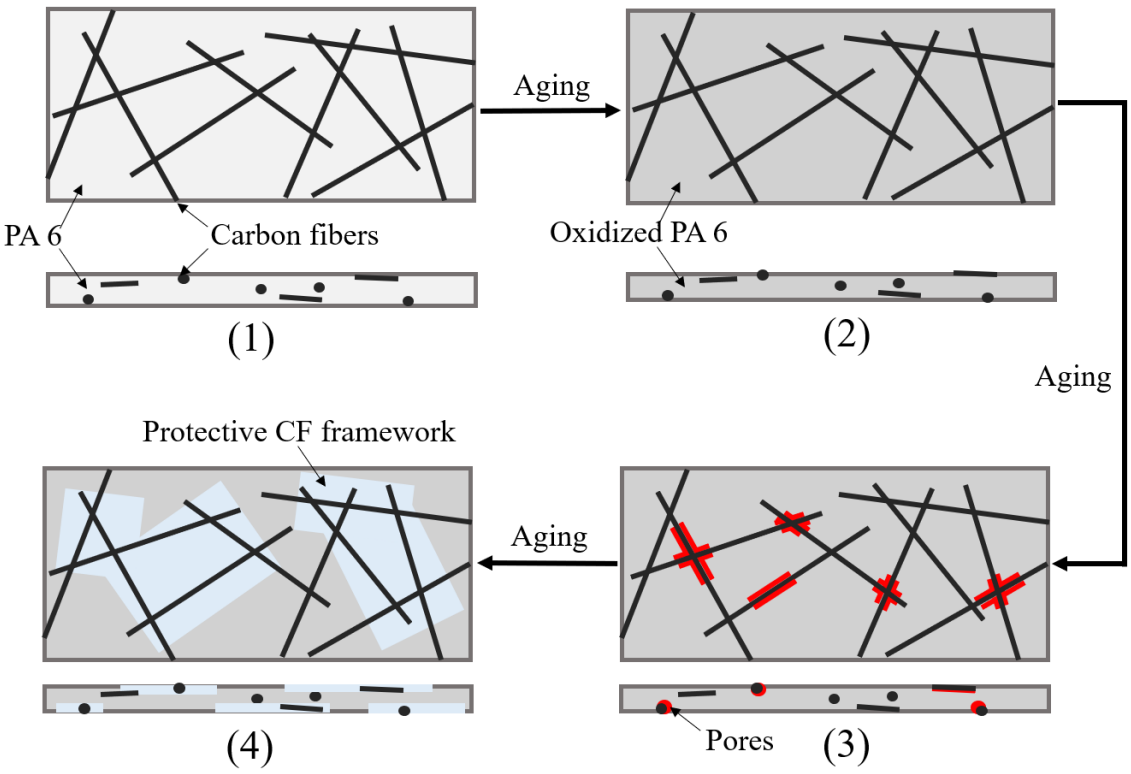

Figure 4-15 The schematic diagram of the mechanism of thermo-oxidative resistance

4.4 Summary

In this research, the effects of the thermo-oxidative aging were researched. The CPT specimens were proved to have good thermo-oxidative resistance. The maximum application temperature of CPT was also determined.

Because PA6 resin in CPT material decomposes under thermo-oxidative exposure when the temperature is above 200 ℃, CPT using PA6 as matrix is not suitable for fire rescue equipment which is close to fire site.

During the thermo-oxidative aging, the higher the temperature is, the easier the resin on the surface decomposes and exfoliates. Carbon fibers are easy to slip from the original positions, and exfoliate from the resin matrix bulk under the effect of load, which lead to the failure of the specimen.

Furthermore, under the thermo-oxidative effects, the framework structure of carbon fibers can establish a protective atmosphere near the specimen surface. This fiber framework can protect the internal unoxidized PA6 and slow down the oxidation speed to some extent. So, CPT material is considered to have thermo-oxidative resistance owning to the carbon fiber framework. But further study is also needed to confirm the long-term thermo-oxidation resistance of CPT material.

This research also provides guidance for future application of CPT material for fire rescue. This material has the potential to be used in remote fire-fighting equipment which has moderate distance from the fire site.

Chapter 5. Conclusions

5.1 Summary

The recycling of carbon fibers are urgent issues for both economic and environmental reasons. As the majority of recycled fibers, the properties and performance of short and semi-long fibers need to be evaluated. Considering the mechanical properties, molding properties and other factors, these recycled fibers are considered suitable for use as reinforcement in thermoplastics. Among these short and semi-long carbon fiber reinforced thermoplastics, as a kind of carbon fiber mat reinforced thermoplastics, CPT material stands out and is expected to have wider applications. The evaluation of the properties of CPT material become critical.

Meanwhile, environmental effects should be studied because the performance of polymer-based composites is seriously affected by environmental factors. In this research, the influence of environmental factors on the performance of CPT material was studied.

5.1.1 Water absorption and its effects

PA6 resin is easy to absorb water from environment, and its performance is affected by water content, so it is necessary to study the water absorption behavior and mechanical properties of CPT materials after water absorption. As the water absorption results shows, CPT material shows similar absorption behavior in fresh and sea water. The retention rate of the flexural properties of saturated CPT in fresh and sea water are both over 50%. The droplet test after water absorption indicates that water molecules reduce the IFSS between resin matrix and carbon fibers, leading to the decline of mechanical properties. In addition, the results of cyclic absorption-desorption test suggest that the mechanical properties of dry or saturated CPT material are not greatly affected by switching between wet and dry environment.

5.1.2 Long-term performance in water environment

In order to meet the long-term use demand in water rich environment, the properties of CPT material after long-term aging in fresh and sea water were analyzed. CPT shows better resistance to sea water than that to fresh water. After long-term aging, the degradation of resin is serious in fresh water, but it is relatively gentle in sea water, reflected by the crystallinity, FTIR results of resin, and surface roughness of specimens. The hydrothermal effect from the aging process results in the main chain scission of PA6 resin and the mechanical properties decline. The different performance between fresh and sea water be because PA6 resin is resistant to alkali and most salt solutions, while sea water is weakly alkaline. Meanwhile, the analysis on critical length, RoM and factor *C* also indicate the reason for flexural properties decline. The degradation of resin matrix plays a key role in the degradation of properties of CPT material.

5.1.3 Thermo-oxidative resistance

To validate the applicability of CPT material in thermo-oxidative environment for further use in fire rescue, the thermo-oxidative resistance of CPT material was examined. The results of thermo-oxidative aging test indicate that the maximum use temperature for CPT material should not exceed 200℃. Furthermore, the results of three-point bending shows that CPT can maintain good mechanical properties when the aging temperature is below 160 ℃. The observation of the micro morphology of CPT material also confirms that the resin on the surface and inside the specimens does not degrade seriously below 160 ℃. Through the discussion on the surface morphology of the aged CPT, it is found that the carbon fiber framework close to the original surface of the specimen can play an important role in the thermo-oxidative resistance of CPT material. So, CPT material may have the potential to be applied in fire-fighting equipment which has moderate distance from fire sites. But further study on the long-term thermo-oxidation resistance of CPT material is also needed to confirm its performance.

5.2 Outlook

This research promoted intensive understanding on the effects of environmental factors, including moisture, sea water, long-term aging and thermo-oxidation, on the performance of short and semi-long carbon fiber reinforced thermoplastics. Considering the good long-term performance of CPT in sea water, this material is recommended to be used in marine industry. However, the properties after water absorption also show that it is imperative to conduct waterproof treatment on this material. Besides, CPT material exhibits some thermo-oxidative resistance, which may broaden its application in the field of fire-fighting. At the same time, its high temperature resistance still needs to be deeply developed so that it can be further used close to fire sites.

5.3 Impact of this research

In this research, study on one kind of carbon fiber mat reinforced thermoplastics for mass production was carried out. As a kind of short fiber prepreg material, CPT was taken as the research object since it is expected to be applied in a broader field in the future. For practical use, concerning the influence of environment factors, the mechanical properties of CPT contributing to the safety were examined; the effects of moisture, sea water, temperature, and thermo-oxidation on the performance of CPT was investigated. Important knowledge in the application of CPT to the mass production, outdoor applications and assurance of products safety.

This research is expected to contribute to carbon fiber recycling industry of high recycling and utilization rate and carbon fiber reinforced plastics manufacturing industry of high mechanical performance and environmental tolerance. We also look forward to the further application of short carbon fiber reinforced materials and recycled carbon fiber reinforced materials in various fields

References

[1] Donnet, J. B. and R.C. Bansal, *Carbon fibers*. 1998: CRC Press.

[2] S. CHAND, *Review Carbon fibers for composites*. Journal of Materials Science, 2000; 35: p. 1303 – 1313.

[3] P. Morgan, *Carbon fibers and their composites*. 2005: CRC Press.

[4] J. Kadla, et al. *Lignin-based carbon fibers for composite fiber applications*. Carbon, 2002; 40: p. 2913–2920.

[5] W. Zhang, J. Liu, and G. Wu. *Evolution of structure and properties of PAN precursors during their conversion to carbon fibers*. Carbon, 2003; 41: p. 2805-2812.

[6] A. GuptaI and R. Harrison. *New aspects in the oxidative stabilization of PAN-based carbon fibers*. Carbon, 1996; 34: p. 1427-1445.

[7] K. Naito, et al. *Tensile properties of ultrahigh strength PAN-based, ultrahigh modulus pitch-based and high ductility pitch-based carbon fibers*. Carbon, 2008; 46: p. 189-195.

[8] A.Wazir, and L. Kakakhel. *Preparation and characterization of pitch-based carbon fibers*. New Carbon Materials, 2009; 24: p.83-88.

[9] J. Shim, S. Park, and S. Ryua. *Effect of modification with HNO3 and NaOH on metal adsorption by pitch-based activated carbon fibers*. Carbon, 2001; 39: p.1635-1642.

[10] E. Raymundo-Piñero, et al. *Structural characterization of N-containing activated carbon fibers prepared from a low softening point petroleum pitch and a melamine resin*. Carbon, 2002; 40: p.597-608.

[11] M. Meng, et al. *Multi-scale modelling of moisture diffusion coupled with stress distribution in CFRP laminated composites*. Composite Structures, 2016; 138: p. 295-304.

[12] I. Käppler, et al. *Surface modification of carbon fibres using plasma technique*. AUTEX Research Journal, 2014, 14: p. 34-38.

[13] Y. Nakashima, et al. *Analytical modelling of the behaviour and scatter of the flexural*

modulus of randomly oriented carbon fibre strand thermoplastic composites. Composite Structures, 2017; 178: p. 217–224.

[14] H. Piao, et al. *Influence of Water Absorption and Temperature on the Mechanical Properties of Discontinuous Carbon Fiber Reinforced Polyamide 6*. Fibers and Polymers, 2019; 20: p. 611-619.

[15] R. Dutra, et al. *Hybrid composites based on polypropylene and carbon fiber and epoxy matrix*. Polymer, 2000; 41: p. 3841–3849.

[16] S. Gopalraj and T. Kärki. *A review on the recycling of waste carbon fibre/glass fibre-reinforced composites: fibre recovery, properties and life-cycle analysis*. SN Applied Sciences, 2020; 2: p. 433.

[17] https://www.techsciresearch.com/report/global-cf-cfrp-market/2659.html

[18] N. Shama, et al. *Carbon composites are becoming competitive and cost effective*. White paper, 2018: External Document.

[19] P. Dong, et al. *Economic and environmental assessment of recovery and disposal pathways for CFRP waste management*. Resources, Conservation and Recycling, 2018; 133: p. 63-75.

[20] H. Nguyen, et al. *Cement mortar reinforced with reclaimed carbon fibres, CFRP waste or prepreg carbon waste*. Construction and Building Materials, 2016; 126: p. 321-331.

[21] M. Nakagawa, et al. *Characterization of CFRP Using Recovered Carbon Fibers from Waste CFRP*. The 5th ISFR, 2019: p. 241-244.

[22] M. Das and S. Varughese. *A Novel Sonochemical Approach for Enhanced Recovery of Carbon Fiber from CFRP Waste Using Mild Acid–Peroxide Mixture*. CS Sustainable Chemistry & Engineering, 2016; 4: p. 2080-2087.

[23] K.Obunai, et al. *Carbon fiber extraction from waste CFRP by microwave irradiation*. Composites Part A: Applied Science and Manufacturing, 2015; 78: p. 160-165.

[24] A. Torres, et al. *Recycling by pyrolysis of thermoset composites: characteristics of the liquid and gaseous fuels obtained*. Fuel, 2000; 79: p. 897–902.

[25] C. Lee, et al. *Assessing environmentally friendly recycling methods for composite bodies*

of railway rolling stock using life-cycle analysis. Transportation Research Part D, 2010; 15: p. 197–203.

[26] C. Thomas, et al. *Epoxy composites containing CFRP powder wastes*. Composites: Part B, 2014; 59: p. 260–268.

[27] S. Pimenta and S. Pinho. *Recycling carbon fibre reinforced polymers for structural applications: Technology review and market outlook*. Waste Management, 2011; 31: p. 378–392.

[28] M. Nahil and P. Williams. *Recycling of carbon fibre reinforced polymeric waste for the production of activated carbon fibres*. Journal of Analytical and Applied Pyrolysis, 2011; 91: p. 67–75.

[29] E. Lester, et al. *Microwave heating as a means for carbon fibre recovery from polymer composites: A technical feasibility study*. Materials Research Bulletin, 2004; 39: p. 1549–1556.

[30] K. Yoo,n et al. *Recycling of unsaturated polyester resin using propylene glycol*. Polymer, 1997; 38: p. 2281–2285.

[31] H. Zhang, et al. *Investigation on degradation of polyethylene to oil in a continuous supercritical water reactor*. Ranliao Huaxue Xuebao/Journal Fuel Chemistry Technology, 2007; 35: p. 487–491.

[32] W. Dan,g et al. *An approach to chemical recycling of epoxy resin cured with amine and nitric acid*. Polymer, 2002; 43: p. 2953–2958.

[33] S. Pimenta and S. Pinho. *Recycling carbon fibre reinforced polymers for structural applications: Technology review and market outlook*. Waste Management, 2011; 31: p. 378–392.

[34] K. Won,g et al. *Recycled carbon fibre reinforced polymer composite for electromagnetic interference shielding*. Composites: Part A, 2010; 41: p. 693–702.

[35] E. Worrell and M. Reuter. *Handbook of Recycling: State-of-the-art for Practitioners, Analysts, and Scientists*. 2014: Elsevier BV.

[36] J. Pascault, et al. *Thermosetting Polymers*. 2002: CRC Press.

[37] O. Olagoke and A. Kolapo. *Handbook of Thermoplastics*. 2016: CRC Press.

[38] Y. Ma, et al. *Higher performance carbon fiber reinforced thermoplastic composites from thermoplastic prepreg technique: Heat and moisture effect*. Composites Part B, 2018; 154: p. 90–98.

[39] H. Obeid, et al. *On the identification of the coefficient of moisture expansion of polyamide-6: Accounting differential swelling strains and plasticization*. Mechanics of Materials, 2018; 118: p. 1–10.

[40] E. Picard, et al. *Water transport properties of polyamide 6 based nanocomposites prepared by melt blending: On the importance of the clay dispersion state on the water transport properties at high water activity*. Journal of Membrane Science, 2008; 313: p. 284–295.

[41] Y. Lei, et al. *Water diffusion in carbon fiber reinforced polyamide 6 composites: Experimental, theoretical, and numerical approaches*. Journal of Reinforced Plastics and Composites, 2019; 38: p.578–587.

[42] P. Le Gac, et al. *Yield stress changes induced by water in polyamide 6: Characterization and modeling*. Polymer Degradation and Stability, 2017; 137: p. 272-280.

[43] M. Broudin, et al. *Water diffusivity in PA66: Experimental characterization and modeling based on free volume theory*. European Polymer Journal, 2015; 67: p. 326–334.

[44] X. Li, et al. *Synergistic effect of polyfunctional silane coupling agent and styrene acrylonitrile copolymer on the water-resistant and mechanical performances of glass fiber–reinforced polyamide 6*. Polymer Advanced Technologies, 2019; 30: p. 1951–1958.

[45] L. Sang, et al. *Moisture diffusion and damage characteristics of carbon fabric reinforced polyamide 6 laminates under hydrothermal aging*. Composites Part A, 2019; 123: p. 242–252.

[46] Z. Kusmono, et al. *Water Absorption Behavior of Different Types of Organophilic Montmorillonite-Filled Polyamide 6/Polypropylene Nanocomposites*. POLYMER COMPOSITES, 2010: p. 196-202.

[47] C. Huang, et al. *Reducing water sorption of injection-molded polyamide 6 bars by*

polymerization-induced diffusion of styrene and grafting with polystyrene. Journal of Applied Polymer Science, 2018: 46243.

[48] V. Do, et al. *Effect of polypropylene on the mechanical properties and water absorption of carbon-fiber-reinforced-polyamide-6/polypropylene composite*. Composite Structures, 2016; 150: p. 240–245.

[49] F. Tian, et al. *Modeling of natural fiber reinforced composites under hydrothermal ageing*. Composite Structures, 2018; 200: p. 144–152.

[50] P. Alam, et al. *Tidal turbine blade composites - A review on the effects of hygrothermal aging on the properties of CFRP*. Composites Part B, 2018; 149: p. 248–259.

[51] F. Tian, et al. *A long-term mechanical degradation model of unidirectional natural fiber reinforced composites under hydrothermal ageing*. Composites Science and Technology, 2017; 142: p. 156-162.

[52] S. Alessi, et al. *Effect of hydrothermal ageing on the thermal and delamination fracture behaviour of CFRP composites*. Composites: Part B, 2014; 67: p. 145–153.

[53] A. Oskouei, et al. *Flexural and web crippling properties of GFRP pultruded profiles subjected to wetting and drying cycles in different sea water conditions*. Polymer Testing, 2018; 69: p. 417–430.

[54] R. Dutra, et al. *Hybrid composites based on polypropylene and carbon fiber and epoxy matrix*. Polymer, 2000; 41: p. 3841–3849.

[55] H. Choi, et al. *Hygroscopic aspects of epoxy/carbon fiber composite laminates in aircraft environments*. Composites: Part A, 2001; 32: p. 709-720.

[56] C. Humeau, et al. *Moisture diffusion under hydrostatic pressure in composites*. Materials and Design, 2016; 96: p. 90–98.

[57] M. Gabr, et al. *Mechanical and thermal properties of carbon fiber/polypropylene composite filled with nano-clay*. Composites: Part B, 2015; 69: p. 94–100.

[58] I. Ksouri, et al. *Long term ageing of polyamide 6 and polyamide 6 reinforced with 30% of glass fibers: physicochemical, mechanical and morphological characterization*. Journal of Polymers Research, 2017; 24: p. 133.

[59] R. Li, et al. *Long-Term Hydrothermal Aging Behavior and Aging Mechanism of Glass Fibre Reinforced Polyamide 6 Composites*. Journal of Macromolecular Science, Part B, 2018; 57: p. 67–82.

[60] I. Ksouri and N. Haddar. *Long term ageing of polyamide 6 and polyamide 6 reinforced with 30% of glass fibers: temperature effect*. Journal of Polymers Research, 2018; 25: p. 153.

[61] B. Yang, et al. *Effect of fiber surface modification on water absorption and hydrothermal aging behaviors of GF/pCBT composites*. Composites Part B, 2015; 82: p. 84-91.

[62] M. Arhant, et al. *Effect of sea water and humidity on the tensile and compressive properties of carbon-polyamide 6 laminates*. Composites: Part A, 2016; 91: p. 250–261.

[63] P. Davies, et al. Influence of Sea Water Aging on the Mechanical Behaviour of Acrylic Matrix Composites. Applied Composite Material, 2017; 24: p. 97–111.

[64] B. Lu, et al. *Comparison of PCL degradation in different aquatic environments: Effects of bacteria and inorganic salts*. Polymer Degradation and Stability, 2018; 150: p. 133–139.

[65] P. Davies. *Environmental degradation of composites for marine structures: new materials and new applications*. Philosophical Transactions A, 2016: p. 1-13.

[66] L. Sang, et al. *Thermo-oxidative ageing effect on mechanical properties and morphology of short fibre reinforced polyamide composites – comparison of carbon and glass fibres*. RSC Advances, 2017; 7: p. 43334.

[67] W. Dong et al. *Influence of temperature on the thermo-oxidative degradation of polyamide 6 films*. Polymer Degradation and Stability, 2010; 95: p. 1054-1062.

[68] I. Zope, et al. *Influence of metal ions on thermo-oxidative stability and combustion response of polyamide 6/clay nanocomposites*. Polymer, 2016; 92: p. 102-113.

[69] H. Seefeld, et al. *Flame retardancy of glass fiber reinforced high temperature polyamide by use of aluminum diethylphosphinate: thermal and thermo-oxidative effects*. Polymer International, 2013; 62: p. 1608–1616.

[70] U. Braun, et al. *Flame retardancy mechanisms of aluminium phosphinate in combination*

with melamine polyphosphate and zinc borate in glass-fibre reinforced polyamide 6,6. Polymer Degradation and Stability, 2007; 92: p. 1528-1545.

[71] T. Kashiwagi, et al. *Flame retardant mechanism of polyamide 6–clay nanocomposites*. Polymer, 2004; 45: p. 881-891.

[72] L. Song, et al. *Preparation and properties of halogen-free flame-retarded polyamide 6/organoclay nanocomposite*. Polymer Degradation and Stability, 2004; 86: p. 535-540.

[73] Y. Chen, et al. *Preparation, properties and characterizations of halogen-free nitrogen–phosphorous flame-retarded glass fiber reinforced polyamide 6 composite*. Polymer Degradation and Stability, 2006; 91: p. 2003-2013.

[74] P. Gijsman, et al. *Differences in the flame retardant mechanism of melamine cyanurate in polyamide 6 and polyamide 66*. Polymer Degradation and Stability, 2002; 78: p. 219-224.

[75] A. Dasari, et al. *Flame retardancy of highly filled polyamide 6/clay nanocomposites*. Nanotechnology, 2007; 18: p. 44.

[76] C. Gao, et al. *Moisture absorption and cyclic absorption-desorption characters of fibre-reinforced epoxy composites*. Journal of Material Science, 2019; 54: p.8289-8301.

[77] S. Pillay, et al. *Effects of moisture and UV exposure on liquid molded carbon fabric reinforced nylon 6 composite laminates*. Composites Science Technology, 2009; 69 : p. 839-846.

[78] P. Scott, et al. *Water, salt water, and alkaline solution uptake in epoxy thin films*. Journal of Applied Polymer Science, 2013; 130: p. 1898-1908.

[79] L. VACCAREZZA, et al. *Kinetics of moisture movement during air drying of sugar beet root*. Institute of Food Science Technology, 1974; 9: p. 317-327.

[80] P. Paradisi, et al. *The fractional Fick's law for non-local transport processes*. Physica A: Statistical Mechanics and its Applications, 2001; 293: p. 130-142.

[81] B. Milligen, et al. *On the applicability of Fick's law to diffusion in inhomogeneous systems*. European Journal of Physics, 2005; 26: p. 913.

[82] X. Chen, et al. *Moisture Absorption and Diffusion Characterization of Molding*

Compound. Journal of Electronic Packaging, 2005; 127: p. 460-465.

[83] T. Chang, et al. *Advancing Boundary Model for Moisture Diffusion in A Composite Laminate*. Journal of COMPOSITE MATERIALS, 2008; 42: p. 957-973.

[84] J. Lowney, et al. *The Use of Fick's Law in Modeling Diffusion Processes*. IEEE Transactions on Electron Devices, 1980; 27: p. 1795-1798.

[85] D. Poirier and G. Geiger. *Fick's Law and Diffusivity of Materials*. Transport Phenomena in Materials Processing, 2016: p. 419-461.

[86] C. Gao, et al. *Moisture absorption and cyclic absorption–desorption characters of fibre-reinforced epoxy composites*. Journal of Material Science, 2019; 54: p. 8289–8301.

[87] U. Gaur, et al. *Effect of hydrothermal ageing on bond strength*. Composites, 1994; 25: p. 609-612.

[88] C. Peng. *Effect of coating resin for reinforcing carbon fibers on the interlaminar shear strength of PA6 composites*. Composite Interfaces, 2019; 26: p. 183-191.

[89] S. Kang, et al. *Fiber/epoxy interfacial shear strength measured by the microdroplet test*. Composites Science and Technology, 2009; 69: p. 245–251.

[90] H. Heilhecker, et al. *The vice angle in the microbond test*. Journal of materials science letters, 2000; 19: p. 2145 – 2147.

[91] X. Wang, et al. E*ffects of thermal residual stress on interfacial properties of polyphenylene sulphide/carbon fibre (PPS/CF) composite by microbond test*. Journal of Material Science, 2016; 51: p. 334-343.

[92] X. Gabrion, et al. *About the thermomechanical behaviour of a carbon fibre reinforced high-temperature thermoplastic composite*. Composites Part B, 2016; 95: p. 386-394.

[93] L. Gao, et al. *Long-Term Hydrothermal Aging Behavior and LifeTime Prediction of Polyamide 6*. Journal of Macromolecular Science Part B, 2015; 54: p. 239–252.

[94] P. Kiliaris, et al. *Influence of accelerated aging on clay-reinforced polyamide 6*. Polymer Degradation and Stability, 2009; 94: p. 389–396.

[95] L. Sang, et al. *Effects of hydrothermal aging on moisture absorption and property prediction of short carbon fiber reinforced polyamide 6 composites*. Composites Part B:

Engineering, 2018; 153: p. 306-314.

[96] P. Atali, et al. *The effect of different bleaching methods on the surface roughness and hardness of resin composites*. Journal of Dentistry and Oral Hygiene, 2011; 3: p. 10-17.

[97] J. Liang, et al. *Mechanical properties, crystallization and melting behaviors of carbon fiber-reinforced PA6 composites*. Journal of Thermal Analysis and Calorimetry, 2014; 115: p. 209–218.

[98] H. Wei. *Research on carbon fiber mat reinforced thermoplastics for advanced use of recycled carbon fibers*. The University of Tokyo, School of Engineering, Department of Systems Innovation, doctoral thesis, 2018.

[99] W. Thodsaratpreeyakul, et al. *The Determination of Interfacial Shear Strength in Short Fiber Reinforced Poly Ethylene Terephthalate by Kelly-Tyson Theory*. Open Journal of Composite Materials, 2017; 7: p. 218-226.

[100] G. Cai. *Effects of superheated steam on the tensile and interfacial adhesion properties of recycled carbon fiber*. The University of Tokyo, School of Engineering, Department of Systems Innovation, doctoral thesis, 2019.

[101] X. Bertran, et al. *Oxidation Behavior of PAN-based Carbon Fibers and the Effect on Mechanical Properties*. Oxidation of Metals, 2013; 80: p. 299–309.

[102] X. Zhao, et al. *Stress–Thermooxidative Aging Behavior of Polyamide 6*. Journal of Applied Polymer Science, 2013: 38616.

Acknowledgement

First and foremost I would like to express my sincere appreciation to my supervisor, Professor Takahashi Jun. I appreciate all his constructive comments, considerations, novel ideas and funding. He continues to provide professional guidance and outstanding assistance to me by his immense knowledge, patience, passion and broad view. I would not finish my research without his best support. It has been an honor to be one of his Ph. D. students. I'll keep this experience for the rest of my life.

I would also like to show my truly appreciation to Dr. Isamu Ohsawa. I am grateful for his considerable supports and wonderful ideas during the past three years, and I will always remember his kind, enthusiastic, healthy and positive lifestyle.

I also want to appreciate to all fellow members in the University of Tokyo. I really appreciate the suggestions and help from seniors, Dr. Yi Wan, Dr. Haowen Wei, Dr. Hao Piao, Dr. Qitao Guo, Dr. Guangbin Cai, Dr. Bing Xiao and Mr. Yiran Wang. I also want to thank Dr. Shaoping Qian, Dr. Peng Qu, Mr. Linshu Meng, Mr. Ye Zhang, Ms. Yunqian Zhang, Mr. Wataru Sato, Mr. Yuto Nakashima, Mr. Daiki Kobayashi, Ms. Natsumi Okano, Mr. Hideki Toyoda, Mr. Tiansheng Han, Ms. Siyi Shao, Mr. Yasuyuki Furuta, Mr. Jun Li, Mr. Hisaki Matsuda, Mr. Hao Wu, Mr. Gutao Shen, Mr. Xiaohang Tong, Mr. Yue Wang, Mr. Ruochen Xu, Mr. Zihao Zhao and Mr. Sixin Yan for their constant help and supports.

Last but not least, I would like to thank my family who are firmly supporting my study abroad. I would not start this journey and complete it without their understanding, trust, encouragement, support and love.

May 2020

Xiangdong He

List of Publications

1. Journal Papers

〔Peer-reviewed〕

1) W. Zhang, **X. He**, T. Song, Q Jiao, R Yang. "The influence of the phosphorus-based flame retardant on the flame retardancy of the epoxy resins", Polymer Degradation and Stability, No. 26,Vol.109, (2014-11), pp.209-217.
2) Q. Sun, M. Zou, X. Guo, R. Yang, H. Huang, P. Huang, **X. He**. "A study of hydrogen generation by reaction of an activated Mg–$CoCl_2$ (magnesium–cobalt chloride) composite with pure water for portable applications", Energy, Vol. 79, No. 28, (2015-2), pp.310-314.
3) W. Zhang, **X. He**, T. Song, Q Jiao, R Yang. "Comparison of intumescence mechanism and blowing-out effect in flame-retarded epoxy resins", Polymer Degradation and Stability, Vol.112, No. 6, (2015-2), pp.43-51.
4) **X. He**, W. Zhang, D. Yi, and R. Yang. "Flame retardancy of ammonium polyphosphate–montmorillonite nanocompounds on epoxy resin", Journal of Fire Sciences, Vol. 34, No. 11, (2016-3), pp.212-225.
5) Z. Qi, W. Zhang, **X. He**, and R. Yang. "High-efficiency flame retardancy of epoxy resin composites with perfect T8 caged phosphorus containing polyhedral oligomeric silsesquioxanes (P-POSSs)", Composites Science and Technology, Vol.127, No. 2, (2016-4), pp.8-19.
6) **X. He**, W. Zhang, and R. Yang. "The Characterization of DOPO/MMT nanocompound and its effect on flame retardancy of epoxy resin", Composites: Part A, Vol. 98, No. 13, (2017-7), pp.124-135.
7) Y. Wang, Y. Gao, J. Takahashi, Y. Wan, Y. Li, M. Li, C. Zhang, B. Xiao, **X. He**, J. Li, Q. Liu and C. Zhou, "Effect of plating time on surface evolution of chromium modified graphite powder by multi-arc ion plating", Surface Topography: Metrology and Properties, Vol.7, No.1, (2019-1), pp.1-7.
8) Y. Wang, Y. Gao, J. Takahashi, Y. Wan, B. Xiao, Y. Zhang, **X. He** and J. Li, "Titanium-modified graphite reinforced Cu-Ni composite by multi-arc ion plating technology", Vacuum, Vol.168, (2019-10), 108829.
9) Y. Wang, Y. Gao, J. Takahashi, Y. Wan, Y. Zhang, B. Xiao, **X. He** and J. Li, "Effect of graphite content on Cu-Ni-graphite composite for use as switch slide baseplate materials sliding against U75V steel", Journal of Tribology, Vol.141, No.12, (2019-12), 121603-1.
10) Y. Wang, Y. Gao, J. Takahashi, Y. Wan, M. Li, B. Xiao, Y. Zhang, **X. He**. " Investigation of modification of Cu-Ni-graphite composite by silver", Materials Chemistry and Physics, Vol. 239, (2020-1), 121990.

11) Y. Wang, Y. Gao, J. Takahashi, Y. Wan, **X. He**, Y. Zhang, B. Xiao and C. Zhang, "The study of microstructure characterization: Cu modified Cu-Ni-graphite composite", Composite Interfaces, Composite Interfaces, Vol.27, No.3, (2020-3), pp.249-262.

〔Under review〕

12) **X. He**, I. Ohsawa, J. Takahashi. "Influence of marine and harsh environments on the performance of carbon fiber paper reinforced polyamide 6" (under review).
13) **X. He**, B. Xiao, J. Takahashi. "Morphological, physicochemical, and flexural characterization of carbon fiber paper-reinforced polyamide 6 for long-term application in aqueous environments" (under review).
14) **X. He**, Y. Wang, J. Takahashi. "Evaluation of the thermo-oxidative resistance property of carbon fiber paper reinforced polyamide 6 material"(to be submitted in July 2020).

2. International Conference Proceeding

〔peer-reviewed ○: Presenter〕

1) ○**X. He**, W. Zhang, and R. Yang. "Influence of APP-MMT nanocompound on the properties of flame retardant epoxy resins", China Academic Annual Conference on flame retardancy, No.S-305, (2016-5).
2) ○**X. He**, I. Ohsawa and J. Takahashi, "The effects of moisture and temperature on the flexural properties of carbon fiber paper reinforced thermoplastics/polyamide 6", 22nd international conference on composite materials, No.P090, (2019-8).
3) ○**X. He**, I. Ohsawa, Y. Wan and J. Takahashi, "The effects of sea water and temperature on the flexural property of carbon fiber reinforced polyamide 6", 16th Japan international SAMPE symposium and exhibition, No.S-06, (2019-9).

3. Patent

1) R. Yang, **X. He**, and W. Zhang. "Phosphorus containing small molecule/montmorillonite nano-composite flame-retardant epoxy resin composite and preparation method thereof", China patent CN105713352A, (2017-4), (in Chinese).
2) W. Zhang, **X. He**, and R. Yang , "DOPO/MMT nano-composite flame retardant and preparation method thereof", China patent CN105694103A, (2017-4), (in Chinese).

4. Award

1) **X. He**, G. Zhu, P. Huang, P. Tu, Y. Wu, and Y. Li. "In situ nano synergistic flame retardant polyurethane foam insulation material", "National College Students' Extracurricular Academic Scientific and Technological Works Competition", The Challenge Cup, Beijing competition area, China, Second Award, (2014-11).
2) Y. Furuta, **X. He**, Y. Wang, T. Han, J. Li. IHI / SAMPE Japan Student Bridge Contest,

Second Award, (2018-2).